8-2015

Evaluating Accuracy and Bias in Genetic Monitoring Under Scenarios of Population Decline

Susan K. Munster
Grand Valley State University

Evaluating Accuracy and Bias in Genetic Monitoring Under Scenarios of Population Decline

Susan Kasko Munster

A Thesis Submitted to the Graduate Faculty of

GRAND VALLEY STATE UNIVERSITY

In

Partial Fulfillment of the Requirements

For the Degree of

Master of Science

Biology

August 2015

DEDICATION

I would like to dedicate this work to my family, without whom I could not have made the step to return to graduate school or complete my degree. I need to thank first and foremost, my husband, Frank, for his unending support and encouragement. I need to thank my children for their patience and both of my parents for their support and time to make all of this possible. I would also like to thank my sister for all the help she has provided.

I would also like to thank my highly supportive and ever-patient advisor Amy Russell for her willingness to take me on as a graduate student, her guidance and encouragement, as well as her sense of humor. I don't know how I could have done half of this without you.

ACKNOWLEDGEMENTS

I would like to acknowledge Mary Karpen and Chris Lawrence of the Chemistry Department at GVSU for all of their support. Their continual assistance and support made it possible to utilize the msvar program on their cluster and run nearly all of the simulations for this study.

I would also like to thank Greg Wolffe of the Computer Science Department at GVSU for his assistance with improving the performance of msvar as well as access to computational time using the resources of the computer science department for some of the lengthier simulations.

Finally, I would like to thank the Kasko Lab at U. C. L. A. for the use of computational tools for additional analyses used in this research.

ABSTRACT

Accurate and unbiased estimates of current effective population size are of primary importance in making informed decisions for conservation purposes. One species of concern, the eastern red bat (*Lasiurus borealis*), is experiencing ongoing population losses due to wind turbine collisions. The proportion of the population being affected is currently unknown, although recent estimates of total fatalities at wind turbines over the time from 2000-2011 are in the hundreds of thousands for this species alone. The roosting habits of eastern red bats make it difficult to monitor their census population size (N_c); thus, genetic estimates of effective population size (N_e) may provide an alternative monitoring tool. Because they mutate rapidly, microsatellite loci are one of the most promising classes of genetic data for monitoring recent changes in effective population size. To test the accuracy of microsatellite-based estimators for monitoring population declines in large populations, simulated microsatellite data sets were created based on eastern red bat population parameters under multiple scenarios of decline. Simulated data sets were then analyzed using coalescent-based msvar analyses, frequency-based *M*-ratio tests, and simple measures of genetic diversity. When parameters estimated using msvar were compared to the known parameters with which data sets were created, it was found that msvar produced precise and unbiased estimates of ancestral effective population size (N_A), but routinely yielded imprecise estimates of current N_e that were typically biased upwards by an order of magnitude or more. *M*-ratios correctly indicated decline in 40.3% of data sets, mostly those simulated under demographic scenarios with a large N_A. θ (= $4N_e\mu$) was calculated using the known parameters, coalescent point estimates, repeat number variance, homozygosity, and mean allele frequencies. Of these, the coalescent estimates of θ were the least accurate when compared to known θ. These results indicate that caution is warranted when using genetic data to

estimate current N_e, particularly for large ($N_e \geq 1000$) populations, and that coalescent-based estimates of N_e may be of little practical utility in monitoring large populations over short timescales.

TABLE OF CONTENTS

LIST OF TABLES

LIST OF FIGURES

INTRODUCTION

Conservation genetics

A primary concern in any conservation effort is accurately estimating and monitoring changes in census population size. Census population size (N_c) is the number of adults in a population within a given area (Luikart *et al*. 2010). Genetic estimates of N_c are a useful alternative when field counts are impractical or unlikely to be accurate (Luikart *et al.* 2010). Methods for estimating N_c from genetic data are similar to traditional capture-mark-recapture (CMR) methods, the difference being that genetic profiles are used as the identification "tag" for individuals. CMR methods of estimating N_c can be performed on open or closed populations and can be designed to accommodate capture rate variability (Seber 1973). Many of these estimates presume that captures, and recaptures if applicable, are random, and produce more reliable estimates if a significant proportion of the population (20% or more) is captured and/or recaptured (Seber 1973, Luikart *et al.* 2010). If populations are large, widespread, or if capture/recapture rates are low, the use of CMR techniques may produce imprecise or inaccurate estimates of N_c.

It is not always possible to accurately estimate the census size for a species from genetic samples, but the effective population size can be estimated. Effective population size (N_e) is the size of a Wright-Fisher population experiencing the same levels of genetic drift or inbreeding as the population being studied (Kimura & Crow 1963). N_e can be used to estimate N_c using the ratio N_e/N_c, if this relationship is known. It is thought that the N_e/N_c ratio is more likely to be predictable for species with reduced fecundity and temporally stable reproductive rates (Luikart *et al.* 2010). Frankham (1995) found that N_e is typically 10-20% of the census size, although there are published N_e/N_c ratios ranging from 0.04 (Bartley *et al.* 1992) to 1.07 (Driscoll 1999)

utilizing data collected in a single season. Additionally, studies have attempted to estimate N_e/N_c ratios from field observations for a population over multiple decades to assess the stability of this ratio (Hauser *et al.* 2002, Ardren & Kapuscinski 2003), and found annual variation due to reproductive success rates and fluctuations in population size (Ardren & Kapuscinski 2003) and selection, selective sweeps, exploitation of populations, and/or genetic drift (Hauser *et al.* 2002).

Methods for estimating a population's current effective size make use of many different aspects of molecular data. Waples & Do (2010) developed a method to estimate current N_e based on linkage disequilibrium in single-sample genetic data, but the authors found this approach to be accurate only for $N_e < 200$. Two other common methods of estimating current N_e from genetic data are based on loss of heterozygosity and change in allele frequencies (Hill 1972, Waples 1989). Both of these methods detect population decline using one summary statistic, such as when N_e is determined using only changes in allele frequency or by comparing the observed heterozygosity to the expected heterozygosity (Luikart *et al.* 2010). Because these methods assess population decline by examining a single aspect of the data, they may not have sufficient power to detect recent population declines (Girod *et al.* 2011). An alternate method of estimating current N_e from genetic data is to use coalescent-based methods (Wakeley 2009, Wakeley & Sargsyan 2009). Using coalescent theory, mutations are situated within genealogies to allow estimation of the time between coalescent events (Kingman 1982, Wakeley 2009). The shape of coalescent genealogies and distribution of coalescence times allows one to infer characteristics such as current effective population size from genetic samples (Hudson 1991, Nielsen & Slatkin 2013).

Estimates of current effective population size can be pertinent to the conservation status of a species. Estimates of N_e can reveal histories of population size change and shed light on the

relative importance of genetic drift or natural selection in a population (Hare *et al.* 2011). N_e can also be used to assess or predict loss of heterozygosity in a population (Allendorf *et al*. 2013). Considering that N_e may be a small proportion of N_c, the genetic variability of breeding individuals is of great importance to the long-term genetic health of a species (Frankham 2005).

Genetics of species in decline

There are several concerns relating to the genetic diversity of a population experiencing a decrease in size. Over time, populations in decline tend to have less genetic diversity and lower heterozygosity (Peery *et al.* 2012). This effect was seen with the Mauritius kestrel, which showed a 57% decrease in heterozygosity after the population declined to fewer than 50 individuals (Groombridge *et al.* 2000). Declining populations also generally see an increase in inbreeding, which can lead to the loss of allelic diversity and the fixation of detrimental alleles (Amos & Balmford 2001). For example, a significant negative correlation between inbreeding coefficient and sperm quality was found in the endangered Iberian lynx (Ruiz-Lopez *et al.* 2012). Both heterozygosity and inbreeding depression are of concern for species survival in conservation biology (Frankham 1995). For any declining population, genetic variation is expected to decrease over time (Nei *et al.* 1975). Therefore, evaluation and monitoring of the genetic variation found within a species could be used as a tool to determine if the population size is decreasing (Cornuet & Luikart 1996, Luikart *et al.* 2010). If estimates of N_e are found to be effective early indicators of population declines then they might be used to monitor species nearing threatened or endangered status before genetic diversity has decreased to dangerously low levels, potentially compromising the ability of a species to adapt to changing conditions (Frankham 2005).

The importance of genetic diversity to fitness and survival has been a matter of debate. Lande (1988) proposed that species generally went extinct due to environmental changes or Allee effects before genetic factors had a significant impact. This has been shown to apply in cases of extreme population declines (Halliday 1980, Stoner & Ray-Culp 2000), but, in general, extrinsic factors are not alone in decreasing the average fitness of a population (Frankham 2005). Fundamentally, it is assumed that a loss of genetic variation within a species contributes to an increase in the risk of extinction (Frankham 1995). A loss of heterozygosity throughout the genome is typically seen in declining populations (Spielman *et al.* 2004b). Such decreases in heterozygosity may impair a species' ability to cope with novel diseases or other changes in their environment (Spielman *et al.* 2004a). Heterozygosity has also been correlated with other factors that affect fitness, such as reproductive success, mate selection, resistance to parasites, and adaptations to local conditions (Ujvari & Belov 2011). Isle Royale wolves exhibited decreased heterozygosity during the decades since their establishment on the island in 1950 (Hedrick *et al.* 2014). A significant increase in the inbreeding coefficient was also observed as the population declined. The crash of this population may be due to inbreeding effects, loss of heterozygosity, extrinsic factors, or some combination of those forces (Hedrick *et al.* 2014).

One mitigating factor that was thought to counteract the effects of inbreeding in declining populations is the purging of deleterious alleles (Lande 1988). Inbreeding has been found to purge some deleterious alleles, but not enough of them are lost to fully compensate for the negative effects of inbreeding (Spielman *et al.* 2004a). Reed *et al.* (2003) documented that populations with higher levels of inbreeding had increased rates of extinction under experimental conditions. Sixty-one percent of inbred *Drosophila* populations went extinct by the sixtieth generation, and extant groups exhibited impaired fitness compared to controls. The negative

impacts of fixing some deleterious alleles were far greater than any benefits incurred from the purging of other deleterious alleles. Additionally, as population census size dwindles, selection acts less effectively against deleterious alleles, which instead may continue to accumulate in surviving generations. This increases the genetic load on the population and can cause an 'extinction vortex' (Amos and Balmford 2001), which is a negative genetic feedback loop that leads inexorably to extinction.

Genetic data have been used in a number of different ways to assess population trends. Using genetic samples with high mutation rates is desirable in detecting recent population decline, as these should be sensitive to more recent changes in population size. There are multiple types of genetic data from which to choose, including mitochondrial DNA sequences, genome-wide single nucleotide polymorphisms (SNPs), and autosomal microsatellite loci. Mitochondrial DNA is a maternally inherited circular chromosome found within mitochondria. Single nucleotide polymorphisms can be found in any type of DNA and refers to variations found at individual base pairs. Microsatellite loci are regions of DNA that consist of short repeating motifs (Pierce 2014). All of these options have been used in analyses of genetic demography (Moritz 1994, Pritchard *et al.* 1999, Schneider & Excoffier 1999, Sunnucks 2000, Marth *et al*. 2004, Gutenkunst *et al*. 2009), but microsatellites have the highest rate of mutation (International SNP Map Working Group 2001, Kumar & Subramanian 2002, Antao *et al*. 2011) and therefore hold the most promise for detecting recent population declines.

Threats to eastern red bats

Currently, many migratory bat species are suffering population losses due to wind turbine collisions (Arnett *et al.* 2008), white nose syndrome (Blehert *et al*. 2009), mine closures (Ellison *et al*. 2003), and habitat fragmentation (Meyer *et al.* 2009). In North America, the three species

most affected by turbine-related mortality are eastern red bats (*Lasiurus borealis)*, hoary bats (*L. cinereus*), and silver-haired bats (*Lasionycteris noctivagans*; Kunz *et al.* 2007). Eastern red bats are tree-roosting bats that migrate in the fall and spring (Harvey *et al.* 2011), roost singly or in small groups in trees, and are mainly active at night (Shump & Shump 1982). This makes estimating population census size through direct counts very difficult because of their widespread, but sparse and unpredictable, distribution throughout the landscape. There have been multiple studies that have estimated the number of eastern red bats killed per year by wind turbines (Johnson *et al.* 2004, Barclay *et al.* 2007, Kunz *et al.* 2007, Cryan & Barclay 2009, Cryan 2011), but it has not been possible to evaluate these losses as a proportion of the population because the total population census size is unknown.

Projections from the U. S. Department of Energy predict continued growth in installed wind capacity, with an observed increase of 8.2% in 2014 and expected increases of 12.9% and 12.0% in 2015 and 2016, respectively (U.S. Energy Information Adminstration 2015). Losses due to wind turbines are also spatially variable, with disproportionately high rates at some locations (Barclay *et al.* 2007). Considering the expected growth in this energy sector, affected bat species are likely to continue experiencing decreases in population size (Cryan 2011). Unfortunately, legal regulations often present difficulties in monitoring affected populations and assessing population trends over large spatial scales. Utility companies operating wind turbines are not uniformly required to enact mitigation measures unless endangered species are being affected. Wildlife mortality data are often considered to be proprietary information of utility companies (Arnett & Baerwald 2013), and reporting requirements for wildlife fatalities varies across states and provinces. For example, the state of Texas, which had the greatest operating

capacity of wind turbines in 2008, has no requirement for utility companies to report bat or bird fatalities (Arnett *et al.* 2008).

In light of these factors, eastern red bats are likely to be of conservation concern in the near future. Although this species is not legally protected, Arnett and Baerwald (2013) calculated that 143,023 to 287,403 eastern red bats were killed by wind turbines between 2000 and 2011 in the United States and Canada. Without an accurate population census size estimate, it is not possible to know what proportion of the total population is represented by these mortality data. A more circumstantial indicator of decline is the tenfold decrease in the number of eastern red bats submitted for rabies testing over a span of nearly four decades (Winhold *et al.* 2008). However, this study was limited to Michigan and does not necessarily reflect eastern red bat losses over their range in eastern North America (Arroyo-Cabrales *et al.* 2008). Overall, available evidence indicates that eastern red bats are experiencing population declines, which suggests that these populations may be subject to the associated genetic effects of decreasing heterozygosity, increasing rates of inbreeding, and lowered adaptability. Considering the difficulties in estimating census population size for this species, genetic monitoring presents an appealing alternative for estimating effective population size and monitoring population decline. Understanding the accuracy and precision of genetic monitoring techniques is essential before applying these estimates to wildlife management decision-making. Through evaluation of simulated datasets, where population parameters are known, it is possible to determine the accuracy and precision of parameter estimates from genetic samples. Because the true parameter values are not known for wild populations, the accuracy and precision of estimates produced from the genetic monitoring of real populations is difficult if not impossible to assess.

In order to test the potential for using microsatellite loci to monitor recent demographic declines in large populations, I simulated microsatellite data based on population parameters from eastern red bats. I then used coalescent (msvar) and frequency-based (*M*-ratio, θ) analyses of the simulated data to assess the accuracy and bias associated with these analytical methods.

MATERIALS AND METHODS

Simulated sample design

In this study, datasets were simulated using ms (Hudson 2002). Simulated data were created in three sampling scenarios. The first sampling scenario constituted 20 diploid individuals and 50 microsatellite loci, similar to what is commonly done in some analyses of genomic data (David *et al.* 2003). The second sampling scenario was created with 50 diploid individuals each genotyped at 10 microsatellite loci, which has been seen commonly in frequentist population genetic studies (Cornuet *et al.* 1999). A third sampling scenario, intended to emulate data that might be collected for phylogeographic analyses, was created with 20 diploid individuals and 10 microsatellite loci (Hunter *et al.* 2012).

For each sampling scenario, data were simulated under a model of exponential decline in a single panmictic population, as is indicated for eastern red bats (Vonhof & Russell 2015). The population history involved a stable ancestral population of a given effective population size (N_A), experiencing a rate of decline (r) for a specified number of generations (t) to a current effective population size (N_e) at the time of sampling (Table 1, Figure 1). Demographic scenarios included ancestral effective population sizes (N_A) of 1,000, 10,000, and 100,000 diploid individuals. For each of these ancestral effective sizes, populations were simulated under rates of decline (r) of -1%, -5%, -10%, and -50% per generation. The time (t) at which the population decline began was specified as 1, 5, 10, 50, and 100 generations in the past. Current effective population sizes (N_e) were calculated from the previous three parameters using the equation:

$$N_e = N_A(1 + r)^t;$$

where N_e is the current effective population size, N_A is the ancestral effective population size, r is the rate of population decline, and t is time in generations (Malthus 1798). Any simulations in

which N_e was less than 10 were discarded and not used for further analyses. The coalescent-scaled rate of decline α was determined as specified by Hudson (2002):

$$\alpha = -\left(\frac{1}{t}\right)\ln\left(\frac{N_e}{N_A}\right)$$

After the data sets were simulated in ms under the infinite sites model, they were converted to microsatellite data using the script ms2ms.pl (Pidugu & Schlötterer 2006).

Mutation rates for microsatellite loci in bats are unknown. For this study, the mutation rate was estimated at $\mu = 1 \times 10^{-3}$ mutations per locus per generation by taking the geometric mean of multiple mutation rates reported for other mammals (Dietrich *et al.* 1992, Edwards *et al.* 1992, Weissenbach *et al.* 1992, Mahtani & Willard 1993, Weber & Wong 1993, Ellegren 1995, Goldstein & Pollock 1997, Brinkmann *et al.* 1998). This mutation rate was used to calculate θ (= $4N_A\mu$) for the data simulations in ms. An average generation time of 5 years was used based on the life history of eastern red bats. The average generation time for eastern red bats is not known, but individuals become sexually mature during their first fall (Cryan *et al.* 2012) and may live as long as 12 years (Harrad & Jackson 1961), so a mean reproductive age of 5 years seemed reasonable.

Coalescent analyses using msvar

Msvar v.1.3 (Storz & Beaumont 2002) was used to obtain coalescent-based estimates of population parameters for each data set. This program utilizes a closed population model in which a population, at some time in the past, had an ancestral effective population size N_A that decreased by rate r for t generations to the current time at which point the effective population size was N_e. For this analysis, all parameters and settings are given on the $\log_{10}$ scale. Msvar also requires hyperpriors for each parameter (N_A, N_e, μ, and t). The hyperpriors are α, the mean of the normal distribution for each variable, σ, the standard deviation of α, β, the mean of the standard

deviation for each variable, and τ, the standard deviation of the standard deviation. I specified hyperpriors for each parameter, N_A, N_e, μ, and t, as follows. For N_A and N_e, α was set to one order of magnitude higher than the known (*i.e.*, simulated) value to allow for greater variation with each simulation and σ was set to 2, in accordance with Storz & Beaumont (2002). For the mutation rate μ, α was equal to the log of the mutation rate and σ was set to 0.5, also as demonstrated by Storz & Beaumont (2002). For t, α was equal to the log of the number of generations since decline with σ set to 2 (Storz & Beaumont 2002), to allow for flexibility in estimating the parameter. For all parameters, β was set to zero, indicating that there was no variation in model parameters amongst loci, and τ was set to 0.5 in accordance with the examples provided with msvar v.1.3 and Storz and Beaumont (2002). MCMC chains were run for a minimum of 2×10^9 steps (or more as needed to reach convergence) and parameter estimates were assessed every 10,000 steps, resulting in 20,000 estimates for each parameter. Each simulated data set was analyzed three times to allow comparisons of runs generated with different starting random numbers.

When each set of three runs were completed for a data set, the runs were checked for convergence with the Gelman-Rubin statistic in R (R Core Team 2014) using the gelman.diag() function in the CODA package (Plummer *et al.* 2006). The first 50% of each chain was discarded as a burn-in, and the Gelman-Rubin statistic was calculated from the second half of the chains to determine whether convergence occurred within a run. Convergence was assessed from the potential scale reduction factor (PSRF), which compares the variability within each chain to the variability between chains. Any runs that did not have a PSRF ≤ 1.1 (Beaumont 1999) were rerun with more steps, some up to 1×10^{10}, to determine if the run would converge within a reasonable time. Analyses with a PSRF ≤ 1.1 were considered to have converged, and were used

to estimate N_A, N_e, μ, and t to compare to the known parameters used to create the data sets. Analyses with a PSRF ≥ 1.1 were considered as not converging and were discarded. After discarding the first half of the data points collected, data from each of the triplicate runs were combined (Okello *et al.* 2008, Bourke & Frantz 2010, Jordan *et al.* 2013) and modes, highest posterior density (HPD) 90% intervals, posterior probability plots, and boxplots for each parameter estimate were constructed using R. These results are referred to as pooled results. Medians were substituted for any variables that yielded more than one mode for the pooled results. Mode and median were both used because they are not as influenced by outliers as the mean would be. All pooled results were observed to have numerous outliers in boxplots.

Frequentist analyses using M-*ratio and* θ

As a population declines, it is initially expected to lose rare alleles and thus decrease the total number of alleles at a locus. Rare alleles tend to be lost at a higher rate than common alleles through genetic drift. Because drift is a random process, it may result in the loss of any allele in the entire range of allele sizes found at a locus. The *M*-ratio (Garza & Williamson 2001) compares the number of alleles to the allelic range using the formula:

$$M = k/r;$$

where k is the total number of alleles and r is the range of allele sizes. While k is affected by the loss of any alleles, r is only affected when the smallest or largest alleles are lost (Garza & Williamson 2001). It is expected that a population that is in decline would lose rare alleles faster than it would decrease the range size of alleles; thus, k would decrease at a faster rate than would r, and M would be smaller in a declining population than in a population at equilibrium.

M-ratios were calculated for each simulated microsatellite data set using M_P_val.app software (Garza & Williamson 2001). The M_C, or critical value, was also determined for each

data set from 10,000 replicate simulations of an equilibrium population based on the known θ (= $4N_e\mu$), number of loci, sample size, size of the largest mutation, and the proportion of multi-step mutations using the Critical_M software (Garza & Williamson 2001). The M_C given for each data set is the minimum of the 95% confidence interval from those simulations; calculated *M*-ratios below this threshold are indicative of populations in decline (Garza & Williamson 2001).

θ is a basic measure of diversity that combines the current effective population size (N_e) with the mutation rate (μ) for a population. So long as the mutation rate remains constant for a population, θ may be used to monitor for changes in the effective population size (Garza & Williamson 2001, Spong *et al.* 2000). θ was calculated multiple ways to determine whether any particular measure showed potential as a proxy for monitoring changes in population size. θ was determined using the equation:

$$\theta = 4N_e\mu \qquad \text{(Kimura 1968)}$$

This was done first using the known parameters for each data set and is shown as θ. θ_{col} was calculated using the modes of N_e and μ from the msvar output for each scenario for any run that demonstrated convergence. θ was also calculated directly from the simulated microsatellite data using three different methods in the Pegas package in R (Paradis 2010). The theta.msat(x) function in this package calculated θ based on the repeat number variance (θ_v; Kimmel *et al.* 1998), expected homozygosity (θ_h; Kimmel *et al.* 1998), and mean allele frequencies (θ_x; Haasl & Payseur 2010).

RESULTS

Msvar estimates

In nearly all analyses, the ancestral effective population size (N_A) was estimated very accurately and precisely using msvar (Figures 2-11). Posterior distributions for this parameter were characterized by a single mode close to the known parameter value, with relatively little error; an example is shown in Figure 2. Across all pooled results in the 50 loci and 20 individuals sampling scenario, the same level of precision is observed across varying rates of decline and with varying time of decline. In demographic scenarios with N_A = 1000, point estimates range between 3.01 - 3.29 compared to a known log(N_A) = 3.00 (Table 2, Figure 3). Similar levels of accuracy are achieved in estimating larger ancestral effective population sizes of 10,000 (Table 3, Figure 4) and 100,000 (Table 4, Figure 5). Point estimates of N_A range between 4.01 – 4.27 (known log(N_A) = 4.00) when N_A is 10,000 and between 5.03 - 5.21 (known log(N_A) = 5.00) when N_A is 100,000.

Estimates of N_A from other sampling scenarios yielded results that were similarly accurate and precise. Pooled results with a sampling scenario of 50 individuals and 10 loci provided a range of N_A estimates of 2.96 - 3.29 for a known log(N_A) = 3.00 (Table 5, Figure 6). For demographic scenarios with larger N_A, parameter estimates produced in msvar ranged between 3.89 - 4.22 (known log(N_A) = 4.00; Table 6, Figure 7) and between 4.90 - 5.26 (known log(N_A) = 5.00; Table 7, Figure 8). For the sampling scenario with 20 individuals, 10 loci, and an ancestral effective population size of 1000, similar results were seen for N_A estimates (Table 8, Figure 9), with log(N_A) ranging from 2.91 – 3.46 (known log(N_A) = 3.00). Simulations with N_A = 10,000 produced estimates ranging from 3.92 – 4.41 (known log(N_A) = 4.00; Table 9, Figure 10), and those with N_A = 100,000 ranged from 4.89 – 5.19 (known = 5.00; Table 10, Figure 11).

Ancestral effective population size estimates are both accurate and precise when compared to the known value (Figure 3). This accuracy is consistent regardless of the time since decline, rate of decline, or initial effective population size (N_A, Figures 3-5). Sampling scenarios with 20 individuals and 50 loci and those with 50 individuals and 10 loci also demonstrate similarly accurate estimates of N_A (Figures 4 and 7). Less accuracy is seen with a less intense sampling effort (20 individuals and 10 loci, Figures 9-11).

This level of precision and accuracy was not seen in estimates of current effective population size (N_e). Multiple examples demonstrate the range of patterns seen in N_e estimates (Figure 12A-D). More than half of the simulated data sets yielded posterior probability plots for N_e similar to Figure 12A, with imprecise and inaccurate estimation of the known. Some analyses showed considerable variation in estimates of N_e among individual runs (*e.g.,* Figure 12B). Some analyses (*e.g.,* Figure 12C) showed improved precision over those exemplified in Figure 12A, but lacked accuracy in estimating N_e. A small number of simulations accurately and precisely estimated N_e, with little inter-run variation (*e.g.,* Figure 12D). In simulations with 20 individuals, 50 loci, and $N_A = 1000$, nine of the fourteen converging pooled results were ±0.5 orders of magnitude or more from the known (Table 2, Figure 13). Five of the pooled results produced point estimates that were more precise, deviating between 0.024 orders of magnitude less and 0.453 orders of magnitude more than the known. For demographic scenarios of $N_A = 10{,}000$ (Table 3, Figure 14), N_e was overestimated by half an order of magnitude or more in twelve of fifteen simulations, with point estimates deviating between 0.727 orders of magnitude and 2.056 orders of magnitude greater than the known. Three simulations produced point estimates that were more precise, deviating by only 0.229 orders of magnitude less to 0.311 orders of magnitude more than the known. Only three simulations converged from the demographic

scenario with N_A = 100,000 (Table 4, Figure 15). All three overestimated the current effective population size, with point estimates of this parameter deviating between 0.704 – 1.537 orders of magnitude greater than the known.

Results from the 50 individuals and 10 loci sampling scenario were similar. In the demographic scenario that had an N_A = 1000, pooled results from seven of fourteen simulations overestimated the current effective population size by a half of an order of magnitude or more, with point estimates deviating between 0.503 – 1.732 orders of magnitude greater than the known N_e (Table 5, Figure 16). The remaining seven pooled results were more precise, with point estimates deviating by 0.084 orders of magnitude less to 0.374 orders of magnitude greater than the known. In the demographic scenario with an N_A of 10,000 (Table 6, Figure 17), N_e was overestimated by half of an order of magnitude or more in pooled results from fifteen of seventeen simulations; estimates deviated between 0.664 – 3.401 orders of magnitude greater than the known value for N_e. Pooled results from the simulations modeling -1% decline over 100 generations (estimate = 3.730, known log(N_e) = 3.566) and -10% decline over 1 generation (estimate = 4.090, known log(N_e) = 3.957) were more precise than other simulations within this sampling scenario. Only nine simulations converged for the demographic scenario with N_A = 100,000 (Table 7, Figure 18). The current effective population size was overestimated by half of an order of magnitude or more (deviation of 0.933 – 1.888 orders of magnitude greater than the known) for seven of nine simulated data sets. Pooled results from two data sets (-1% decline over 50 generations and -5% decline over 100 generations) yielded more precise estimates of N_e (estimate = 5.270, known log(N_e) = 4.783; estimate = 2.860, known log(N_e) =2.829; respectively) than other simulations in this sampling scenario.

Pooled results from the 20 individuals and 10 loci sampling scenario yielded levels of precision in estimating N_e comparable to the previous two sampling scenarios. In nine of fourteen demographic scenarios with N_A = 1000, point estimates of N_e deviated from the known by half of an order of magnitude or more (0.644 less than to 1.686 orders of magnitude greater than the known, Table 8, Figure 19). Data sets from the five remaining scenarios produced estimates that deviated between 0.061 less than to 0.367 orders of magnitude greater than the known value of N_e. Point estimates of N_e overestimated the known in fourteen of seventeen demographic scenarios with an ancestral effective population size of 10,000, with estimates deviating between 0.582 and 2.056 orders of magnitude greater than the known value for N_e (Table 9, Figure 20). Three pooled results yielded better precision in estimating N_e, with point estimates deviating between 0.459 less than to 0.389 orders of magnitude greater than the known. N_e was overestimated in eleven of fifteen data sets simulated under a demographic scenario with N_A = 100,000, with the point estimate deviating between 0.542-1.976 orders of magnitude greater than the known N_e (Table 10, Figure 21). Point estimates of N_e from the remaining four data sets deviated from the known by 0.178 less than to 0.447 orders of magnitude greater than the known. Across all sampling scenarios and demographic scenarios, of the pooled results producing estimates within a half an order of magnitude of the known, most (28 of 32) data sets were simulated under conditions of population decline lasting for 50-100 generations and/or with a rate of decline of -1% or -5%.

Although N_e was not accurately estimated, there were some general trends that were demonstrated by the boxplots. For most analyses, the known value fell within the second quartile of the posterior distribution (*e.g.*, Figure 13A), and the point estimate was typically greater than the known. Demographic scenarios with smaller N_A (= 1000, Figure 16) yielded estimates that

were more accurate rather than those with a larger N_A (= 10,000, Figure 17; = 100,000, Figure 18), with the known typically falling within the second quartile for scenarios with N_A = 1000. Results from sampling scenarios with 20 individuals and 50 loci were fairly similar to those with 50 individuals and 10 loci as shown in Figure 13B and 16B, where simulations at 1, 5, and 10 generations produce broad and imprecise estimates of N_e and simulations at 50 generations actually underestimate the known N_e. Simulation results for the 20 individuals and 50 loci and the 50 individuals and 10 loci sampling scenarios each also had knowns that were narrowly outside of the second quartile (13A, C, D, 16B, D). Both of these sampling scenarios produced more accurate results than the 20 individuals and 10 loci sampling scenario (Figure 19) where the known is not within the second quartile in multiple simulations, and there were two estimates that have second quartiles far removed from the known (Figure 19A at 10 generations; 19D at 5 generations). The sampling scenario with 20 individuals and 50 loci did have two simulations (Figure 13A at 100 generations, 13B at 50 generations) that precisely estimated the known N_e, whereas the sampling scenario with 50 individuals and 10 loci only had one scenario precisely estimating N_e (Figure 16B at 50 generations). The sampling scenario with 20 individuals and 10 loci (Figure 19) did not have any precise estimates of N_e, indicative of the effects of both the number of individuals and the number of loci sampled on resolution power.

Additionally, estimates of current effective population size tended to lose precision over time, with notable deviations between the point estimate and known at 50 or 100 generations of decline (*e.g.*, Figure 17B, C, D). Of all data sets tested, only 32 of 119 (26.9%) estimated the current effective population size within half an order of magnitude and 16 of those 32 occurred at the most extreme number of generations (t) of decline: at -1% decline for 50 or 100 generations, -5% decline for 50 or 100 generations, or -10% decline for 50 generations (Tables 2, 3, 5-10).

Nine data sets (Tables 2, 3, 5, 8, 9, 10) actually underestimated the known N_e. Seven of the nine underestimates were also seen at the most extreme number of generations (*t)* of decline: at 50 or 100 generations since decline, and at -1%, -5% or -10% rate of decline. Most (7 of 9) of these data sets were characterized by few alleles per locus, as would be expected after many generations of strong genetic drift. One hundred and ten of 119 data sets (92.4%) provided point estimates of N_e that were greater than N_A for the given scenario, yielding a false signal of population growth rather than decline. Additionally, posterior probability plots (Figure 12) and 90% HPD intervals are indicative of the lack of precision for N_e estimates (Tables 2-10). For example, with a known $\log(N_e) = 3.00$, the 90% HPD typically ranged between 1 to 7 (= 10 to 10 million, Table 2). In summary, the imprecision of N_e point estimates indicates they should be viewed as an unreliable measure for short-term population monitoring. In addition, N_e point estimates were consistently biased upward from the known across pooled results, regardless of sampling scenario or demographic scenario.

Msvar accurately and precisely estimated the known mutation rate, $\log(10^{-3}) = -3.00$. This result was observed in nearly all simulations performed. Posterior density curves illustrate unimodal distributions with modes very close to the known value and little deviation between runs (Figure 22). No changes in precision were observed from differing scenarios, regardless of the ancestral effective population size, number of microsatellite loci sampled, or the number of individuals sampled. All pooled results from the 50 loci and 20 individual sampling scenario produced estimates of μ that were within 0.3 orders of magnitude or less of the known (Tables 2-4, Figures 23-25). The 50 individual and 10 loci sampling scenario similarly estimated μ within 0.4 orders of magnitude of the known (Tables 5-7, Figures 26-28). All pooled results from the 20

individuals and 10 loci sampling scenario produced estimates of μ that were within 0.3 orders of magnitude of the known (Tables 8-10, Figures 29-31).

Estimates of μ are precise but do tend to underestimate the known (*e.g.*, Figure 23). Estimates from sampling scenarios of 20 individuals and 50 loci and those with 50 individuals and 10 loci show this pattern (*e.g.*, Figures 24 and 27). The sampling scenario with 20 individuals and 10 loci (Figures 29-31) yielded results that were slightly less accurate than the other sampling scenarios. Additionally, mutation rate estimates did not vary in precision or accuracy across demographic scenarios with N_A = 1000, N_A = 10,000, or N_A = 100,000 (Figures 26-28).

Estimates of the time since decline (t) are less reliable than those seen for the mutation rate. Posterior probability plots illustrate large margins of error (*e.g.,* Figures 32A, B), significant deviation from the known value (*e.g.,* Figure 32C), and considerable variation among replicate runs (*e.g.,* Figure 32D). Results from the sampling scenario with 50 loci and 20 individuals yielded point estimates that deviated from 1.539 orders of magnitude less to 1.781 orders of magnitude more than the known (Tables 2-4, Figures 33-35). Pooled results from sixteen of 32 data sets in this sampling scenario are within ±0.5 orders of magnitude of the known. Estimates of time since decline from data sets simulated under the sampling scenario with 10 loci and 50 individuals were similarly variable, with point estimates between 1.799 orders of magnitude less than to 2.470 orders of magnitude more than the known (Tables 5-7, Figures 36-38). Twenty-six of the forty data sets simulated under this sampling scenario produced estimates of t that were within ±0.5 orders of magnitude of the known. Estimates of t from the 20 individual and 10 loci sampling scheme deviated by 1.740 orders of magnitude less than to 1.910 orders of magnitude

more than the known (Tables 8-10, Figures 39-41), with eighteen data sets yielding estimates more than 0.5 orders of magnitude different than the known.

Estimates of generations since decline are imprecise. Of all the sampling scenarios, estimates from pooled results with 50 individuals and 10 loci were the most consistent among runs and generally underestimated the known generations (Figures 36-38). Data sets with 20 individuals and 50 loci generally yielded underestimates of time since decline, particularly with more recent declines (1-10 generations, Figures 33-35). Results from the sampling scenario with 20 individuals and 10 loci are comparable (Figures 39-41). Modifications to the demographic scenario (N_A = 1000, N_A = 10,000, or N_A = 100,000; Figures 36-38) did not result in improved accuracy or precision in estimating *t*.

M-*ratio calculations*

M-ratios and critical *M* values (M_C) were determined for all simulated data sets. In accordance with Garza & Williamson (2001), M_C values were simulated based on the sample size, number of loci, and mutation model; calculated *M*-ratio values less than the M_C indicate a significant population decline. In sampling scenarios with 20 individuals and 10 loci, decline was indicated for 14 out of 48 (=29.2%; 2 out of 14 data sets for N_A = 1,000; 6 out of 17 data sets for N_A = 10,000; 6 out of 17 data sets for N_A = 100,000; Table 11) of the simulated data sets. Improving sampling by increasing the number of individuals genotyped (50 individuals and 10 loci) had little effect on the power of this analysis, with *M*-ratios demonstrating decline in 15 out of 48 (=31.3%; 3 out of 14 data sets for N_A = 1,000; 4 out of 17 data sets for N_A = 10,000; 8 out of 17 data sets for N_A = 100,000; Table 12) simulated data sets. However, increasing the number of loci examined (20 individuals and 50 loci) markedly improved statistical power, with *M*-ratios indicating decline in 29 out of 48 (= 60.4%; 6 out of 14 data sets for N_A = 1,000; 10 out of 17

data sets for N_A = 10,000; 13 out of 17 data sets for N_A = 100,000; Table 13) simulated data sets. Overall, 58 of 144 (=40.3%) simulated data sets indicated decline using the *M*-ratio bottleneck test. Of those data sets that did indicate decline, 51 of 58 (=87.9%) were simulated under conditions of -10% or -50% rate of decline and/or 50 or 100 generations of decline.

θ *calculations*

The θ values calculated for each scenario did not demonstrate accuracy or precision throughout all simulated data sets or pooled results. θ_{col} was determined using msvar estimate modes (or in some cases medians) for N_e and μ. θ_{col} was roughly an order of magnitude greater than the known θ for 70 out of 119 (58.8%) of the pooled results (Tables 14-22), and was generally the estimate of θ that was most divergent from the known. Estimates of θ_v, θ_h, and θ_x were determined using repeat number variance, expected homozygosity, and allele frequency means, respectively. These simple summary statistics provided more accurate estimates of the known θ. Among these θ estimates, θ_v typically provided the most accurate estimate of the true θ in demographic scenarios with lower rates of decline (-1% to -5%) and more recent times since the onset of decline (up to 10 generations), whereas θ_x provided more accurate estimates for more extreme scenarios of decline (Tables 14-22). θ_h was generally less accurate than either θ_v or θ_x, with a few exceptions. Sampling scenarios with 50 individuals and 20 loci demonstrated this pattern the most consistently through all three demographic scenarios (N_A = 1000, 10,000, and 100,000; Tables 14-16). Sampling scenarios with 20 individuals and 10 loci did also demonstrate this pattern across demographic scenarios, but with less consistency (Tables 17-19). Sampling scenarios with 50 individuals and 10 loci lacked a consistent pattern for the demographic scenario with N_A = 1000 (Table 20). For example, when N_A = 1000, the most precise estimator of θ was still either θ_v or θ_x, but θ_v was most accurate in some sampling scenarios with high rates of

decline (-50% decline, 1 generations; Table 20) and θ_x was in some cases most accurate in sampling scenarios with low rates of decline (-1% decline, 5 generations; Table 20). In a few cases (1 generation, at -1%, -5%, and -10% decline; Table 20), θ_h most accurately estimated the known θ. Demographic scenarios where N_A = 10,000 (Table 21) or N_A = 100,000 (Table 22) did generally demonstrate better accuracy from θ_v at lower rates of decline over less time and from θ_x at higher rates of decline and/or generations, as seen in previous sampling scenarios.

DISCUSSION

Msvar analyses

My results indicate that msvar is an unbiased estimator of the N_A and μ parameters, but it provides imprecise and often inaccurate estimates of the N_e and t parameters. The accuracy (N_A) and precision (N_A, μ) observed with sampling scenarios with 20 individuals and 50 loci and those with 50 individuals and 10 loci, as compared to those with 20 individuals and 10 loci, indicate that more intense sampling, whether by increasing the number of individuals or number of loci, provides improved statistical power for estimating these population parameters using msvar.

Girod *et al.* (2011) simulated microsatellite data sets with the same ancestral effective population sizes of 1000, 10,000, and 100,000, under similar rates of decline (approximately -0.5% to -50%), and similar timescales (10-500 generations) using msvar. These authors found that their estimates of all parameters were imprecise and inaccurate. Here, I also found that estimates of time and the current effective population size lacked accuracy, but ancestral effective population size and mutation rate were both consistently estimated with accuracy and precision by msvar.

There were some noteworthy differences in the construction of the two studies that may account for these discrepancies. Girod *et al.* (2011) simulated five different data sets for each demographic scenario, estimated parameters from each data set only once, and found that parameter estimates from these data sets were notably different from each other. This approach confounds stochasticity in the coalescent process simulating the data sets with that in the analysis of the data in msvar. Genealogies for single populations can be analyzed to estimate population parameters, taking into account stochastic effects on a population, but the technique used by Girod *et al.* (2011) is analogous to taking samples from five different populations and expecting

them all to produce accurate and precise estimates of population characteristics as if they represented the same population. My study had one simulated data set for each demographic scenario, which was analyzed in triplicate in msvar. Thus, my results better assess the precision, accuracy, and bias inherent to msvar alone.

Girod *et al.* (2011) also permitted broader initial variation of all parameters in msvar in order to test the ability of the program to estimate parameters from uninformative priors. Mutation rate was estimated accurately and precisely in my study, generally within 0.5 orders of magnitude of the known. Girod *et al*. (2011) found much less precision in estimating mutation rate. This may be attributable to a difference in priors. Girod *et al.* (2011) set mutation rate priors very broadly, with a mean of -4 (known was -3) and a standard deviation of 2. I set mutation rate priors more narrowly, as is common in many empirical publications (Okello *et al.* 2008, Bourke & Frantz 2010, Rotheray *et al.* 2012), with a prior of -3 (known was -3) and a standard deviation of 0.5. When each parameter is estimated by msvar, the other parameters are permitted to vary within the bounds set by the user (pers. comm., M. Beaumont). Storz and Beaumont (2002) recommended a general strategy of having broad priors for N_e and N_A but priors that were more informative for the mutation rate, and stated that the N_e, N_A, and t parameters are strongly dependent on the prior for μ. Analyses by Storz and Beaumont (2002) were consistent with Girod *et al.* (2011) in finding that broad priors would produce results dependent on variation in the mutation rate.

M-*ratio tests*

M-ratios less than the M_C value were detected for 58 of 144 data sets, signifying that the *M*-ratio accurately detected population decline in 40.3% of the simulations (Tables 11-13). Two *M*-ratios indicating decline were too close to the M_C value to definitively indicate decline (-5%

decline from an N_A = 1000 for 1 generation, and -1% decline from an N_A = 100,000 for 1 generation, Table 13). Apart from these two results, nearly all (51 of 56) remaining significant *M*-ratios were detected at higher rates of decline (-10% or -50%) and/or longer time intervals (50 or 100 generations). Sampling scenarios with 20 individuals and 10 loci indicated population decline in only 29.2% of data sets (Table 11). Sampling scenarios with 50 individuals and 10 loci had similar power, with *M*-ratios indicating decline in 31.3% of data sets (Table 12). However, sampling scenarios with 20 individuals and 50 loci showed much greater power, with population decline indicated in 56.3% of data sets (Table 13). Compared to a minimal sampling scheme of 20 individuals and 10 loci, increasing the number of loci had a much greater impact on the power of the *M*-ratio test than increasing the number of individuals. The greatest rate of successful identification of population decline was seen with a sampling scenario of 20 individuals and 50 microsatellite loci and a demographic scenario of N_A = 100,000, with *M*-ratios correctly indicating decline for 70.6% of simulated data sets. Although Garza and Williamson (2001) predicted that *M*-ratios would be sensitive to population decline only after 100 generations, very high rates of decline (-50%) were detectable in as little as a single generation under an optimal sampling scenario (20 individuals and 50 loci). There are a small number of data sets that were expected to show significant signals of decline and did not (Table 11, N_A = 1000, 5 gen. and -50%, 10 gen. and -10%; Table 12, N_A = 1000, 10 gen. and -10%, N_A = 100,000, 10 gen. and -10%) as sampling scenarios of fewer generations since decline or rates of decline did indicate population decline. This may be attributable to the stochastic nature of allele loss in declining populations. Alleles, including rare alleles, are presumed to be lost randomly from a declining population. By chance, rare alleles may or may not be lost as a population declines and if too few

rare alleles are lost as a population declines, this could negatively affect the sensitivity of the *M*-ratio to detect population decline.

Significant signals of population decline were seen most frequently (51.0% of data sets) in demographic scenarios with N_A = 100,000. For data sets with N_A = 10,000, population decline was detected in 39.2% of data sets and for data sets with N_A = 1000, population decline was detectable in only 23.8% of data sets, indicating greater sensitivity when the ancestral population sizes are large. Population genetic theory predicts that a larger population will possess more rare alleles than a smaller population. As the *M*-ratio is dependent on the loss of rare alleles, this test is more powerful in demographic scenarios with larger N_A values. This is consistent with other studies that have found that *M*-ratios detect population declines more reliably where there are larger ancestral effective population sizes, as compared to populations with smaller ancestral effective sizes (Kuo & Janzen 2004, Hoban *et al.* 2014).

Diversity estimates

I assessed whether various measures of the genetic diversity parameter θ could serve as meaningful proxies for monitoring population declines. θ_{col} was roughly an order of magnitude greater than the known θ for 70 out of 119 data sets, or 58.8% of the simulations (Tables 14-22). θ_{col} (= $4N_e\mu$) was calculated using msvar point estimates for N_e and μ. The summary statistics θ_v, θ_h, and θ_x were determined using the repeat number variance, expected homozygosity, and allele frequency means, respectively; these estimates were much more similar to the known θ. θ_v typically provided the most accurate estimates of the true θ in less extreme scenarios of decline (-1% decline over 1-10 generations), while θ_x provided more accurate estimates for more extreme rates of decline (-50% decline over 1-10 generations; Table 15). θ_x is expected to reflect declines, especially strong declines, because it is calculated from allele frequencies and thus

should reflect the loss of rare alleles as a population declines (Williamson-Natesan 2005), but has been observed to be downward biased when the true θ is greater than 50 (Haasl & Payseur 2010). The true, or known, θ for the demographic scenarios in this study were $\theta = 4$, 40, and 400, so it is likely that θ_x would produce downward biased estimates of the known θ, particularly when N_A = 10,000 or 100,000. This may provide an explanation for the lack of precision seen for θ_x as compared to other methods of calculating θ. θ_v is determined from changes in the number of repeats observed and would be expected, like allele frequencies, to decrease as a population declines and alleles are lost. Like Haasl & Payseur (2010), I found that θ_h provided overestimates of θ, regardless of the sampling or demographic scenario. Considering the poor estimates of θ produced by msvar parameter estimates, use of the scaled parameter θ derived from msvar could not be recommended.

Implications for conservation

The analyses conducted here indicate that genetic monitoring alone would not be a reliable method of estimating the current effective population size of eastern red bats. While there is circumstantial evidence for a decline in the eastern red bat population (Winhold *et al.* 2008), accurate census estimates are not available. Mortality due to wind turbines has been estimated (Arnett & Baerwald 2013), but the proportion of the populations being killed at wind turbines is still unknown. Current effective population size was recently estimated for eastern red bats (Vonhof & Russell 2015), but estimates of current effective population size are not available for other migrating bat species. Because N_e/N_c for eastern red bats is also unknown, this ratio cannot be used to evaluate the impact of wind turbine mortalities on this species. Additionally, eastern red bats may face an increased risk of extinction due to its migratory behavior (Arnett & Baerwald 2013). Impacts of climate change and habitat fragmentation further increase this risk

(Jones & Rebelo 2013). Additional research is needed in determining what method is most efficacious in estimating a census population size for eastern red bats to monitor population impacts as well as the effectiveness of any mitigation measures designed to curtail wind turbine mortalities.

Eastern red bats have been found to have a single panmictic population (Vonhof & Russell 2015), so any mortalities from wind turbines would not be disproportionately impacting some subpopulations over others. It is generally expected that migratory species do not have structured populations (Moussy *et al.* 2013). While a similar pattern of panmixia has been found for migratory Mexican free-tailed bats (*Tadarida brasiliensis*, Russell *et al.* 2005), not all migratory bat species are necessarily panmictic. Another migratory species, eastern pipistrelles (*Perimyotis subflavus*), has been found to have sex-biased dispersal, with significant structure among females but not males (Martin 2014).

Arnett and Baerwald (2013) estimated wind turbine mortalities from 2000 to 2011 in the U. S. and Canada to be between 143,023 – 287,403 for eastern red bats, 26,004 – 52,255 for the big brown bat (*Eptesicus fuscus*), 247,040 – 633,822 for the hoary bat (*Lasiurus cinereus*), 148,839 – 308,322 for the silver-haired bat (*Lasionycteris noctivagans*), 51,617 – 106,925 for the little brown bat (*Myotis lucifugus*), 45,260 – 93,756 for *P. subflavus*, and 21,282 – 44,087 for *T. brasiliensis*. Significant gaps do exist in our knowledge of population size and population structure for many bat species including some of those listed above, and these gaps impair our ability to assess the effects of turbine-related mortalities on bat populations. This could include potential disproportionate impacts to subpopulations suffering wind turbine mortalities at higher rates than other subpopulations.

Climate change, habitat fragmentation, and other anthropogenic disturbances have negative impacts on bat species (Jones *et al*. 2009). Many bat mortalities are caused by changes to the physical environment in which bats fly, such as the construction of roads through bat foraging routes (Russell *et al.* 2009) or nesting sites (Lesiński 2008). Noise pollution also impacts bats and may interfere with their ability to use echolocation (Simmons *et al.* 2004). The greater mouse eared bat (*M. myotis*) has been found to avoid highways when seeking prey; it is thought that noise from highway traffic interferes with passive listening for insect prey (Siemers & Schaub 2011). In fact, sound-emitting interference has demonstrated some success as a method of deterring bats from wind turbines (Horn *et al.* 2008, Arnett *et al.* 2013). Some bat species are also suffering devastating losses due to white nose syndrome (Coleman & Reichard 2014). Under these combined pressures, multiple bat species are facing extinction threats. *Myotis septentrionalis* was listed as a threatened species in April 2015, primarily because of white nose syndrome, although other impacts included in the listing are wind turbine collisions and climate change (U.S. Fish and Wildlife Service 2015). To address the many negative impacts facing bat species, better quality data on population size, structure, and losses are needed.

Population census size or current effective population size is commonly estimated as a means of genetically monitoring species (Nei & Tajima 1981, Waples 1989, Hare *et al.* 2011). For many species of conservation interest, there are significant barriers to obtaining an accurate census estimate. When populations are widely dispersed across terrestrial or aquatic systems, it can impede accurate census estimates. The use of current effective population size estimates becomes important for conservation monitoring of populations potentially in decline. Coalescent estimates of N_e are thought to be more reliable than other methods of estimating N_e (Luikart *et al*. 2010). My study indicates that, even with specific knowledge of the mutation rate, estimates of

current N_e using msvar are not reliable and routinely overestimate this parameter. Results from msvar produced estimates with very broad 90% HPD intervals spanning, in some cases, up to six orders of magnitude. The large amount of error associated with estimates of N_e also made it difficult to detect significant population declines (*i.e.*, N_e significantly less than N_A for a given simulation) using msvar. Only a few simulated data sets, typically involving decline over 50 or 100 generations, gave a significant signal of decline. Therefore, coalescent-based estimates of current N_e alone should not be used for conservation decisions. Msvar estimates of N_e from simulations with ancestral effective population sizes of 1000 had slightly more precise modes, but still had HPD 90% intervals so broad (from 10 to 10,000,000 for $N_A = 1000$) as to be meaningless. Consequently N_e estimates from msvar were not demonstrably reliable at any of the population sizes tested in this study. Further simulations are needed to determine whether msvar estimates of N_e demonstrate improved accuracy or precision over short timescales if N_A is less than 1000.

Current effective population size, or N_e, is defined as the size of a theoretical population at Wright-Fisher equilibrium that experiences the same rate of genetic drift as the study population. The populations modeled in this study do violate one assumption of a Wright-Fisher equilibrium population in that populations were simulated to be declining in size and therefore not at equilibrium. However, coalescent analyses of populations have been demonstrated to be robust even if violations of the Wright-Fisher population model do occur (Kingman 1982, Möhle 1998). If real data were to be used it would also be necessary to consider additional violations of Wright-Fisher equilibrium, as follows. Eastern red bats are a panmictic population (Vonhof & Russell 2015), meeting the expectation of a single closed population, but it is unlikely that mating is completely random for a species with a range from Canada to northern Mexico

(Arroyo-Cabrales *et al.* 2008). Additionally, it is likely that eastern red bats do have overlapping generations (Cryan *et al.* 2012), further violating the assumptions of a Wright-Fisher equilibrium population. Lastly, the Wright-Fisher model of an equilibrium population also presumes a haploid hermaphroditic population, neither of which is true of eastern red bats. These additional violations for a real population would not be likely to affect the quality of coalescent estimates of populations (Hein *et al.* 2004), so long as the sample size was significantly smaller than the total population size (Fu 2006).

To improve coalescent-based estimates of N_e, it would be important to improve computational capacity to analyze larger data sets with greater speed. Some analyses in this study required only a few hours to run, but many required weeks or months of computational time on a ten-node cluster. I intended to explore demographic scenarios with an N_A of 1,000,000 and sampling scenarios including 100 loci. Neither of these scenarios would run on msvar using the ten-node computer cluster used for the other data sets in this study. Msvar is not designed to handle such large data sets. Alternative computational approaches, such as approximate Bayesian computation, while requiring less computational power, are also less sensitive to detecting past population parameters (Beaumont *et al.* 2002). Both computational capacity and more efficient software would be necessary to take full advantage of the data potentially available from NextGen sequencing, and may provide a more reliable method to assess short-term declines of large populations.

M-ratios are more reliable indicators of population declines, particularly over long periods of time or with rates of decline of -10% or more. Additionally, *M*-ratios demonstrated higher rates of detecting population decline when N_A was large (= 10,000 or 100,000), as it would be expected for these populations to have greater numbers of rare alleles to lose.

Populations with a small N_A (= 1000) would likely have fewer rare alleles and be less sensitive to detecting population decline using *M*-ratios. However, this statistic has limited power to detect lower rates of decline over shorter time frames. *M*- ratios also require knowledge of θ, the estimation of which may involve considerable error.

M-ratios may provide a useful monitoring tool for other migratory species likely to have large ancestral effective population sizes. Some migratory species of conservation concern include scalloped hammerhead sharks (Baum *et al.* 2003), green sea turtles (Jackson *et al.* 2001), and caribou (Vors & Boyce 2009). Like eastern red bats, accurately estimating N_c or N_e for many aquatic and terrestrial migratory species can be problematic. In order to assess impacts to widely dispersed migratory species, it is necessary to monitor species throughout their range (Vonhof and Russell 2015), and *M*-ratios could potentially provide a simple and effective means of monitoring population declines for species with historically large ancestral effective population sizes.

SNPs may be an alternative genetic marker for detecting population bottlenecks, but would require the use of highly polymorphic sites (Morin *et al.* 2004). However, the sole use of highly polymorphic SNP data can potentially cause ascertainment bias in data sets (Morin *et al.* 2012). Mitochondrial DNA has been used for long term conservation planning and identification of evolutionarily significant units (Moritz 1994), but more recently has been determined to potentially provide an incomplete assessment of a species' conservation priority (Rubinoff 2006) and may produce overestimates of current effective population size when compared to N_e estimates from microsatellite loci (Qiu *et al.* 2013). Hypervariable microsatellite loci with mutation rates of 10^{-2} could also be used to monitor N_e and have been found in multiple species including humans (Itsara *et al.* 2010) and birds (Anmarkrud *et al.* 2011). Their use would require

knowledge of locus-specific mutation rates for each species being studied, so that more quickly mutating loci could be identified and analyzed appropriately. Their mutation rate may also be influenced by multiple factors including environmental conditions, sex, or chromosomal location (Anmarkrud *et al.* 2011), and the effects of these factors on accurate N_e estimation are not known. Detailed knowledge of their mutation characteristics would be needed for accurate estimates of N_e from hypervariable microsatellite loci. As indicated by the results of this study and that of Storz and Beaumont (2002), knowledge of mutation rates is essential to estimating any other parameters using coalescent methods such as msvar. Other possibilities that could be pursued in future research would be estimating N_e using large numbers of microsatellite loci, 100 or more. *M*-ratios demonstrated greater sensitivity in this study in sampling scenarios with greater numbers of loci. Felsenstein (2006) also determined that maximizing the number of loci produced better assessments of genetic parameters in coalescent analyses than maximizing the number of individuals. NextGen sequencing has the capacity to provide researchers with data from hundreds of microsatellite loci (Tucker *et al.* 2009). In order to take advantage of the wealth of knowledge available from these data sets, it will be vital for computational capacity to improve.

Table 1. Data simulated for this study were created in three sampling scenarios, one with 20 individuals and 50 microsatellite loci, one with 50 individuals and 10 microsatellite loci, and one with 20 individuals and 10 microsatellite loci. For each sampling scenario, each of the following demographic scenarios was simulated for analysis, resulting in a total of 48 demographic scenarios per sampling scenario:

N_A	r	t
1000	-1% decline	1 generation
	-1% decline	5 generations
	-1% decline	10 generations
	-1% decline	50 generations
	-1% decline	100 generations
	-5% decline	1 generation
	-5% decline	5 generations
	-5% decline	10 generations
	-5% decline	50 generations
	-10% decline	1 generation
	-10% decline	5 generations
	-10% decline	10 generations
	-50% decline	1 generation
	-50% decline	5 generations
10,000	-1% decline	1 generation
	-1% decline	5 generations
	-1% decline	10 generations
	-1% decline	50 generations
	-1% decline	100 generations
	-5% decline	1 generation
	-5% decline	5 generations
	-5% decline	10 generations
	-5% decline	50 generations
	-5% decline	100 generations
	-10% decline	1 generation
	-10% decline	5 generations
	-10% decline	10 generations
	-10% decline	50 generations
	-50% decline	1 generation
	-50% decline	5 generations
	-50% decline	10 generations
100,000	-1% decline	1 generation
	-1% decline	5 generations
	-1% decline	10 generations
	-1% decline	50 generations
	-1% decline	100 generations
	-5% decline	1 generation
	-5% decline	5 generations

	-5% decline	10 generations
	-5% decline	50 generations
	-5% decline	100 generations
	-10% decline	1 generation
	-10% decline	5 generations
	-10% decline	10 generations
	-10% decline	50 generations
	-50% decline	1 generation
	-50% decline	5 generations
	-50% decline	10 generations

Table 2. Msvar results showing known vs. estimated parameters for data sets with N_A =1000, 50 microsatellite loci, and 20 individuals, percent decline noted. Estimates are reported as the mode (or *median*) of the posterior distribution with the 90% highest posterior density. All known and estimated parameter values are given on the $\log_{10}$ scale.

time	N_e		N_A		μ		t	
	known	estimate	known	estimate	known	estimate	known	estimate
-1%								
1 gen	2.996	3.92 (1.32, 6.88)	3.00	3.16 (2.23, 3.84)	-3.00	-3.17 (-3.95, -2.37)	0.00	-0.02 (-3.19, 2.56)
5 gen	2.978	3.18 (1.19, 6.95)	3.00	3.29 (2.33, 3.92)	-3.00	-3.14 (-3.94, -2.37)	0.70	-0.78 (-3.11, 2.26)
10 gen	2.957	3.41 (1.08, 7.16)	3.00	3.27 (2.35, 3.94)	-3.00	-3.25 (-3.97, -2.39)	1.00	-0.41 (-3.31, 1.91)
50 gen	2.783	3.15 (1.61, 6.84)	3.00	3.16 (2.29, 4.09)	-3.00	-3.12 (-3.99, -2.41)	1.70	0.16 (-3.18, 3.61)
100 gen	2.566	2.5 (0.49, 4.02)	3.00	3.25 (2.33, 4.02)	-3.00	-3.29 (-3.98, -2.41)	2.00	2.60 (-0.39, 4.60)
-5%								
1 gen	2.978	3.93 (1.12, 7.16)	3.00	3.07 (2.37, 3.96)	-3.00	-3.06 (-3.94, -2.36)	0.00	-0.55 (-3.22, 2.28)
5 gen	2.891	3.60 (1.16, 6.94)	3.00	3.01 (2.29, 3.91)	-3.00	-3.17 (-3.96, -2.39)	0.70	0.37 (-2.98, 2.36)
10 gen	2.783	3.15 (1.81, 6.75)	3.00	3.2 (2.20, 4.38)	-3.00	-3.12 (-3.90, -2.32)	1.00	1.00 (-2.01, 5.95)
50 gen	1.914	1.89 (0.1, 2.76)	3.00	3.08 (2.33, 3.86)	-3.00	-3.24 (-4.01, -2.49)	1.70	2.70 (0.89, 3.53)
-10%								
1 gen	2.957	4.42 (1.46, 7.33)	3.00	3.14 (2.33, 3.93)	-3.00	-3.09 (-3.96, -2.38)	0.00	-0.08 (-3.30, 2.17)
5 gen	2.783	3.86 (1.62, 6.88)	3.00	3.24 (2.31, 4.02)	-3.00	-3.22 (-3.94, -2.37)	0.70	-0.03 (-3.36, 3.42)
10 gen	2.566	3.15 (1.07, 7.00)	3.00	3.24 (2.35, 4.01)	-3.00	-3.20 (-4.00, -2.42)	1.00	*0.25* (-2.88, 2.39)
-50%								
1 gen	2.783	4.16 (1.30, 7.40)	3.00	3.26 (2.33, 3.93)	-3.00	-3.16 (-3.96, -2.38)	0.00	*-0.58* (-3.40, 1.88)
5 gen	1.914	*2.53* (-0.27, 6.01)	3.00	3.11 (2.41, 4.02)	-3.00	-3.29 (-4.02, -2.44)	0.70	1.16 (-2.03, 3.07)

Table 3. Msvar results showing known vs. estimated parameters for data sets with N_A =10,000, 50 microsatellite loci, and 20 individuals, percent decline noted. Estimates are reported as the mode (or *median*) of the posterior distribution with the 90% highest posterior density. All known and estimated parameter values are given on the $\log_{10}$ scale.

time	N_e		N_A		μ		t	
	known	estimate	known	estimate	known	estimate	known	estimate
-1%								
1 gen	3.996	3.89 (2.14, 8.15)	4.00	4.08 (3.31, 4.92)	-3.00	-3.08 (-3.96, -2.37)	0.00	0.12 (-3.51, 2.16)
5 gen	3.978	4.86 (2.40, 8.13)	4.00	4.23 (3.33, 4.92)	-3.00	-3.19 (-3.94, -2.37)	0.70	0.47 (-2.58, 2.82)
10 gen	3.957	5.27 (2.46, 8.10)	4.00	4.08 (3.33, 4.92)	-3.00	-3.23 (-3.94, -2.37)	1.00	0.35 (-2.59, 2.96)
50 gen	3.783	5.15 (2.87, 8.04)	4.00	4.16 (3.29, 4.92)	-3.00	-3.33 (-3.94, -2.37)	1.70	1.80 (-1.88, 3.24)
100 gen	3.566	5.19 (2.59, 7.83)	4.00	4.11 (3.27, 4.88)	-3.00	-3.34 (-3.97, -2.41)	2.000	1.12 (-1.79, 3.13)
-5%								
1 gen	3.978	5.45 (2.25, 8.20)	4.00	4.19 (3.31, 4.89)	-3.00	-3.20 (-3.94, -2.36)	0.00	-0.14 (-3.17, 2.19)
5 gen	3.891	*5.15* (1.97, 7.99)	4.00	4.05 (3.31, 4.89)	-3.00	-3.03 (-3.90, -2.33)	0.70	*0.31* (-2.52, 2.94)
10 gen	3.783	4.51 (2.40, 7.81)	4.00	4.13 (3.35, 4.96)	-3.00	-3.20 (-3.93, -2.35)	1.00	*0.54* (-2.46, 3.21)
100 gen	1.829	1.6 (0.89, 2.47)	4.00	4.27 (3.43, 4.97)	-3.00	-3.12 (-4.02, -2.52)	2.00	3.18 (2.50, 4.09)
-10%								
1 gen	3.957	4.89 (2.24, 8.11)	4.00	4.13 (3.33, 4.92)	-3.00	-3.20 (-3.94, -2.35)	0.00	-0.35 (-3.06, 2.62)
5 gen	3.783	4.76 (2.24, 8.00)	4.00	4.07 (3.35, 4.92)	-3.00	-3.00 (-3.92, -2.36)	0.70	0.26 (-2.45, 2.88)
10 gen	3.566	4.97 (2.49, 8.23)	4.00	4.01 (3.31, 4.88)	-3.00	-3.26 (-3.93, -2.38)	1.00	0.34 (-2.41, 2.76)
50 gen	1.829	2.14 (1.45, 3.01)	4.00	4.15 (3.35, 4.88)	-3.00	-3.15 (-3.98, -2.47)	1.70	3.48 (2.70, 4.27)
-50%								
1 gen	3.783	5.25 (2.36, 8.04)	4.00	4.20 (3.33, 4.92)	-3.00	*-3.12* (-3.96, -2.38)	0.00	-0.55 (-3.06, 2.92)
5 gen	2.914	*4.97* (2.32, 8.17)	4.00	4.17 (3.33, 4.92)	-3.00	-3.27 (-3.94, -2.37)	0.70	0.38 (-2.60, 2.48)

Table 4. Msvar results showing known vs. estimated parameters for data sets with N_A =100,000, 50 microsatellite loci, and 20 individuals, percent decline noted. Estimates are reported as the mode (or *median*) of the posterior distribution with the 90% highest posterior density. All known and estimated parameter values are given on the $\log_{10}$ scale.

time	N_e		N_A		μ		t	
	known	estimate	known	estimate	known	estimate	known	estimate
-1%								
1 gen	4.996	5.7 (3.09, 9.36)	5.00	5.21 (4.22, 5.82)	-3.00	-3.20 (-3.95, -2.35)	0.00	-0.79 (-3.17, 2.57)
5 gen	4.978	5.70 (3.22, 9.12)	5.00	5.17 (4.28, 5.85)	-3.00	-3.23 (-3.91, -2.35)	0.70	*0.29* (-2.54, 2.95)
50 gen	4.783	6.32 (3.38, 9.12)	5.00	5.03 (4.25, 5.84)	-3.00	-3.27 (-3.94, -2.37)	1.70	0.84 (-1.79, 3.06)

Table 5. Msvar results showing known vs. estimated parameters for data sets with N_A =1000, 10 microsatellite loci, and 50 individuals, percent decline noted. Estimates are reported as the mode (or *median*) of the posterior distribution with the 90% highest posterior density. All known and estimated parameter values are given on the $\log_{10}$ scale.

	N_e		N_A		μ		t	
time	known	estimate	known	estimate	known	estimate	known	estimate
-1%								
1 gen	2.996	3.66 (1.20, 7.18)	3.00	2.96 (2.27, 3.89)	-3.00	-3.02 (-3.93, -2.37)	0.00	-0.91 (-3.37, 2.20)
5 gen	2.978	3.14 (1.27, 7.06)	3.00	3.29 (2.36, 4.06)	-3.00	-3.09 (-3.96, -2.38)	0.70	-0.17 (-3.08, 2.89)
10 gen	2.957	*3.46* (0.82, 6.81)	3.00	3.15 (2.31, 3.98)	-3.00	-3.19 (-3.94, -2.37)	1.00	0.62 (-2.78, 3.19)
50 gen	2.783	2.75 (0.78, 6.68)	3.00	2.98 (2.09, 4.04)	-3.00	-3.23 (-4.02, -2.44)	1.70	0.91 (-2.38, 4.97)
100 gen	2.566	2.94 (0.94, 6.44)	3.00	3.09 (1.99, 4.16)	-3.00	-3.28 (-4.00, -2.41)	2.00	0.92 (-1.73, 5.87)
-5%								
1 gen	2.978	4.71 (1.62, 7.53)	3.00	3.04 (2.16, 3.82)	-3.00	-3.14 (-3.94, -2.35)	0.00	1.82 (-2.98, 2.90)
5 gen	2.891	3.03 (1.10, 7.27)	3.00	3.14 (2.37, 4.05)	-3.00	-3.14 (-3.96, -2.38)	0.70	0.18 (-3.02, 2.69)
10 gen	2.783	3.43 (1.36, 7.02)	3.00	3.15 (2.27, 4.02)	-3.00	-2.99 (-3.91, -2.33)	1.00	1.01 (-3.11, 3.50)
50 gen	1.914	1.83 (-0.10, 2.69)	3.00	3.21 (2.40, 4.18)	-3.00	-3.36 (-4.01, -2.47)	1.70	2.29 (0.93, 4.09)
-10%								
1 gen	2.957	3.87 (1.16, 7.30)	3.00	3.13 (2.22, 3.87)	-3.00	-3.11 (-3.98, -2.40)	0.00	-0.87 (-3.42, 2.33)
5 gen	2.783	3.07 (0.91, 6.90)	3.00	3.13 (2.18, 3.88)	-3.00	-3.23 (-3.94, -2.36)	0.70	0.47 (-3.03, 3.01)
10 gen	2.566	2.61 (0.53, 6.81)	3.00	3.03 (2.24, 3.95)	-3.00	-3.18 (-4.00, -2.44)	1.00	0.69 (-2.69, 3.07)
-50%								
1 gen	2.783	3.67 (1.08, 7.11)	3.00	3.14 (2.24, 3.89)	-3.00	-3.10 (-3.94, -2.36)	0.00	-0.10 (-3.33, 2.17)
5 gen	1.914	2.85 (0.70, 6.78)	3.00	3.08 (2.14, 3.84)	-3.00	-3.16 (-4.00, -2.42)	0.70	0.45 (-3.14, 2.86)

Table 6. Msvar results showing known vs. estimated parameters for data sets with N_A =10,000, 10 microsatellite loci, and 50 individuals, percent decline noted. Estimates are reported as the mode (or *median*) of the posterior distribution with the 90% highest posterior density. All known and estimated parameter values are given on the $\log_{10}$ scale.

	N_e		N_A		μ		t	
time	known	estimate	known	estimate	known	estimate	known	estimate
-1%								
1 gen	3.996	4.66 (2.47, 8.34)	4.00	3.99 (3.23, 4.85)	-3.00	-3.05 (-3.90, -2.33)	0.00	*0.23* (-2.98, 3.46)
5 gen	3.978	4.93 (3.15, 8.29)	4.00	4.12 (3.22, 4.84)	-3.00	-2.94 (-3.79, -2.23)	0.70	2.48 (-1.77, 4.02)
10 gen	3.957	5.06 (2.64, 8.36)	4.00	4.06 (3.29, 4.93)	-3.00	-3.00 (-3.92, -2.33)	1.00	2.21 (-2.33, 3.16)
50 gen	3.783	4.74 (2.81, 8.23)	4.00	4.02 (3.29, 5.02)	-3.00	-3.0 (-3.94, -2.36)	1.70	2.03 (-2.07, 4.14)
100 gen	3.566	3.73 (1.65, 7.60)	4.00	4.10 (3.35, 5.01)	-3.00	-3.20 (-4.02, -2.45)	2.000	0.99 (-1.86, 3.86)
-5%								
1 gen	3.978	5.19 (2.56, 8.39)	4.00	4.11 (3.30, 4.94)	-3.00	-3.12 (-3.88, -2.29)	0.00	-0.38 (-2.87, 3.03)
5 gen	3.891	4.80 (2.22, 8.36)	4.00	4.18 (3.35, 4.95)	-3.00	-3.16 (-3.96, -2.38)	0.70	0.80 (-2.61, 2.57)
10 gen	3.783	4.91 (2.30, 8.04)	4.00	4.08 (3.31, 4.92)	-3.00	-3.01 (-3.99, -2.41)	1.00	0.45 (-2.42, 3.09)
50 gen	2.914	3.87 (2.47, 8.27)	4.00	4.10 (3.31, 4.96)	-3.00	-3.12 (-3.96, -2.39)	1.70	1.04 (-2.29, 3.11)
100 gen	1.829	4.08 (2.45, 8.00)	4.00	4.22 (3.29, 5.01)	-3.00	-3.14 (-4.00, -2.43)	2.000	1.14 (-2.51, 3.54)
-10%								
1 gen	3.957	4.09 (1.86, 8.10)	4.00	4.22 (3.33, 4.93)	-3.00	-3.29 (-3.93, -2.36)	0.00	*-0.31* (-3.26, 2.30)
5 gen	3.783	4.99 (2.23, 8.20)	4.00	3.97 (3.26, 4.89)	-3.00	-3.18 (-4.00, -2.40)	0.70	1.06 (-2.55, 2.97)
10 gen	3.566	5.74 (2.89, 8.28)	4.00	3.89 (3.16, 4.80)	-3.00	-3.17 (-3.90, -2.33)	1.00	2.52 (-1.87, 3.67)
50 gen	1.829	4.07 (1.69, 7.80)	4.00	4.17 (3.39, 5.05)	-3.00	-3.13 (-3.96, -2.39)	1.70	1.48 (-2.05, 3.35)
-50%								
1 gen	3.783	5.41 (2.79, 8.76)	4.00	3.99 (3.29, 4.96)	-3.00	-2.97 (-3.88, -2.27)	0.00	2.47 (-2.87, 3.54)
5 gen	2.914	4.29 (1.90, 8.03)	4.00	4.04 (3.33, 4.93)	-3.00	-3.15 (-3.95, -2.39)	0.70	0.80 (-2.59, 2.66)
10 gen	1.829	*5.23* (2.40, 8.08)	4.00	3.94 (3.31, 4.93)	-3.00	-3.04 (-3.96, -2.39)	1.00	1.27 (-2.53, 3.00)

Table 7. Msvar results showing known vs. estimated parameters for data sets with N_A =100,000, 10 microsatellite loci, and 50 individuals, percent decline noted. Estimates are reported as the mode (or *median*) of the posterior distribution with the 90% highest posterior density. All known and estimated parameter values are given on the $\log_{10}$ scale.

	N_e		N_A		μ		t	
time	known	estimate	known	estimate	known	estimate	known	estimate
-1%								
50 gen	4.783	5.27 (3.57, 9.03)	5.00	4.90 (4.19, 5.81)	-3.00	-3.16 (-3.94, -2.38)	1.70	1.41 (-1.67, 4.51)
-5%								
1 gen	4.978	*6.06* (3.05, 9.25)	5.00	4.98 (4.15, 5.75)	-3.00	-3.01 (-3.96, -2.37)	0.00	-0.29 (-3.17, 2.36)
5 gen	4.891	*6.05* (3.14, 9.18)	5.00	5.03 (4.19, 5.76)	-3.00	-3.03 (-3.94, -2.38)	0.70	0.72 (-2.61, 2.64)
10 gen	4.783	6.67 (3.42, 9.31)	5.00	5.09 (4.19, 5.80)	-3.00	-3.16 (-3.90, -2.31)	1.00	1.34 (-2.17, 3.39)
100 gen	2.829	2.86 (2.00, 3.59)	5.00	5.26 (4.37, 5.89)	-3.00	-3.17 (-3.99, -2.49)	2.000	3.46 (2.62, 4.21)
-10%								
1 gen	4.957	6.32 (2.95, 9.20)	5.00	5.08 (4.18, 5.78)	-3.00	-3.14 (-3.94, -2.35)	0.00	0.14 (-3.11, 2.75)
5 gen	4.783	5.74 (3.20, 9.18)	5.00	5.05 (4.24, 5.83)	-3.00	-3.20 (-3.97, -2.39)	0.70	0.69 (-2.42, 3.09)
10 gen	4.566	5.50 (3.22, 9.39)	5.00	4.96 (4.19, 5.78)	-3.00	-3.18 (-3.98, -2.41)	1.00	0.79 (-2.33, 2.88)
-50%								
1 gen	4.783	6.12 (3.26, 9.20)	5.00	4.96 (4.08, 5.72)	-3.00	-2.93 (-3.87, -2.28)	0.00	0.45 (-2.90, 4.31)

Table 8. Msvar results showing known vs. estimated parameters for data sets with N_A =1000, 10 microsatellite loci, and 20 individuals, percent decline noted. Estimates are reported as the mode (or *median*) of the posterior distribution with the 90% highest posterior density. All known and estimated parameter values are given on the $\log_{10}$ scale.

	N_e		N_A		μ		t	
time	known	estimate	known	estimate	known	estimate	known	estimate
-1%								
1 gen	2.996	3.75 (1.35, 7.22)	3.00	3.02 (2.16, 3.84)	-3.00	-2.99 (-3.90, -2.33)	0.00	1.00 (-3.17, 2.77)
5 gen	2.978	3.1 (1.30, 7.17)	3.00	3.17 (2.40, 4.06)	-3.00	-3.25 (-4.00, -2.41)	0.70	-0.03 (-2.84, 2.70)
10 gen	2.957	4.26 (2.29, 8.45)	3.00	2.94 (1.96, 3.80)	-3.00	-2.98 (-3.82, -2.24)	1.00	2.57 (-1.42, 4.04)
50 gen	2.783	2.81 (1.11, 6.83)	3.00	3.22 (2.24, 4.14)	-3.00	-3.27 (-3.96, -2.37)	1.70	0.89 (-2.19, 5.10)
100 gen	2.566	2.81 (1.35, 6.72)	3.00	2.91 (1.77, 4.06)	-3.00	-3.32 (-3.96, -2.38)	2.000	1.27 (-1.81, 5.55)
-5%								
1 gen	2.978	*4.02* (0.91, 7.00)	3.00	3.21 (2.39, 4.02)	-3.00	-3.19 (-3.94, -2.37)	0.00	-0.38 (-3.28, 2.43)
5 gen	2.891	2.83 (1.06, 7.14)	3.00	3.31 (2.41, 4.07)	-3.00	-3.14 (-3.93, -2.36)	0.70	0.81 (-2.92, 2.81)
10 gen	2.783	3.15 (1.36, 7.09)	3.00	3.19 (2.07, 3.86)	-3.00	-3.20 (-3.95, -2.37)	1.00	*0.55* (-2.92, 3.24)
50 gen	1.914	1.27 (-0.59, 2.45)	3.00	3.46 (2.60, 4.27)	-3.00	-3.19 (-4.06, -2.52)	1.70	2.32 (0.68, 3.53)
-10%								
1 gen	2.957	4.43 (1.53, 7.42)	3.00	3.16 (2.35, 4.01)	-3.00	-3.18 (-3.88, -2.29)	0.00	*-0.10* (-3.1, 2.73)
5 gen	2.783	3.34 (0.98, 6.99)	3.00	3.29 (2.29, 4.02)	-3.00	-3.03 (-3.97, -2.37)	0.70	0.53 (-3.17, 2.96)
10 gen	2.566	3.43 (1.09, 7.07)	3.00	2.99 (2.22, 4.02)	-3.00	-3.2 (-3.97, -2.39)	1.00	*0.55* (-2.96, 3.31)
-50%								
1 gen	2.783	3.45 (0.93, 7.02)	3.00	3.21 (2.37, 4.02)	-3.00	-3.23 (-3.96, -2.38)	0.00	-0.04 (-3.29, 2.49)
5 gen	1.914	3.60 (1.16, 7.12)	3.00	2.91 (2.00, 3.73)	-3.00	-3.21 (-3.96, -2.39)	0.70	0.26 (-2.96, 2.86)

Table 9. Msvar results showing known vs. estimated parameters for data sets with N_A =10,000, 10 microsatellite loci, and 20 individuals, percent decline noted. Estimates are reported as the mode (or *median*) of the posterior distribution with the 90% highest posterior density. All known and estimated parameter values are given on the $\log_{10}$ scale.

time	N_e		N_A		μ		t	
	known	estimate	known	estimate	known	estimate	known	estimate
-1%								
1 gen	3.996	*5.41* (2.22, 8.51)	4.00	4.20 (3.33, 5.00)	-3.00	-3.07 (-3.90, -2.29)	0.00	0.44 (-2.86, 3.65)
5 gen	3.978	4.56 (2.47, 8.29)	4.00	4.31 (3.40, 5.02)	-3.00	-3.13 (-3.93, -2.35)	0.70	*0.38* (-2.68, 3.26)
10 gen	3.957	5.18 (2.32, 8.11)	4.00	4.20 (3.41, 5.05)	-3.00	*-3.12* (-3.90, -2.33)	1.00	0.01 (-2.42, 3.40)
50 gen	3.783	*4.96* (2.32, 8.07)	4.00	4.30 (3.38, 5.05)	-3.00	-3.03 (-3.97, -2.39)	1.70	1.61 (-2.07, 3.58)
100 gen	3.566	3.52 (1.39, 7.47)	4.00	4.41 (3.42, 5.10)	-3.00	-3.22 (-3.98, -2.41)	2.00	1.02 (-1.69, 3.89)
-5%								
1 gen	3.978	*4.97* (1.91, 8.15)	4.00	4.18 (3.24, 4.85)	-3.00	-3.04 (-3.95, -2.37)	0.00	-0.49 (-3.27, 2.34)
5 gen	3.891	4.28 (1.90, 8.03)	4.00	4.08 (3.28, 4.89)	-3.00	*-3.14* (-3.96, -2.39)	0.70	0.76 (-2.68, 2.90)
10 gen	3.783	*4.81* (1.78, 8.49)	4.00	4.25 (3.33, 4.97)	-3.00	-3.10 (-3.98, -2.41)	1.00	0.68 (-2.57, 2.84)
50 gen	2.914	4.94 (2.98, 8.49)	4.00	4.10 (3.13, 4.81)	-3.00	-3.19 (-3.88, -2.31)	1.70	2.22 (-1.49, 3.96)
100 gen	1.829	2.46 (0.76, 3.27)	4.00	4.39 (3.54, 5.13)	-3.00	-3.18 (-4.01, -2.49)	2.000	2.91 (1.54, 3.92)
-10%								
1 gen	3.957	4.95 (2.22, 8.17)	4.00	3.92 (3.10, 4.80)	-3.00	-3.00 (-3.92, -2.33)	0.00	-0.07 (-3.32, 3.31)
5 gen	3.783	4.66 (2.18, 8.12)	4.00	4.10 (3.25, 4.89)	-3.00	-3.11 (-3.96, -2.37)	0.70	0.15 (-2.65, 2.90)
10 gen	3.566	5.42 (2.29, 8.28)	4.00	4.03 (3.27, 4.88)	-3.00	-3.17 (-3.98, -2.41)	1.00	*0.51* (-2.60, 2.97)
50 gen	1.829	1.37 (-0.08, 2.59)	4.00	4.13 (3.33, 5.02)	-3.00	-3.22 (-4.06, -2.54)	1.70	2.96 (1.44, 4.02)
-50%								
1 gen	3.783	4.62 (2.12, 8.18)	4.00	4.07 (3.35, 5.01)	-3.00	-3.1 (-3.94, -2.36)	0.00	-0.02 (-3.34, 3.35)
5 gen	2.914	4.97 (2.14, 8.20)	4.00	4.18 (3.30, 4.91)	-3.00	-3.19 (-3.93, -2.35)	0.70	0.86 (-2.59, 2.96)
10 gen	1.829	*2.52* (1.02, 3.77)	4.00	4.17 (3.35, 4.93)	-3.00	-3.09 (-3.97, -2.43)	1.00	2.91 (1.29, 4.26)

Table 10. Msvar results showing known vs. estimated parameters for data sets with N_A =100,000, 10 microsatellite loci, and 20 individuals, percent decline noted. Estimates are reported as the mode (or *median*) of the posterior distribution with the 90% highest posterior density. All known and estimated parameter values are given on the $\log_{10}$ scale.

time	N_e		N_A		μ		t	
	known	mode	known	mode	known	mode	known	mode
-1%								
1 gen	4.996	5.57 (3.06, 9.27)	5.00	5.08 (4.23, 5.83)	-3.00	-3.01 (-3.98, -2.38)	0.00	-0.25 (-3.26, 2.86)
5 gen	4.978	4.80 (2.90, 9.27)	5.00	5.03 (4.28, 5.89)	-3.00	-3.26 (-3.99, -2.39)	0.70	0.94 (-2.53, 2.87)
10 gen	4.957	*6.09* (3.14, 9.20)	5.00	5.14 (4.24, 5.83)	-3.00	-3.08 (-3.96, -2.39)	1.00	0.5 (-2.28, 3.15)
50 gen	4.783	6.61 (3.32, 9.16)	5.00	5.04 (4.07, 5.74)	-3.00	-3.16 (-3.92, -2.36)	1.70	2.13 (-1.58, 4.47)
100 gen	4.566	5.57 (3.29, 9.19)	5.00	4.96 (4.24, 5.85)	-3.00	-3.17 (-3.93, -2.37)	2.000	*1.27* (-1.61, 3.62)
-5%								
1 gen	4.978	5.52 (3.01, 9.27)	5.00	5.09 (4.24, 5.83)	-3.00	-2.97 (-3.94, -2.36)	0.00	0.15 (-3.27, 2.73)
5 gen	4.891	*6.11* (3.36, 9.23)	5.00	5.19 (4.24, 5.84)	-3.00	-3.05 (-3.92, -2.34)	0.70	0.60 (-2.66, 3.88)
10 gen	4.783	5.21 (3.23, 9.25)	5.00	5.10 (4.20, 5.81)	-3.00	-3.14 (-3.96, -2.37)	1.00	0.66 (-2.29, 3.28)
50 gen	3.914	5.56 (3.23, 9.12)	5.00	5.01 (4.24, 5.85)	-3.00	-3.01 (-3.92, -2.34)	1.70	1.18 (-1.67, 3.60)
-10%								
1 gen	4.957	*5.96* (2.83, 9.10)	5.00	5.14 (4.16, 5.75)	-3.00	-2.95 (-3.94, -2.37)	0.00	0.35 (-3.29, 3.30)
5 gen	4.783	5.23 (3.06, 9.11)	5.00	4.89 (4.24, 5.83)	-3.00	-3.11 (-3.96, -2.38)	0.70	0.29 (-2.61, 3.11)
10 gen	4.566	5.57 (3.30, 9.29)	5.00	5.13 (4.22, 5.81)	-3.00	-3.25 (-3.97, -2.39)	1.00	0.59 (-2.18, 3.36)
50 gen	2.829	2.93 (1.08, 3.86)	5.00	5.08 (4.32, 5.87)	-3.00	*-3.26* (-4.02, -2.49)	1.70	2.93 (1.43, 4.02)
-50%								
1 gen	4.783	5.72 (3.07, 9.28)	5.00	5.12 (4.15, 5.77)	-3.00	-3.04 (-3.96, -2.36)	0.00	-0.27 (-3.18, 3.05)
5 gen	3.914	5.89 (3.27, 9.23)	5.00	5.04 (4.19, 5.81)	-3.00	-3.04 (-3.94, -2.35)	0.70	*0.65* (-2.50, 3.88)

Table 11. *M*-ratios and critical *M* values (presented as estimated *M*-ratio, M_C) for all simulations listed for 20 individuals, 10 microsatellite loci. N_A is noted for each set. *M*-ratios that are lower than M_C, indicating population decline, are highlighted in grey.

	% decline			
N_A = 1000	-1%	-5%	-10%	-50%
1 gen.	0.948, 0.853	0.949, 0.854	0.941, 0.865	0.968, 0.879
5 gen.	0.935, 0.853	0.897, 0.865	0.851, 0.878	0.975, 0.950
10 gen.	0.967, 0.857	0.936, 0.878	0.969, 0.900	
50 gen.	0.898, 0.879	0.743, 0.950		
100 gen.	0.975, 0.903			
	% decline			
N_A = 10,000	-1%	-5%	-10%	-50%
1 gen.	0.804, 0.641	0.807, 0.644	0.851, 0.651	0.848, 0.697
5 gen.	0.818, 0.643	0.779, 0.669	0.770, 0.696	0.804, 0.864
10 gen.	0.778, 0.650	0.828, 0.695	0.746, 0.748	0.699, 0.954
50 gen.	0.743, 0.696	0.788, 0.862	0.600, 0.954	
100 gen.	0.774, 0.748	0.612, 0.984		
	% decline			
N_A = 100,000	-1%	-5%	-10%	-50%
1 gen.	0.575, 0.341	0.491, 0.344	0.529, 0.351	0.594, 0.401
5 gen.	0.424, 0.346	0.482, 0.370	0.465, 0.402	0.555, 0.663
10 gen.	0.476, 0.351	0.523, 0.401	0.466, 0.467	0.472, 0.873
50 gen.	0.558, 0.401	0.485, 0.663	0.516, 0.873	
100 gen.	0.524, 0.468	0.373, 0.874		

Table 12. *M*-ratios and critical *M* values (presented as estimated *M*-ratio, M_C) for all simulations listed for 50 individuals, 10 microsatellite loci. N_A is noted for each set. *M*-ratios that are lower than M_C, indicating population decline, are highlighted in grey.

	% decline			
N_A = 1000	-1%	-5%	-10%	-50%
1 gen.	0.924, 0.896	1.000, 0.898	0.986, 0.899	0.986, 0.910
5 gen.	0.988, 0.898	0.946, 0.904	0.917, 0.909	0.930, 0.950
10 gen.	0.921, 0.899	0.875, 0.909	0.957, 0.920	
50 gen.	0.983, 0.908	0.795, 0.988		
100 gen.	0.967, 0.922			
	% decline			
N_A = 10,000	-1%	-5%	-10%	-50%
1 gen.	0.969, 0.806	0.844, 0.809	0.836, 0.811	0.928, 0.830
5 gen.	0.882, 0.808	0.836, 0.819	0.882, 0.828	0.875, 0.902
10 gen.	0.835, 0.813	0.890, 0.829	0.853, 0.849	0.858, 0.950
50 gen.	0.926, 0.830	0.915, 0.901	0.837, 0.950	
100 gen.	0.854, 0.850	0.869, 0.950		
	% decline			
N_A = 100,000	-1%	-5%	-10%	-50%
1 gen.	0.734, 0.637	0.703, 0.641	0.548, 0.644	0.741, 0.682
5 gen.	0.640, 0.639	0.767, 0.658	0.664, 0.682	0.806, 0.815
10 gen.	0.746, 0.645	0.618, 0.681	0.757, 0.723	0.625, 0.906
50 gen.	0.719, 0.682	0.657, 0.815	0.548, 0.906	
100 gen.	0.725, 0.721	0.356, 0.907		

Table 13. *M*-ratios and critical *M* values (presented as estimated *M*-ratio, M_C) for all simulations listed for 20 individuals, 50 microsatellite loci. N_A is noted for each set. *M*-ratios that are lower than M_C, indicating population decline, are highlighted in grey.

	% decline			
N_A = 1000	-1%	-5%	-10%	-50%
1 gen	0.938, 0.903	0.904, 0.905	0.942, 0.907	0.901, 0.920
5 gen	1.099, 0.905	0.922, 0.912	0.949, 0.921	0.907, 0.967
10 gen	0.936, 0.906	0.928, 0.921	0.934, 0.936	
50 gen	0.942, 0.921	0.900, 0.968		
100 gen	0.928, 0.936			
	% decline			
N_A = 10,000	-1%	-5%	-10%	-50%
1 gen.	0.765, 0.763	0.851, 0.766	0.811, 0.770	0.796, 0.803
5 gen.	0.813, 0.766	0.799, 0.783	0.799, 0.803	0.775, 0.910
10 gen.	0.781, 0.771	0.793, 0.838	0.790, 0.837	0.661, 0.970
50 gen.	0.830, 0.803	0.773, 0.910	0.564, 0.970	
100 gen.	0.813, 0.837	0.536, 0.970		
	% decline			
N_A = 100,000	-1%	-5%	-10%	-50%
1 gen.	0.530, 0.531	0.504, 0.504	0.544, 0.510	0.513, 0.562
5 gen.	0.784, 0.505	0.484, 0.530	0.539, 0.563	0.514, 0.778
10 gen.	0.713, 0.510	0.527, 0.562	0.493, 0.626	0.500, 0.917
50 gen.	0.504, 0.562	0.563, 0.779	0.404, 0.917	
100 gen.	0.522, 0.626	0.410, 0.945		

Table 14. θ calculations for each data set for the 50 microsatellite loci & 20 individuals sampling scenario. N_A = 1000, θ_A = 4, generations, and percent decline noted for each scenario. $\theta = 4N_e\mu$ was calculated from 'known' parameters, $\theta_{col} = 4N_e\mu$ was calculated from msvar point estimates, θ_v was determined using the repeat number variance, θ_h was determined using expected homozygosity, and θ_x was determined using mean allele frequencies.

	θ	θ_{col}	θ_v	θ_h	θ_x
-1%					
1 gen.	3.960	22.494	3.534	5.266	1.796
5 gen.	3.805	4.386	3.716	6.177	2.219
10 gen.	3.619	5.782	4.070	6.015	2.281
50 gen.	2.426	4.286	3.546	7.007	2.391
100 gen.	1.472	0.649	4.223	5.742	1.714
-5%					
1 gen.	3.805	29.652	4.664	6.175	2.216
5 gen.	3.115	10.766	4.031	6.270	2.046
10 gen.	2.426	4.286	8.404	6.459	2.150
50 gen.	0.328	0.179	2.273	2.927	0.851
-10%					
1 gen.	3.619	85.518	4.440	6.528	2.151
5 gen.	2.426	17.461	3.810	6.168	2.350
10 gen.	1.472	3.565	5.028	6.450	2.230
-50%					
1 gen.	2.426	40.000	5.812	6.507	2.192
5 gen.	0.328	0.695	4.053	5.953	1.914

Table 15. θ calculations for each data set for the 50 microsatellite loci & 20 individuals sampling scenario. N_A = 10,000, θ_A = 40, generations, and percent decline noted for each scenario. $\theta = 4N_e\mu$ was calculated from 'known' parameters, $\theta_{col} = 4N_e\mu$ was calculated from msvar point estimates, θ_v was determined using the repeat number variance, θ_h was determined using expected homozygosity, and θ_x was determined using mean allele frequencies. N/A indicates a scenario that did not converge, so θ_{col} was not reported.

	θ	θ_{col}	θ_v	θ_h	θ_x
-1%					
1 gen.	39.602	25.826	43.985	59.34	10.136
5 gen.	38.049	187.094	41.694	59.935	10.689
10 gen.	36.193	438.591	49.357	86.14	12.11
50 gen.	24.261	264.277	35.076	64.94	10.791
100 gen.	14.715	283.178	36.523	54.198	9.314
-5%					
1 gen.	38.049	711.312	32.618	58.783	10.405
5 gen.	31.152	527.303	36.662	69.391	11.001
10 gen.	24.261	81.670	41.35	73.945	11.195
50 gen.	3.283	N/A	34.617	41.746	8.559
100 gen.	0.270	0.121	22.113	2.162	0.539
-10%					
1 gen.	36.193	195.912	33.384	66.99	10.795
5 gen.	24.261	230.176	54.761	68.06	11.22
10 gen.	14.715	205.145	38.184	53.14	10.416
50 gen.	0.270	0.391	25.149	5.022	1.698
-50%					
1 gen.	24.261	539.585	39.557	61.574	10.769
5 gen.	3.283	200.475	52.830	73.616	11.411
10 gen.	0.270	N/A	35.094	29.040	6.516

Table 16. θ calculations for each data set for the 50 microsatellite loci & 20 individuals sampling scenario. N_A = 100,000, θ_A = 400, generations, and percent decline noted for each scenario. $\theta = 4N_e\mu$ was calculated from 'known' parameters, $\theta_{col} = 4N_e\mu$ was calculated from msvar point estimates, θ_v was determined using the repeat number variance, θ_h was determined using expected homozygosity, and θ_x was determined using mean allele frequencies. N/A indicates a scenario that did not converge, so θ_{col} was not reported.

	θ	θ_{col}	θ_v	θ_h	θ_x
-1%					
1 gen.	396.020	1264.911	537.160	1421.210	28.660
5 gen.	380.492	1180.484	355.500	873.510	27.300
10 gen.	361.935	N/A	389.920	722.980	26.600
50 gen.	242.612	4488.074	628.710	883.800	27.150
100 gen.	147.152	N/A	390.900	3.661E+31	27.410
-5%					
1 gen.	380.492	N/A	291.720	367.870	26.532
5 gen.	311.520	N/A	632.390	1145.300	28.240
10 gen.	242.612	N/A	433.710	1019.750	27.650
50 gen.	32.834	N/A	326.850	919.100	26.920
100 gen.	2.695	N/A	270.710	79.088	12.016
-10%					
1 gen.	361.935	N/A	321.620	3.661E+31	27.020
5 gen.	242.612	N/A	338.240	3.661E+31	26.870
10 gen.	147.152	N/A	460.320	1553.860	27.890
50 gen.	2.695	N/A	380.040	180.210	17.720
-50%					
1 gen.	242.612	N/A	456.530	1283.360	28.020
5 gen.	32.834	N/A	464.190	1199.100	26.960
10 gen.	2.695	N/A	316.990	3.661E+31	24.960

Table 17. θ calculations for each data set for the 10 microsatellite loci & 20 individuals sampling scenario. N_A = 1000, θ_A = 4, generations, and percent decline noted for each scenario. $\theta = 4N_e\mu$ was calculated from 'known' parameters, $\theta_{col} = 4N_e\mu$ was calculated from msvar point estimates, θ_v was determined using the repeat number variance, θ_h was determined using expected homozygosity, and θ_x was determined using mean allele frequencies.

	θ	θ_{col}	θ_v	θ_h	θ_x
-1%					
1 gen.	3.960	23.018	7.269	7.497	3.344
5 gen.	3.805	2.832	5.419	7.509	2.862
10 gen.	3.619	76.218	2.662	4.631	1.875
50 gen.	2.426	1.387	4.155	7.670	2.306
100 gen.	1.472	1.236	2.471	5.713	1.494
-5%					
1 gen.	3.805	27.043	4.585	7.571	2.694
5 gen.	3.115	1.959	5.761	6.582	2.406
10 gen.	2.426	3.565	4.509	5.240	1.869
50 gen.	0.328	0.048	3.174	2.941	0.956
-10%					
1 gen.	3.619	71.131	3.848	5.278	2.494
5 gen.	2.426	8.167	5.785	5.996	2.119
10 gen.	1.472	6.793	2.749	6.916	1.794
-50%					
1 gen.	2.426	6.638	6.413	8.975	2.806
5 gen.	0.328	9.819	1.927	3.884	1.344

Table 18. θ calculations for each data set for the 10 microsatellite loci & 20 individuals sampling scenario. N_A = 10,000, θ_A = 40, generations, and percent decline noted for each scenario. $\theta = 4N_e\mu$ was calculated from 'known' parameters, $\theta_{col} = 4N_e\mu$ was calculated from msvar point estimates, θ_v was determined using the repeat number variance, θ_h was determined using expected homozygosity, and θ_x was determined using mean allele frequencies.

	θ	θ_{col}	θ_v	θ_h	θ_x
-1%					
1 gen.	39.602	875.105	48.907	148.809	13.125
5 gen.	38.049	107.661	35.435	57.470	11.238
10 gen.	36.193	459.261	42.791	72.200	11.431
50 gen.	24.261	340.455	31.193	72.020	10.731
100 gen.	14.715	7.981	50.664	65.960	11.040
-5%					
1 gen.	38.049	340.455	24.872	38.888	9.069
5 gen.	31.152	55.215	34.103	41.180	8.569
10 gen.	24.261	205.145	32.962	43.280	9.269
50 gen.	3.283	224.937	33.028	86.219	10.106
100 gen.	0.270	0.762	35.921	24.007	5.869
-10%					
1 gen.	36.193	356.500	18.229	45.830	8.494
5 gen.	24.261	141.925	48.774	58.350	10.175
10 gen.	14.715	711.312	39.954	51.510	10.770
50 gen.	0.270	0.057	43.737	4.422	1.219
-50%					
1 gen.	24.261	132.452	45.936	66.180	10.970
5 gen.	3.283	241.024	40.995	46.160	8.794
10 gen.	0.270	1.077	39.620	24.310	6.631

Table 19. θ calculations for each data set for the 10 microsatellite loci & 20 individuals sampling scenario. N_A = 100,000, θ_A = 400, generations, and percent decline noted for each scenario. $\theta = 4N_e\mu$ was calculated from 'known' parameters, $\theta_{col} = 4N_e\mu$ was calculated from msvar point estimates, θ_v was determined using the repeat number variance, θ_h was determined using expected homozygosity, and θ_x was determined using mean allele frequencies. N/A indicates a scenario that did not converge, so θ_{col} was not reported.

N_a=100,000	θ	θ_{col}	θ_v	θ_h	θ_x
-1%					
1 gen.	396.020	1452.312	319.620	783.200	28.200
5 gen.	380.492	138.695	510.000	1841.940	30.310
10 gen.	361.935	4093.172	425.720	795.220	28.250
50 gen.	242.612	11273.532	197.000	1238.400	24.520
100 gen.	147.152	1004.755	735.930	724.680	26.230
-5%					
1 gen.	380.492	1419.254	432.720	1951.100	29.490
5 gen.	311.520	4592.614	391.800	1134.000	28.490
10 gen.	242.612	469.959	594.960	798.200	26.860
50 gen.	32.834	1419.254	326.000	720.600	27.340
100 gen.	2.695	N/A	297.860	56.533	11.494
-10%					
1 gen.	361.935	4093.172	417.240	835.390	26.980
5 gen.	242.612	527.303	638.300	1928.700	29.880
10 gen.	147.152	835.718	566.920	1667.600	28.170
50 gen.	2.695	1.871	173.250	169.420	17.344
-50%					
1 gen.	242.612	1914.520	294.250	871.200	28.460
5 gen.	32.834	2831.783	261.010	839.800	27.370
10 gen.	2.695	N/A	420.850	495.790	25.000

Table 20. θ calculations for each data set for the 10 microsatellite loci & 50 individuals sampling scenario. N_A = 1000, θ_A = 4, generations, and percent decline noted for each scenario. $\theta = 4N_e\mu$ was calculated from 'known' parameters, $\theta_{col} = 4N_e\mu$ was calculated from msvar point estimates, θ_v was determined using the repeat number variance, θ_h was determined using expected homozygosity, and θ_x was determined using mean allele frequencies.

	θ	θ_{col}	θ_v	θ_h	θ_x
-1%					
1 gen.	3.960	17.461	3.644	3.697	2.944
5 gen.	3.805	4.488	4.034	7.025	3.844
10 gen.	3.619	7.448	4.322	6.233	2.956
50 gen.	2.426	1.325	2.440	6.311	2.044
100 gen.	1.472	1.828	2.463	3.720	2.188
-5%					
1 gen.	3.805	148.614	2.518	4.142	2.469
5 gen.	3.115	3.105	3.826	6.451	3.381
10 gen.	2.426	11.017	6.408	4.981	3.362
50 gen.	0.328	0.118	4.845	2.074	0.688
-10%					
1 gen.	3.619	23.018	3.082	4.002	2.650
5 gen.	2.426	2.767	3.118	4.054	2.500
10 gen.	1.472	1.077	2.130	4.255	2.150
-50%					
1 gen.	2.426	14.861	3.002	6.665	2.237
5 gen.	0.328	1.959	3.752	4.778	2.369

Table 21. θ calculations for each data set for the 10 microsatellite loci & 50 individuals sampling scenario. N_A = 10,000, θ_A = 40, generations, and percent decline noted for each scenario. $\theta = 4N_e\mu$ was calculated from 'known' parameters, $\theta_{col} = 4N_e\mu$ was calculated from msvar point estimates, θ_v was determined using the repeat number variance, θ_h was determined using expected homozygosity, and θ_x was determined using mean allele frequencies.

	θ	θ_{col}	θ_v	θ_h	θ_x
-1%					
1 gen.	39.602	162.952	21.643	42.550	16.650
5 gen.	38.049	390.895	45.762	49.450	20.920
10 gen.	36.193	459.261	56.160	55.580	21.760
50 gen.	24.261	219.816	37.046	65.170	22.331
100 gen.	14.715	13.554	46.747	61.500	21.988
-5%					
1 gen.	38.049	469.959	47.563	49.791	20.712
5 gen.	31.152	174.606	47.473	50.260	19.030
10 gen.	24.261	317.731	35.956	50.420	19.031
50 gen.	3.283	22.494	27.684	42.620	18.490
100 gen.	0.270	34.839	44.502	60.920	20.044
-10%					
1 gen.	36.193	25.238	50.562	62.120	20.962
5 gen.	24.261	258.262	31.461	51.090	17.125
10 gen.	14.715	1486.141	51.180	43.880	16.494
50 gen.	0.270	34.839	34.870	53.020	20.640
-50%					
1 gen.	24.261	1101.691	41.180	68.490	22.890
5 gen.	3.283	55.215	29.471	46.895	19.081
10 gen.	0.270	619.527	34.034	41.150	18.120

Table 22. θ calculations for each data set for the 10 microsatellite loci & 50 individuals sampling scenario. N_A = 100,000, θ_A = 400, generations, and percent decline noted for each scenario. $\theta = 4N_e\mu$ was calculated from 'known' parameters, $\theta_{col} = 4N_e\mu$ was calculated from msvar point estimates, θ_v was determined using the repeat number variance, θ_h was determined using expected homozygosity, and θ_x was determined using mean allele frequencies. N/A indicates a scenario that did not converge, so θ_{col} was not reported.

	θ	θ_{col}	θ_v	θ_h	θ_x
-1%					
1 gen.	396.020	N/A	263.400	571.400	87.650
5 gen.	380.492	N/A	527.780	530.700	84.660
10 gen.	361.935	N/A	246.650	475.800	81.900
50 gen.	242.612	515.300	375.230	615.800	92.210
100 gen.	147.152	N/A	430.200	430.700	79.430
-5%					
1 gen.	380.492	4488.074	258.980	518.500	79.330
5 gen.	311.520	4188.514	262.700	484.300	81.040
10 gen.	242.612	12943.746	712.330	628.500	95.900
50 gen.	32.834	N/A	371.200	479.100	82.410
100 gen.	2.695	1.959	413.620	67.120	31.500
-10%					
1 gen.	361.935	6054.245	322.540	496.000	83.010
5 gen.	242.612	1386.947	522.950	894.800	96.780
10 gen.	147.152	835.718	318.540	539.800	86.230
50 gen.	2.695	N/A	323.180	141.460	41.760
-50%					
1 gen.	242.612	6195.266	326.300	508.560	82.810
5 gen.	32.834	N/A	220.200	570.100	87.720
10 gen.	2.695	N/A	464.500	399.700	79.290

Figure 1. Population model for the sampling scenarios created using ms. N_A is the ancestral effective population size, r is the rate of decline, t is the time in generations for the length of the decline, and N_e is the current effective population size.

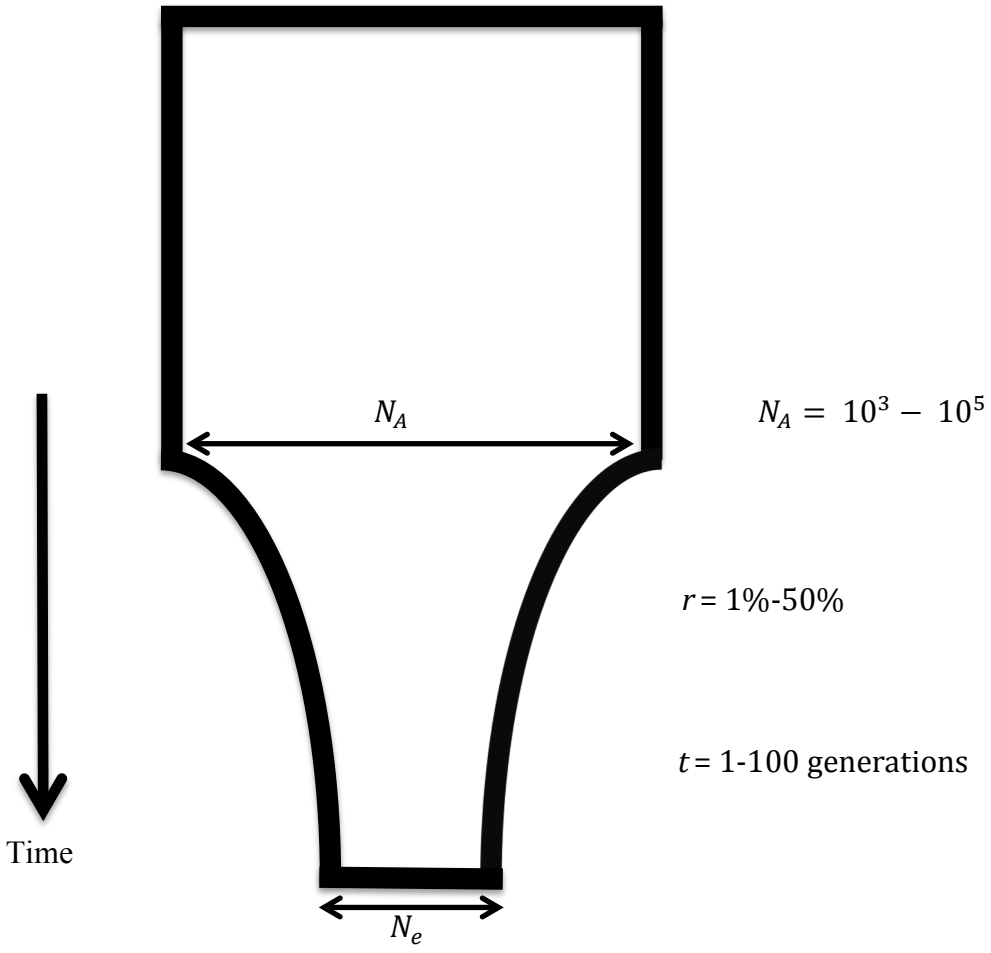

Figure 2. Example posterior probability plot for N_A. Results are from a demographic scenario of -1% decline over 100 generations from an ancestral population size of 1000. The sampling scenario involved 20 individuals genotyped at 50 loci. The red line indicates the known parameter value; posterior distributions for the three independent runs are shown as blue, green, and purple curves.

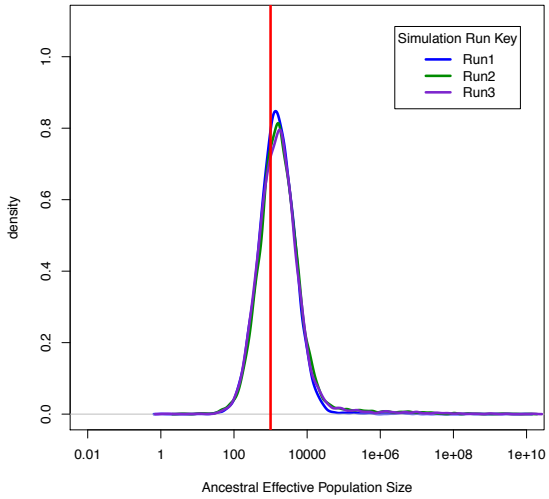

Figure 3. Estimated vs. known N_A for scenarios with 20 individuals, 50 microsatellite loci, and N_A =1000. (A) -1% decline, (B) -5% decline, (C) -10% decline, (D) -50% decline. The red line indicates the known value of N_A. Results are shown only for analyses that converged. Results of individual runs are shown in green (run 1), yellow (run 2), and pink (run 3), with the pooled results of the three runs in blue.

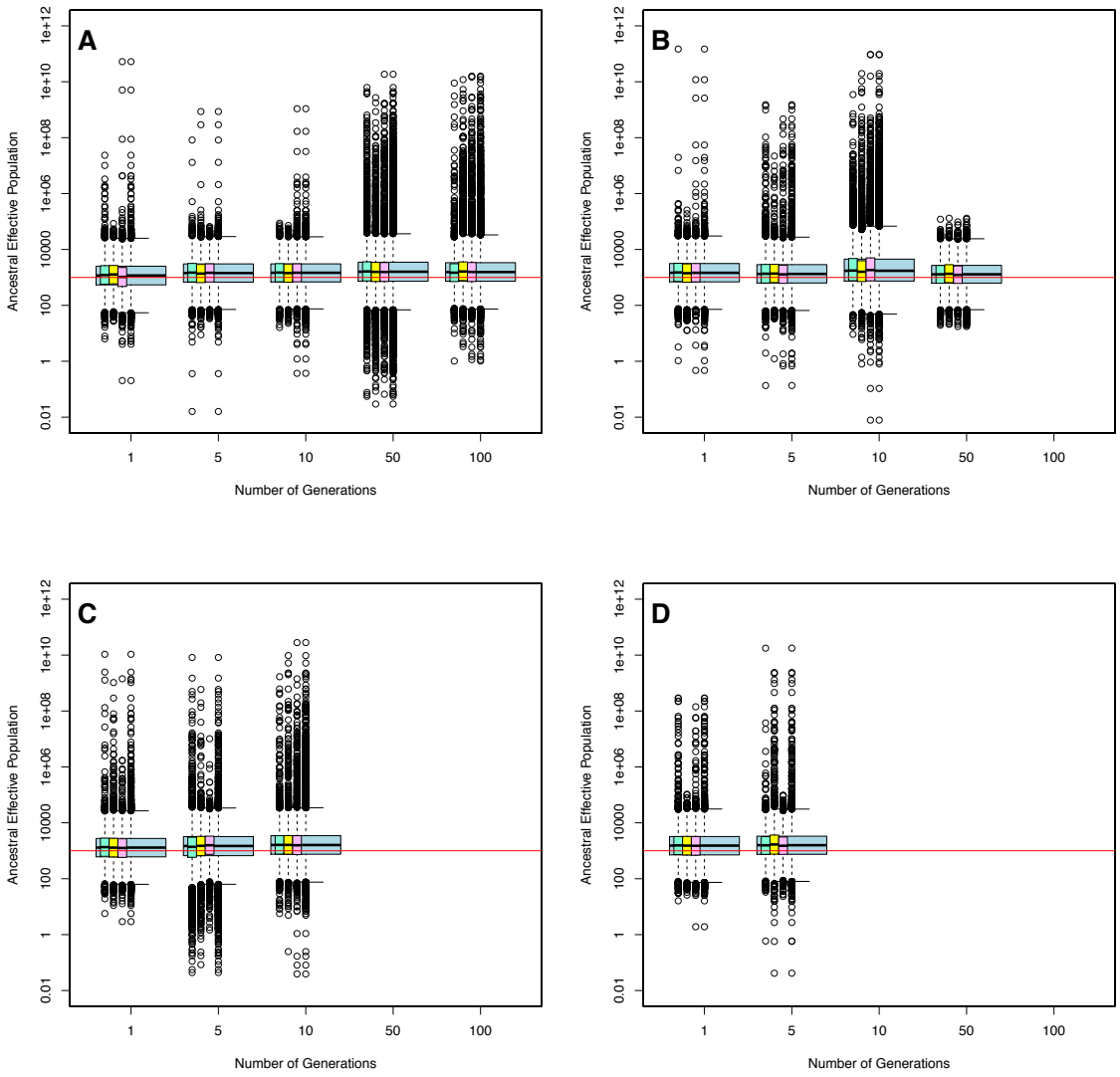

Figure 4. Estimated vs. known N_A for scenarios with 20 individuals, 50 microsatellite loci, and N_A =10,000. (A) -1% decline, (B) -5% decline, (C) -10% decline, (D) -50% decline. The red line indicates the known value of N_A. Results are shown only for analyses that converged. Results of individual runs are shown in green (run 1), yellow (run 2), and pink (run 3), with the pooled results of the three runs in blue.

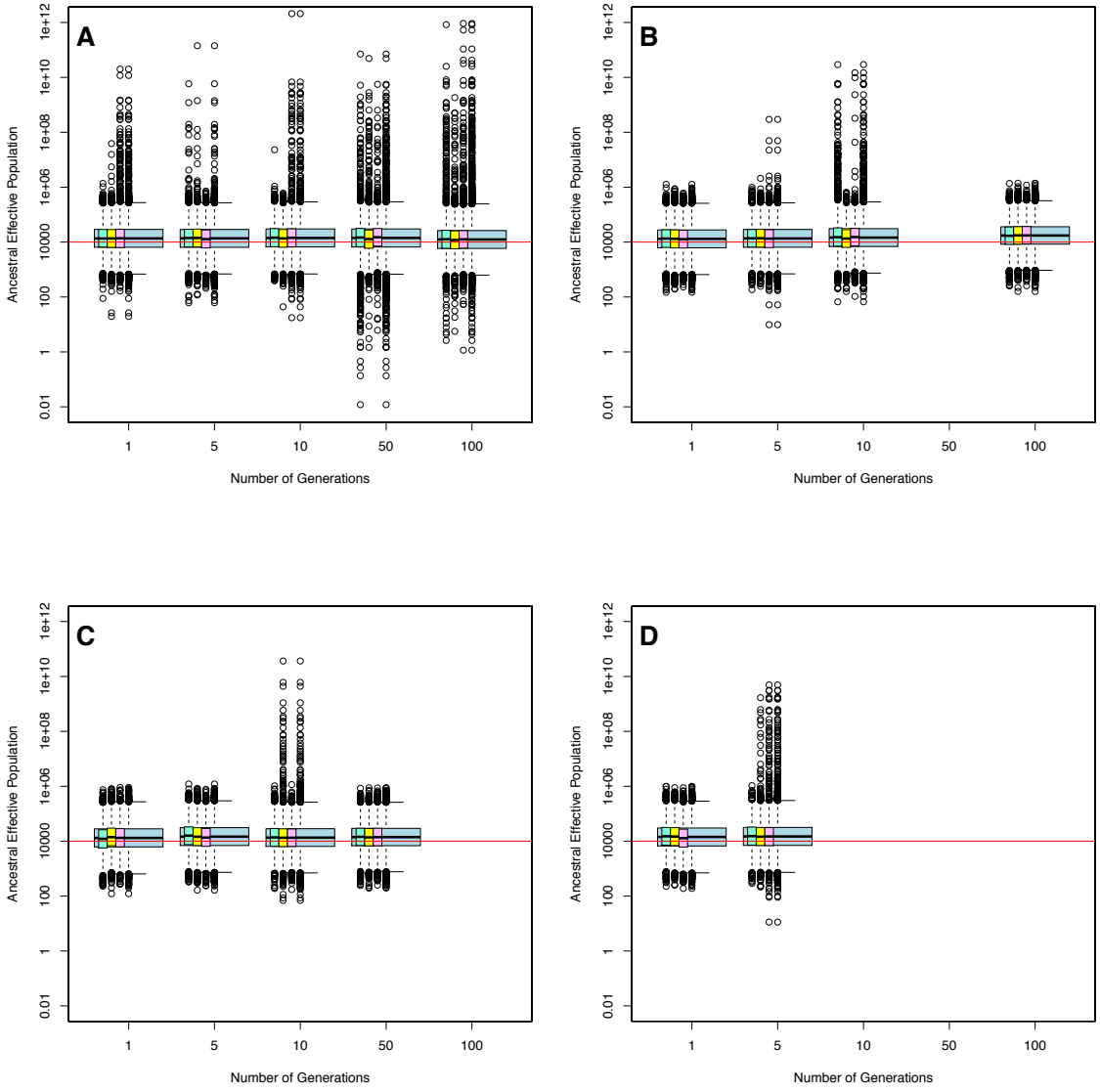

Figure 5. Estimated vs. known N_A for scenarios with 20 individuals, 50 microsatellite loci, N_A =100,000, and -1% decline. The red line indicates the known value of N_A. Results are shown only for analyses that converged. Results of individual runs are shown in green (run 1), yellow (run 2), and pink (run 3), with the pooled results of the three runs in blue.

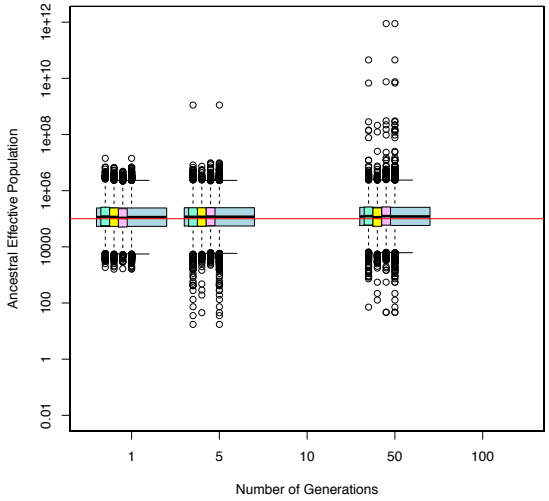

Figure 6. Estimated vs. known N_A for scenarios with 50 individuals, 10 microsatellite loci, and N_A =1000. (A) -1% decline, (B) -5% decline, (C) -10% decline, (D) -50% decline. The red line indicates the known value of N_A. Results are shown only for analyses that converged. Results of individual runs are shown in green (run 1), yellow (run 2), and pink (run 3), with the pooled results of the three runs in blue.

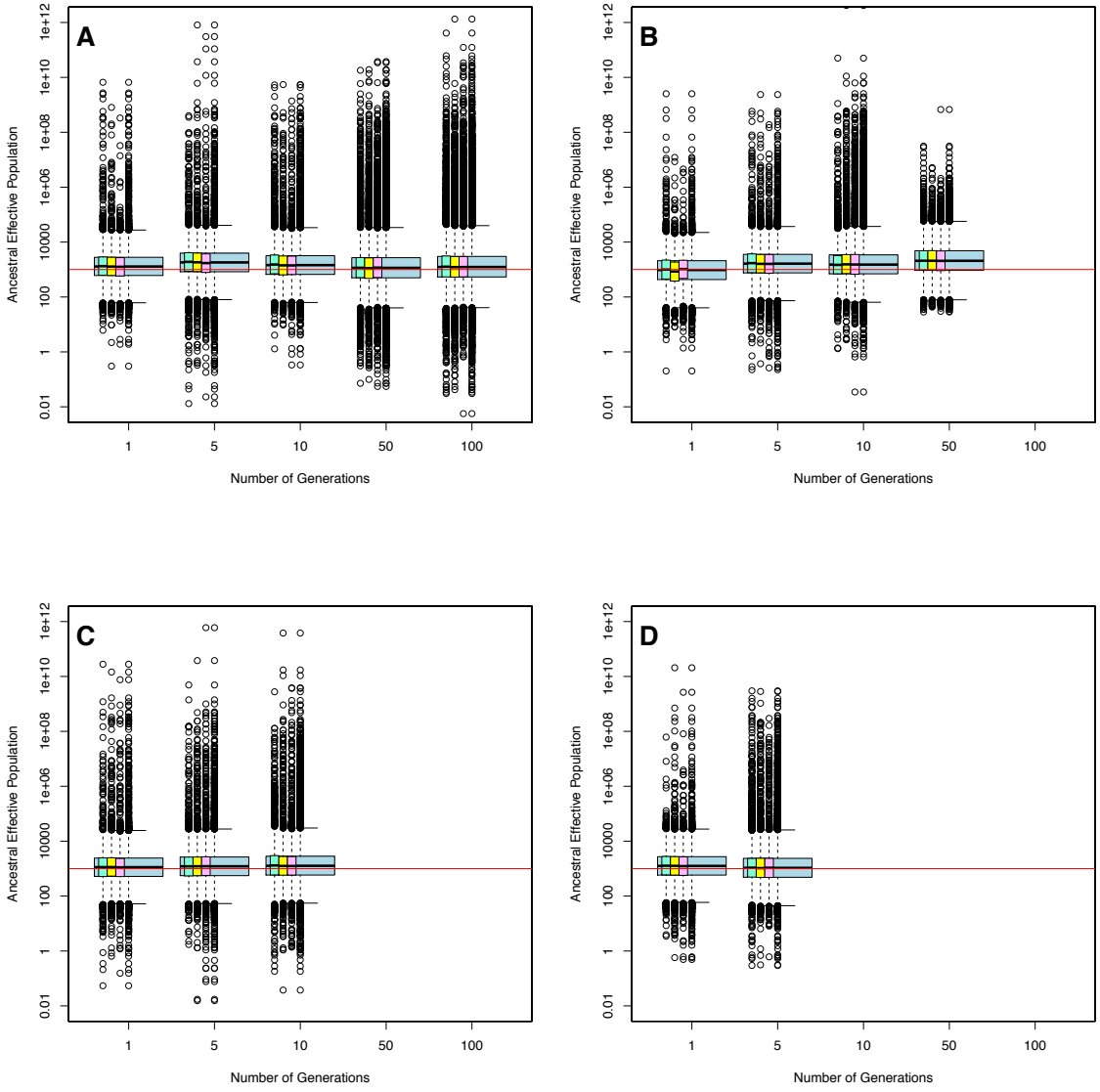

Figure 7. Estimated vs. known N_A for scenarios with 50 individuals, 10 microsatellite loci, and N_A =10,000. (A) -1% decline, (B) -5% decline, (C) -10% decline, (D) -50% decline. The red line indicates the known value of N_A. Results are shown only for analyses that converged. Results of individual runs are shown in green (run 1), yellow (run 2), and pink (run 3), with the pooled results of the three runs in blue.

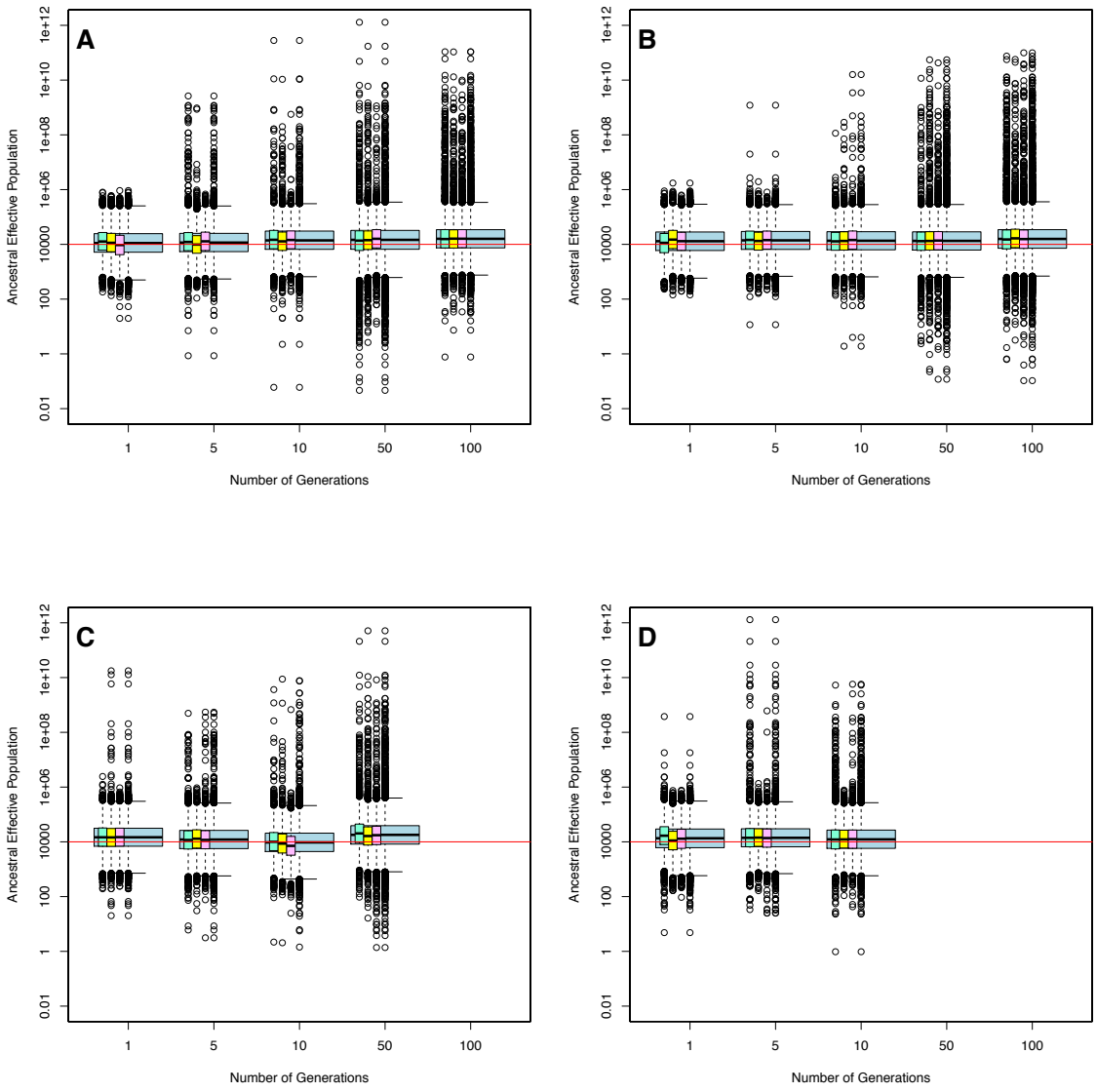

Figure 8. Estimated vs. known N_A for scenarios with 50 individuals, 10 microsatellite loci, and N_A =100,000. (A) -1% decline, (B) -5% decline, (C) -10% decline, (D) -50% decline. The red line indicates the known value of N_A. Results are shown only for analyses that converged. Results of individual runs are shown in green (run 1), yellow (run 2), and pink (run 3), with the pooled results of the three runs in blue.

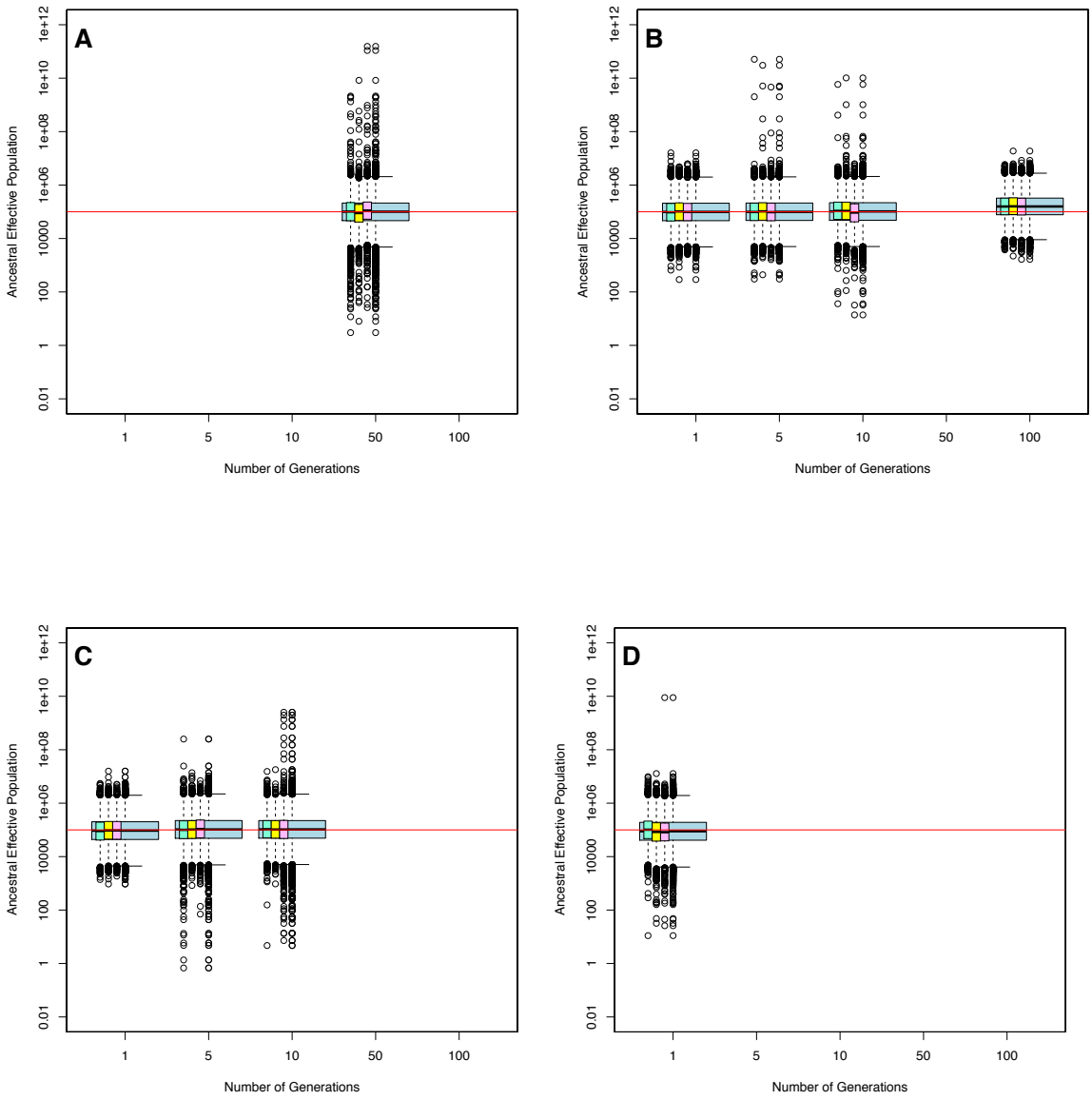

Figure 9. Estimated vs. known N_A for scenarios with 20 individuals, 10 microsatellite loci, and N_A =1000. (A) -1% decline, (B) -5% decline, (C) -10% decline, (D) -50% decline. The red line indicates the known value of N_A. Results are shown only for analyses that converged. Results of individual runs are shown in green (run 1), yellow (run 2), and pink (run 3), with the pooled results of the three runs in blue.

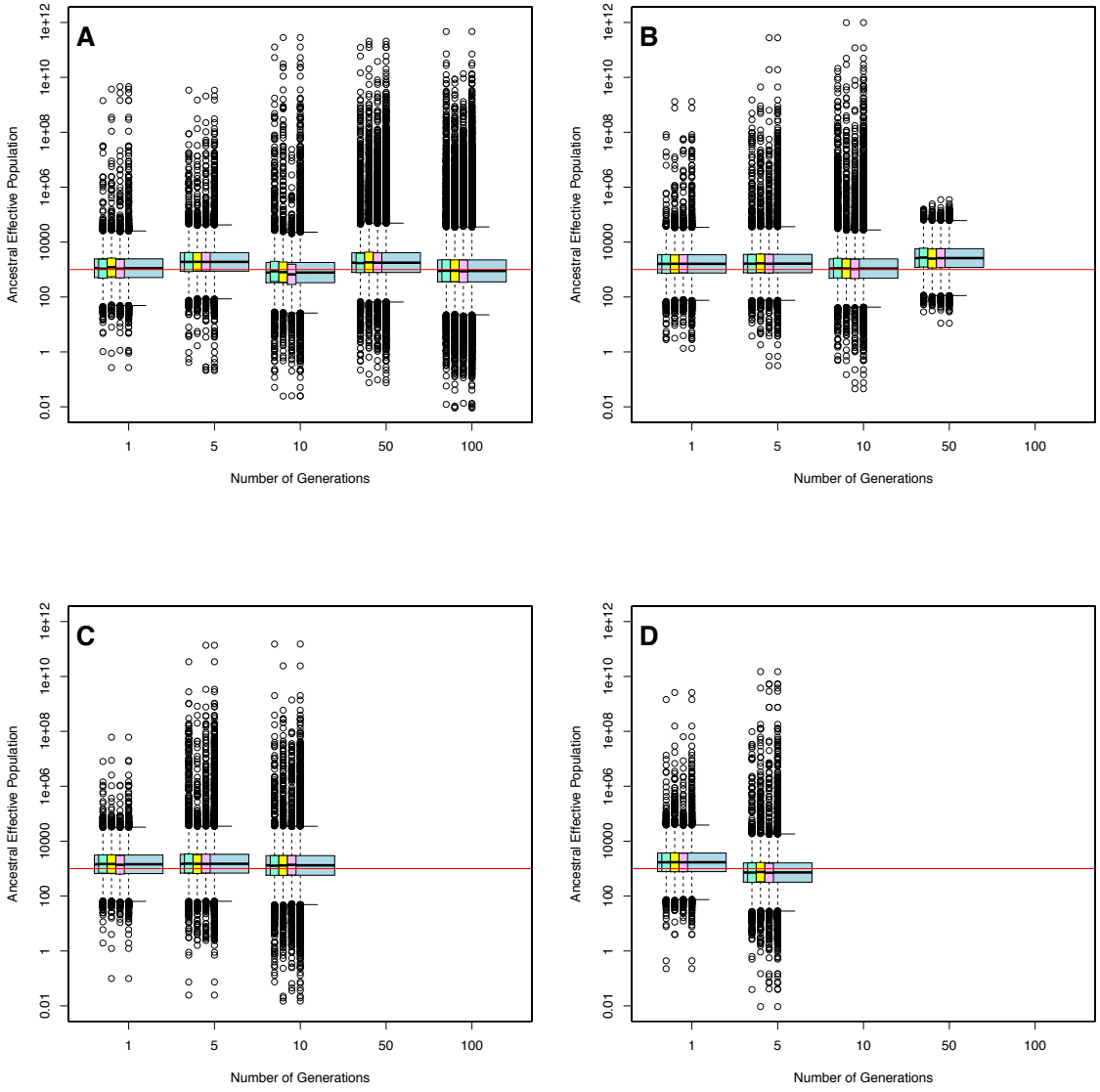

Figure 10. Estimated vs. known N_A for scenarios with 20 individuals, 10 microsatellite loci, and N_A =10,000. (A) -1% decline, (B) -5% decline, (C) -10% decline, (D) -50% decline. The red line indicates the known value of N_A. Results are shown only for analyses that converged. Results of individual runs are shown in green (run 1), yellow (run 2), and pink (run 3), with the pooled results of the three runs in blue.

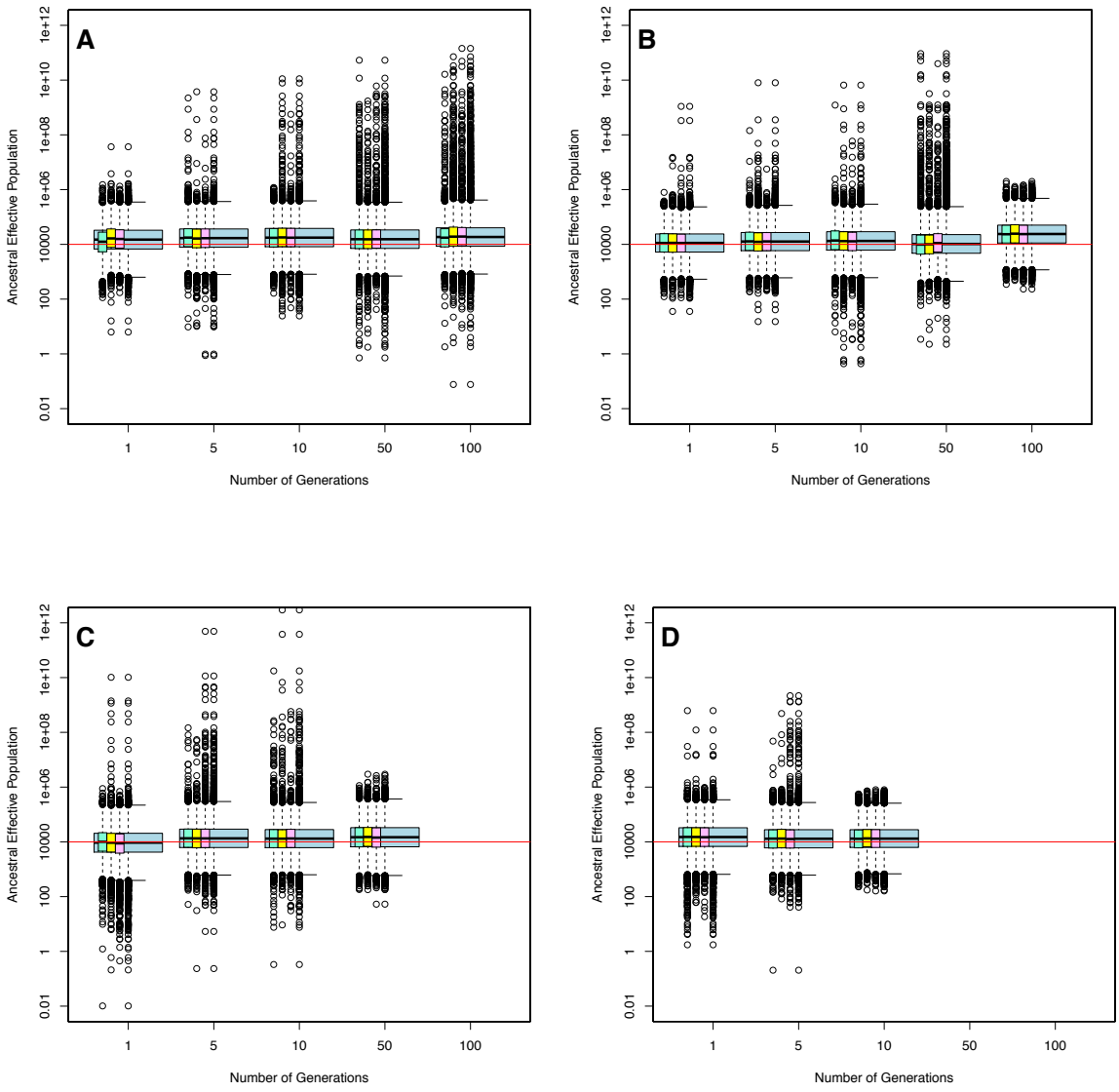

Figure 11. Estimated vs. known N_A for scenarios with 20 individuals, 10 microsatellite loci, and N_A =100,000. (A) -1% decline, (B) -5% decline, (C) -10% decline, (D) -50% decline. The red line indicates the known value of N_A. Results are shown only for analyses that converged. Results of individual runs are shown in green (run 1), yellow (run 2), and pink (run 3), with the pooled results of the three runs in blue.

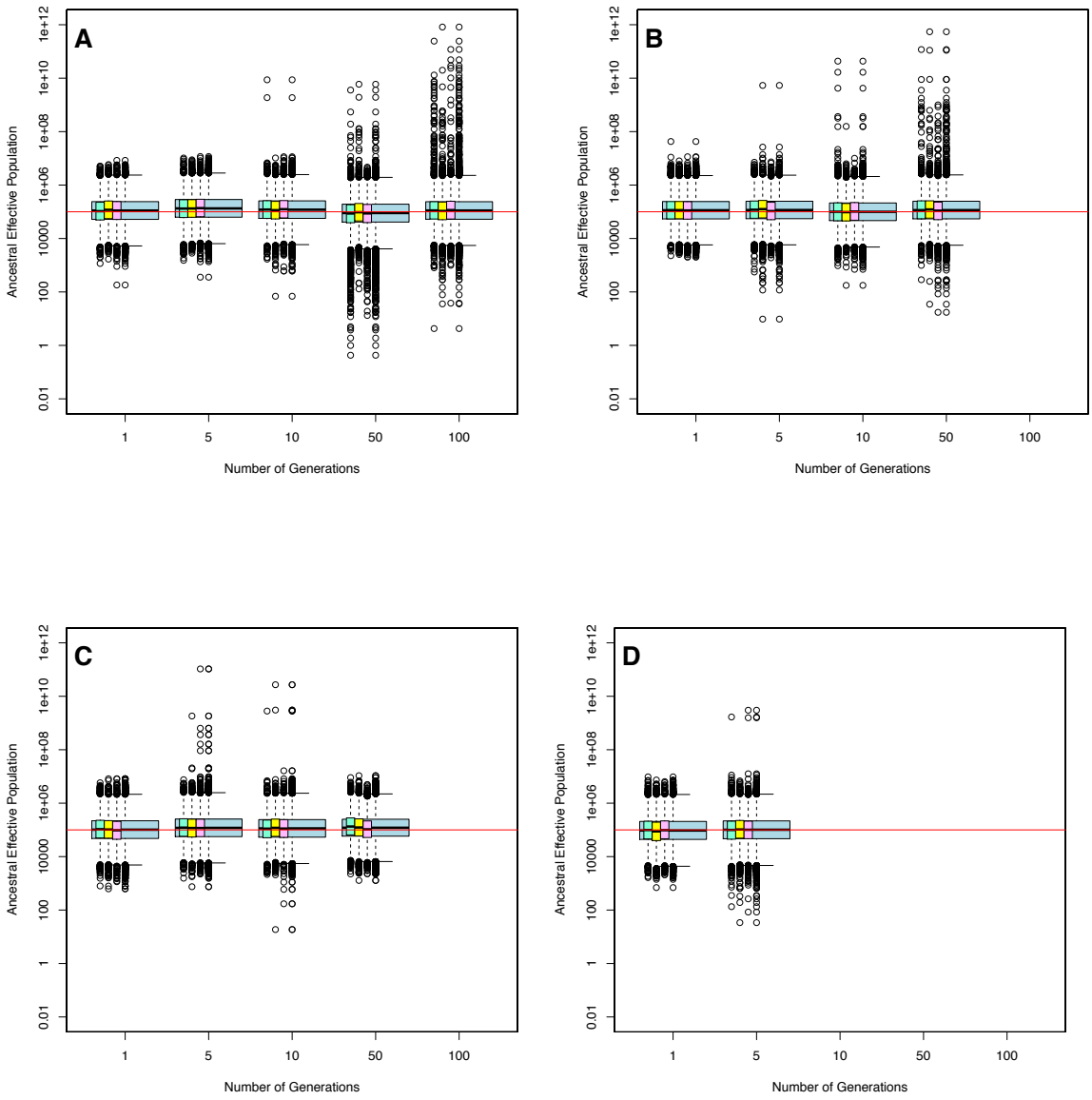

Figure 12. Example posterior probability plots for N_e. Red lines indicate the known parameter value; posterior distributions for the three independent runs are shown as blue, green, and purple curves. A. Results from a demographic scenario of -1% decline over 1 generation from an ancestral population size of 1000 and a sampling scenario of 20 individuals and 10 loci. B. Results from a demographic scenario of -10% decline over 1 generation from an ancestral population size of 100,000 and a sampling scenario of 20 individuals and 10 loci. C. Results from a demographic scenario of -1% decline over 100 generations from an ancestral population size of 10,000 and a sampling scenario of 50 individuals and 10 loci. D. Results from a demographic scenario of -1% decline over 100 generations from an ancestral population size of 10,000 and a sampling scenario of 20 individuals and 50 loci.

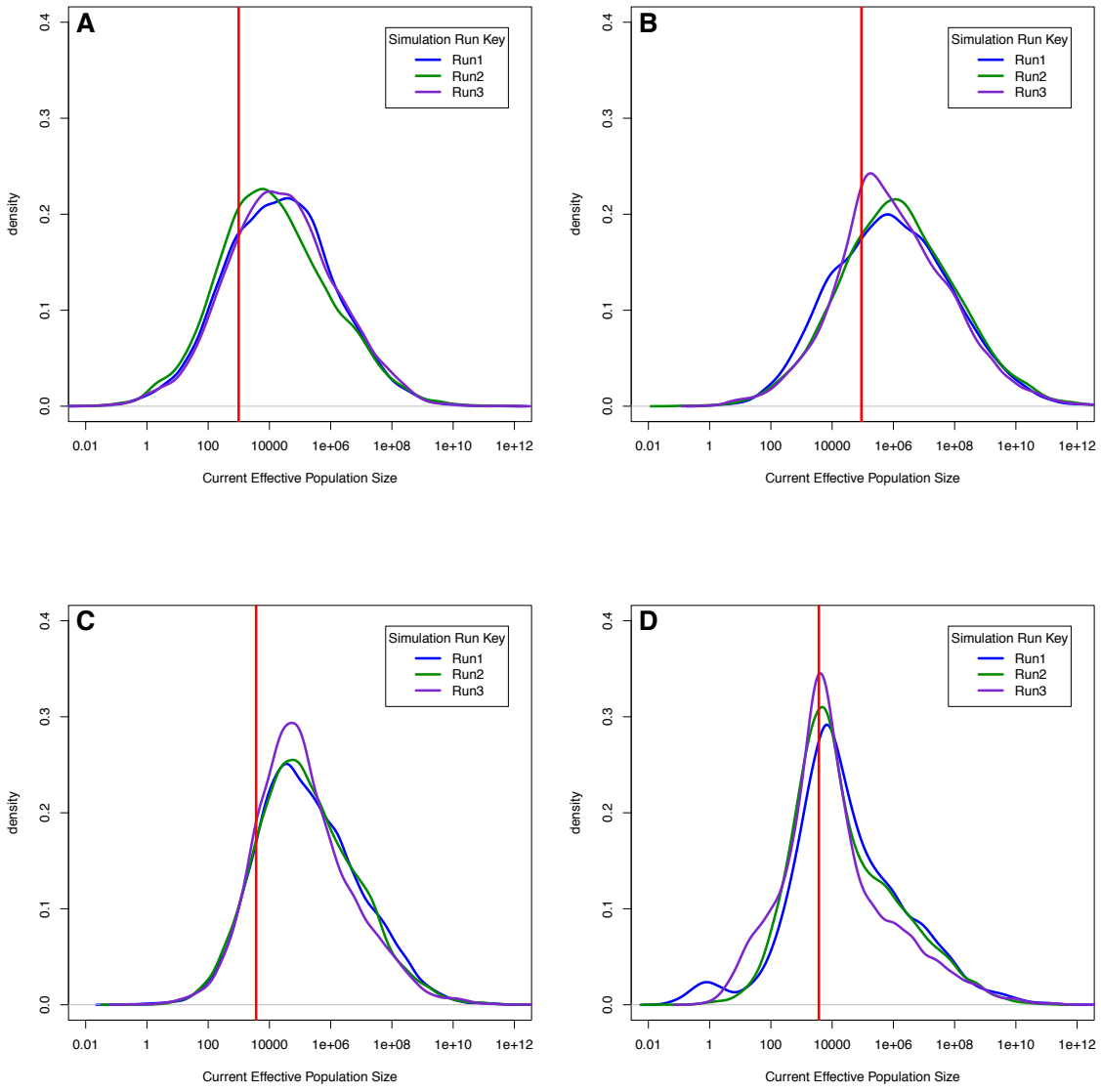

Figure 13. Estimated vs. known N_e for scenarios with 20 individuals, 50 microsatellite loci, and N_A =1000. (A) -1% decline, (B) -5% decline, (C) -10% decline, (D) -50% decline. Red lines indicate the known values of N_e at each timepoint. Results are shown only for analyses that converged. Results of individual runs are shown in green (run 1), yellow (run 2), and pink (run 3), with the pooled results of the three runs in blue.

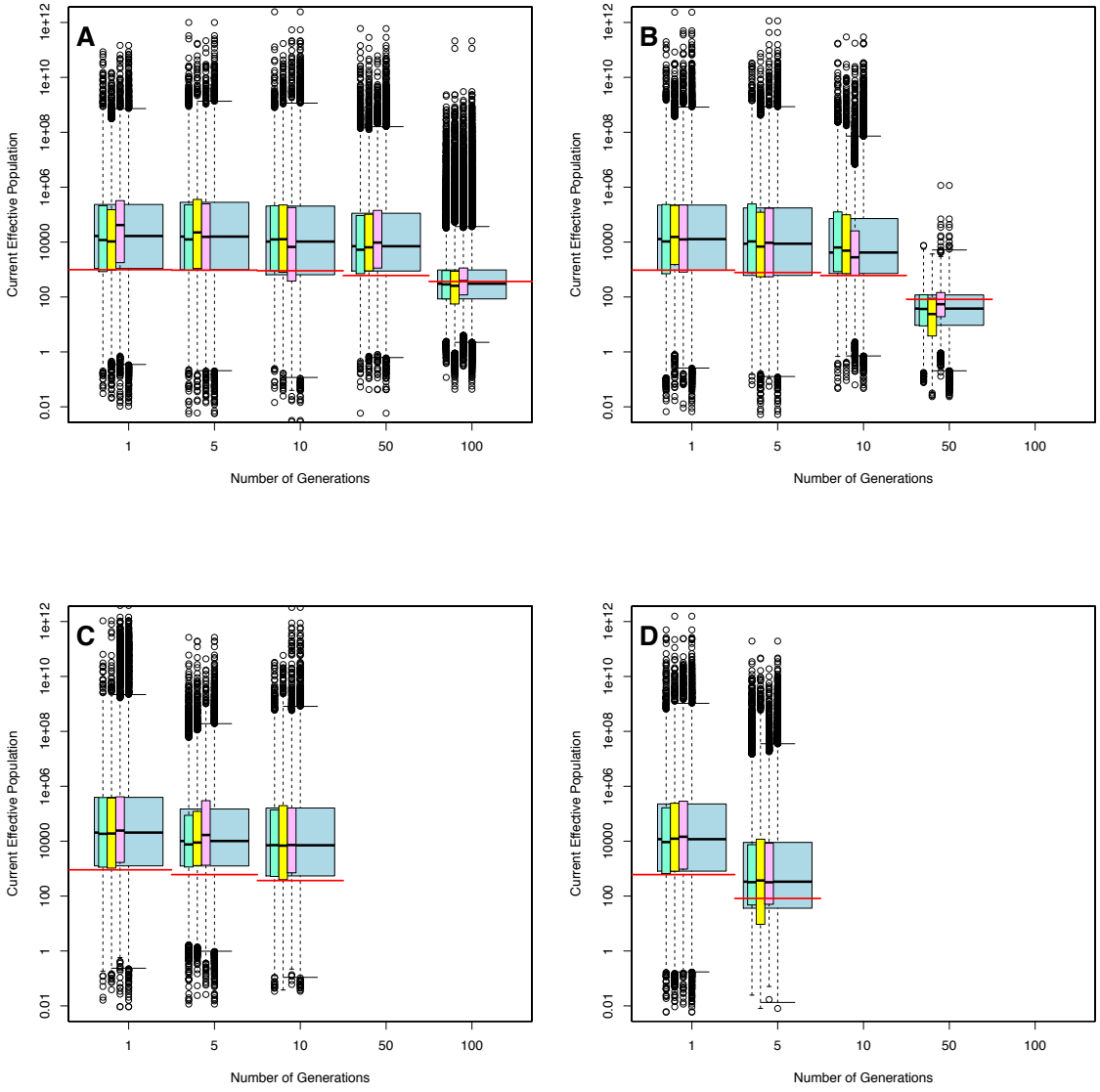

Figure 14. Estimated vs. known N_e for scenarios with 20 individuals, 50 microsatellite loci, and N_A =10,000. (A) -1% decline, (B) -5% decline, (C) -10% decline, (D) -50% decline. Red lines indicate the known values of N_e at each timepoint. Results are shown only for analyses that converged. Results of individual runs are shown in green (run 1), yellow (run 2), and pink (run 3), with the pooled results of the three runs in blue.

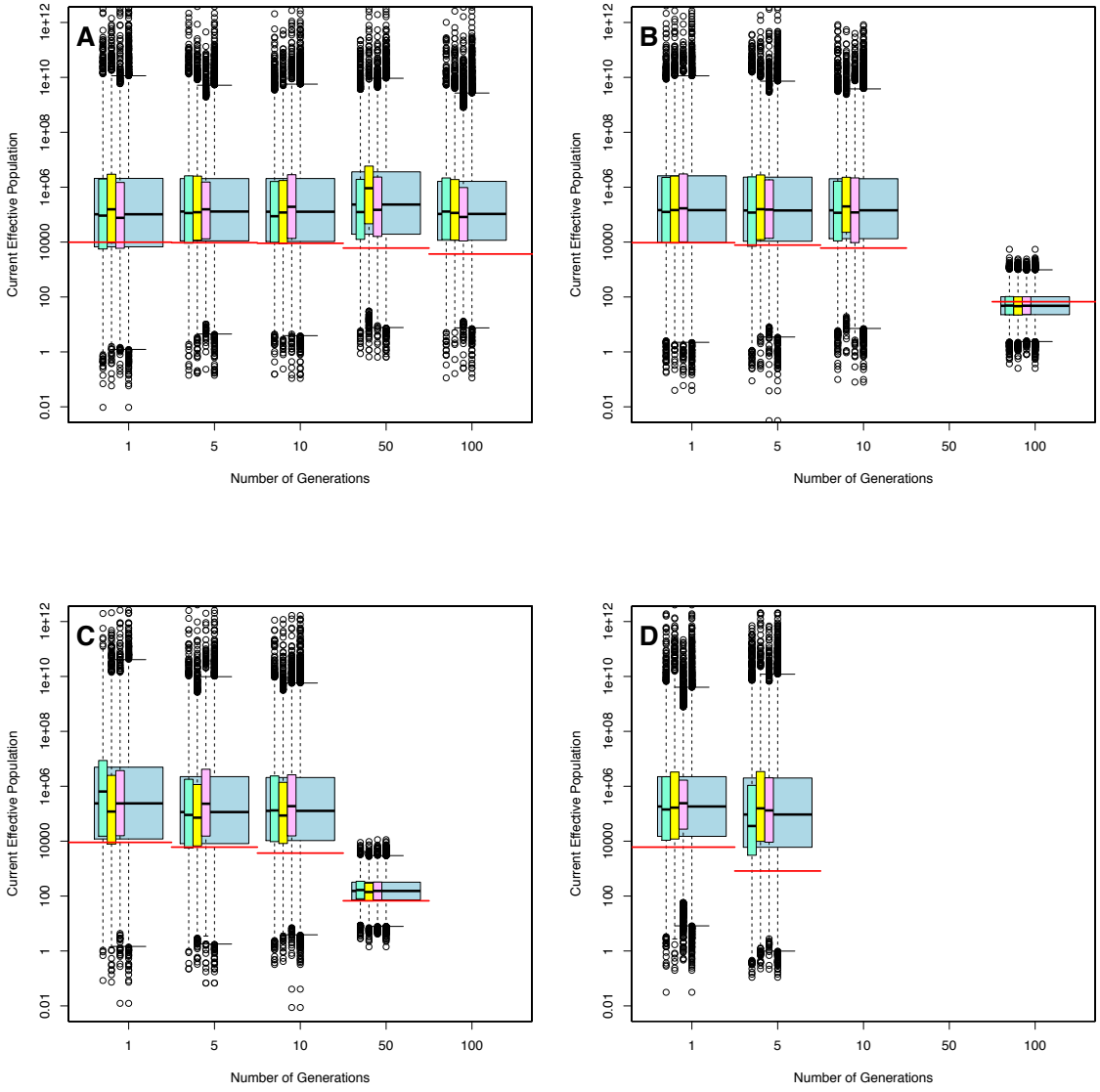

Figure 15. Estimated vs. known N_e for scenarios with 20 individuals, 50 microsatellite loci, N_A =100,000, and -1% decline. Red lines indicate the known values of N_e at each timepoint. Results are shown only for analyses that converged. Results of individual runs are shown with each box plot in green (run 1), yellow (run 2), and pink (run 3), with the pooled results of the three runs in blue.

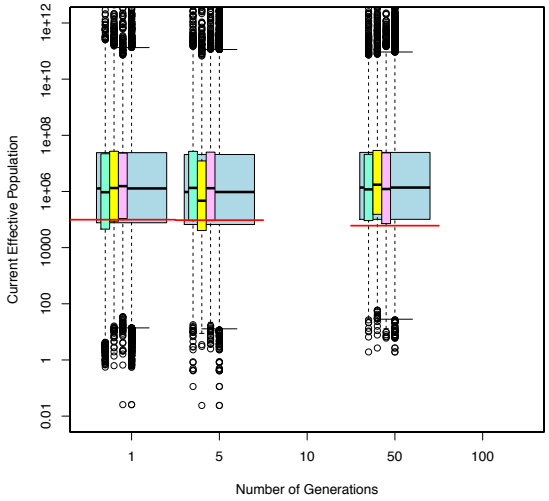

Figure 16. Estimated vs. known N_e for scenarios with 50 individuals, 10 microsatellite loci, and N_A =1000. (A) -1% decline, (B) -5% decline, (C) -10% decline, (D) -50% decline. Red lines indicate the known values of N_e at each timepoint. Results are shown only for analyses that converged. Results of individual runs are shown in green (run 1), yellow (run 2), and pink (run 3), with the pooled results of the three runs in blue.

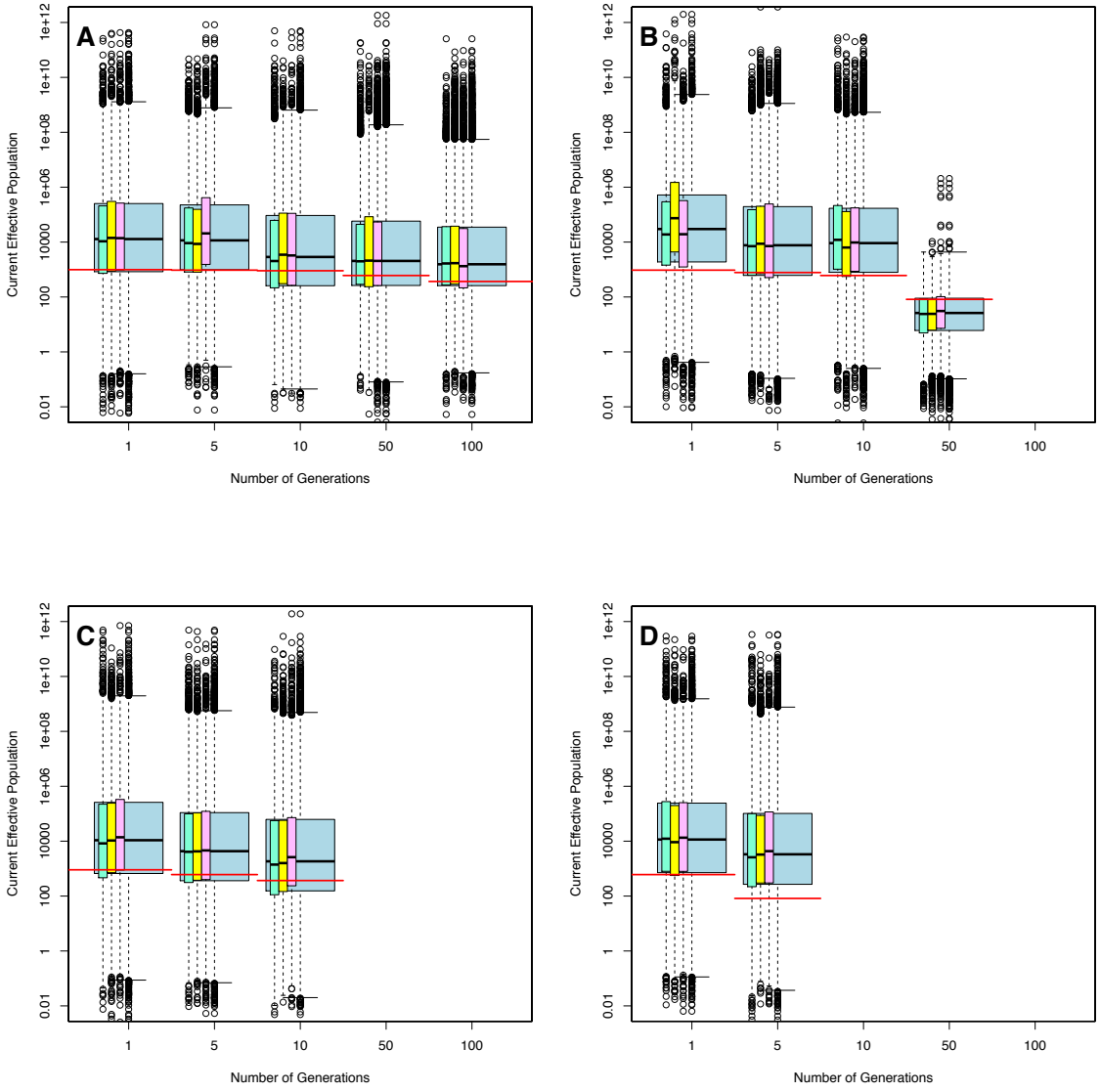

Figure 17. Estimated vs. known N_e for scenarios with 50 individuals, 10 microsatellite loci, and N_A =10,000. (A) -1% decline, (B) -5% decline, (C) -10% decline, (D) -50% decline. Red lines indicate the known values of N_e at each timepoint. Results are shown only for analyses that converged. Results of individual runs are shown in green (run 1), yellow (run 2), and pink (run 3), with the pooled results of the three runs in blue.

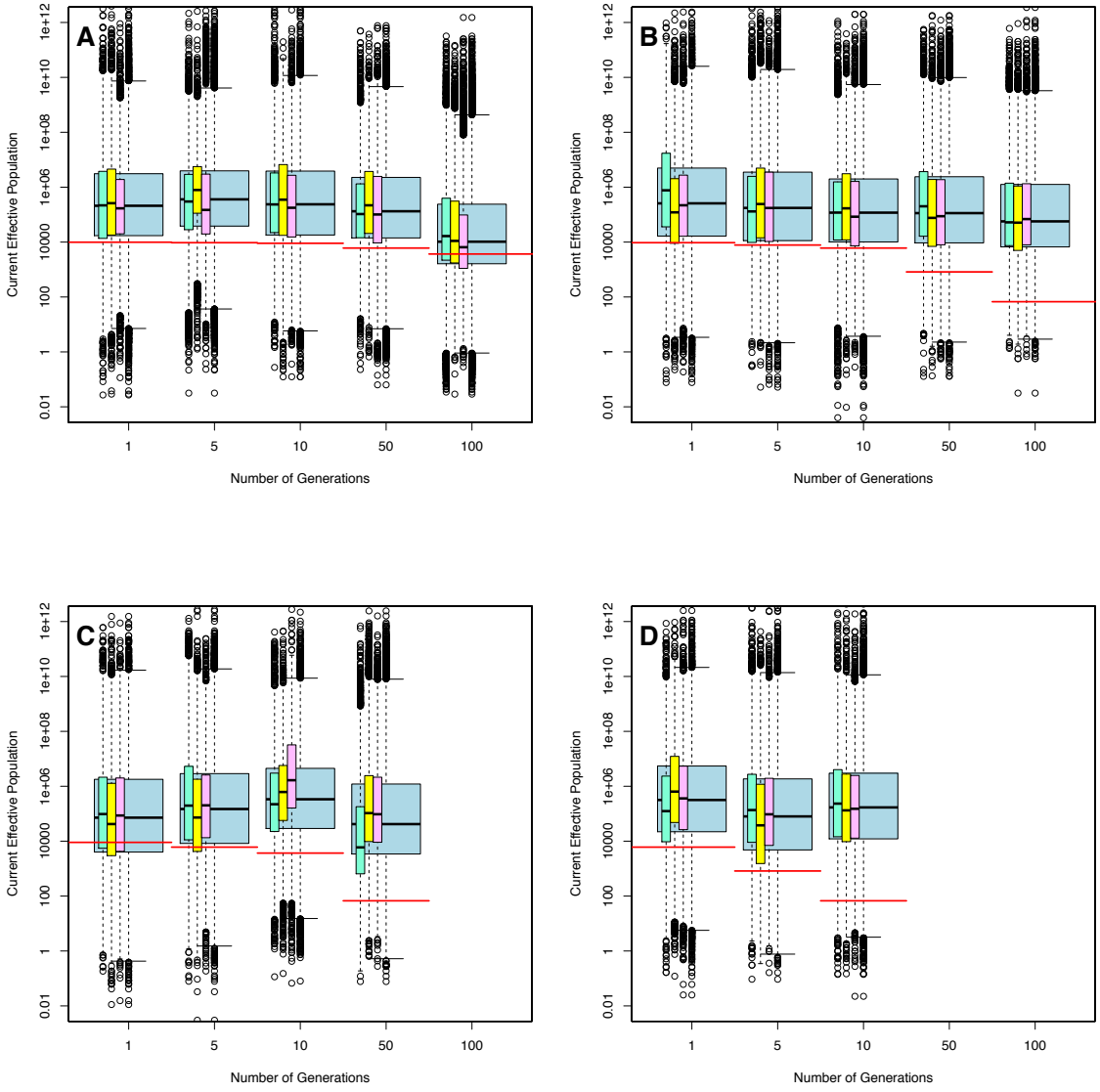

Figure 18. Estimated vs. known N_e for scenarios with 50 individuals, 10 microsatellite loci, and N_A =100,000. (A) -1% decline, (B) -5% decline, (C) -10% decline, (D) -50% decline. Red lines indicate the known values of N_e at each timepoint. Results are shown only for analyses that converged. Results of individual runs are shown in green (run 1), yellow (run 2), and pink (run 3), with the pooled results of the three runs in blue.

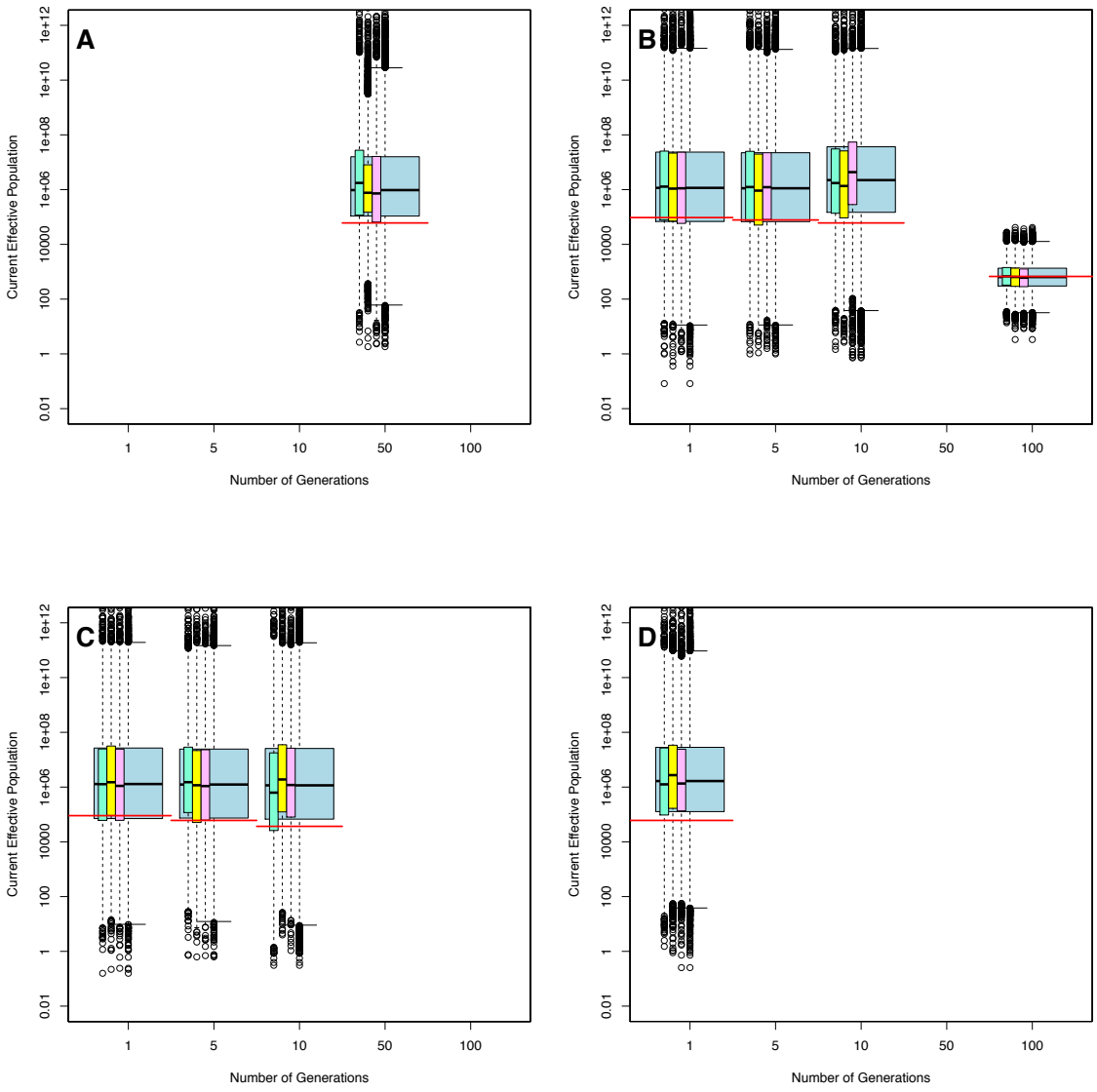

Figure 19. Estimated vs. known N_e for scenarios with 20 individuals, 10 microsatellite loci, and N_A =1000. (A) -1% decline, (B) -5% decline, (C) -10% decline, (D) -50% decline. Red lines indicate the known values of N_e at each timepoint. Results are shown only for analyses that converged. Results of individual runs are shown in green (run 1), yellow (run 2), and pink (run 3), with the pooled results of the three runs in blue.

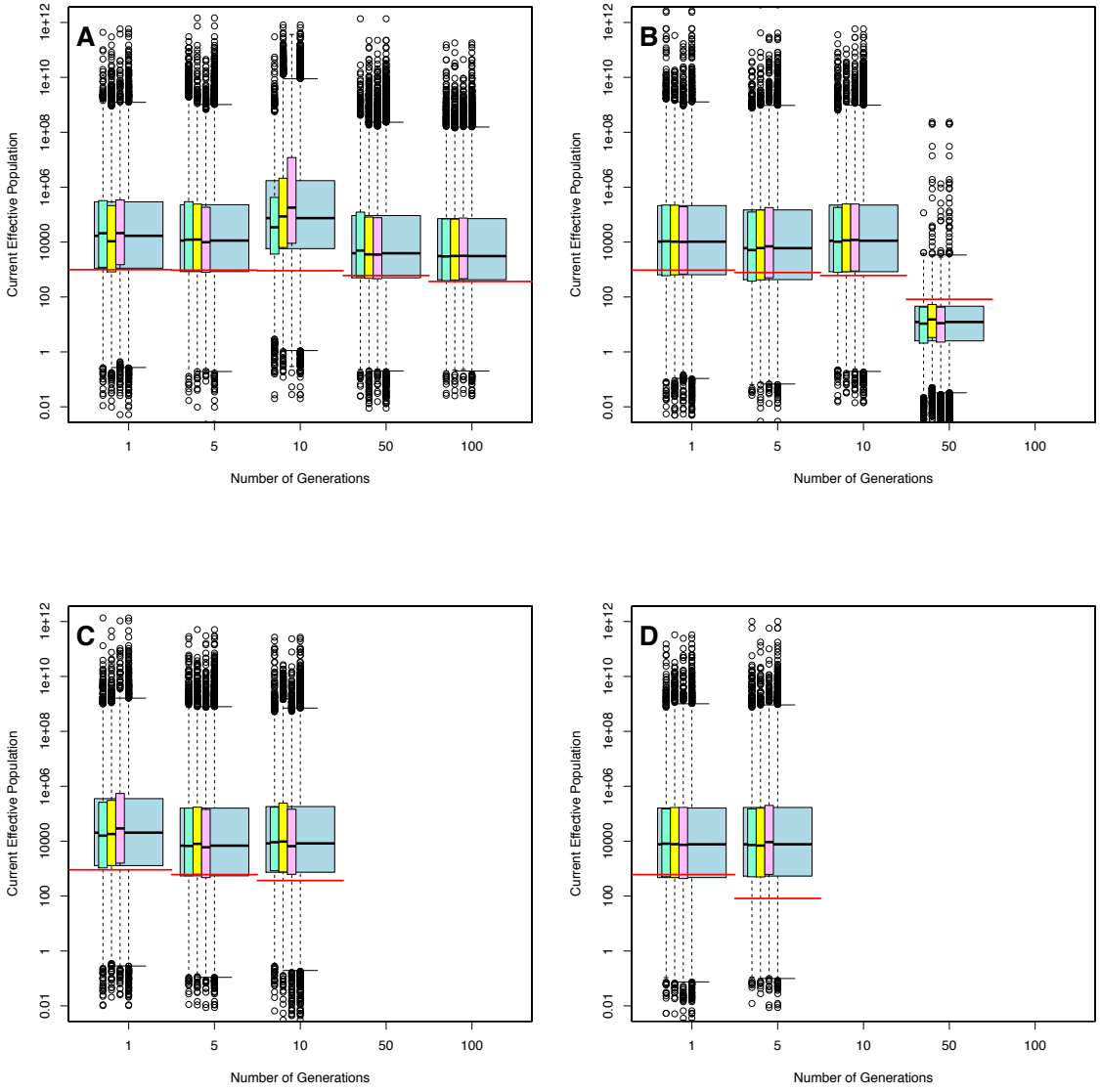

Figure 20. Estimated vs. known N_e for scenarios with 20 individuals, 10 microsatellite loci, and N_A =10,000. (A) -1% decline, (B) -5% decline, (C) -10% decline, (D) -50% decline. Red lines indicate the known values of N_e at each timepoint. Results are shown only for analyses that converged. Results of individual runs are shown in green (run 1), yellow (run 2), and pink (run 3), with the pooled results of the three runs in blue.

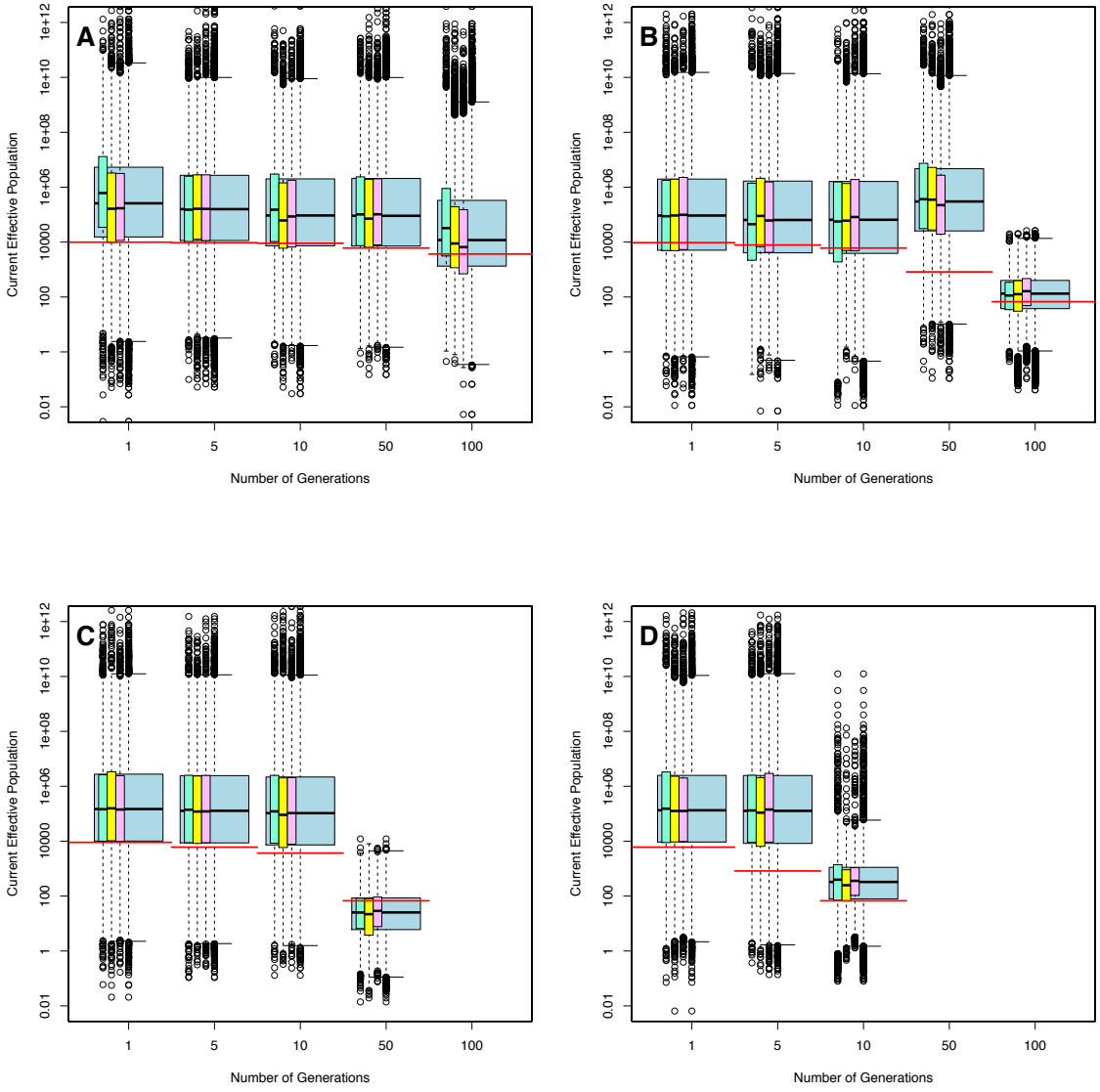

Figure 21. Estimated vs. known N_e for scenarios with 20 individuals, 10 microsatellite loci, and N_A =100,000. (A) -1% decline, (B) -5% decline, (C) -10% decline, (D) -50% decline. Red lines indicate the known values of N_e at each timepoint. Results are shown only for analyses that converged. Results of individual runs are shown in green (run 1), yellow (run 2), and pink (run 3), with the pooled results of the three runs in blue.

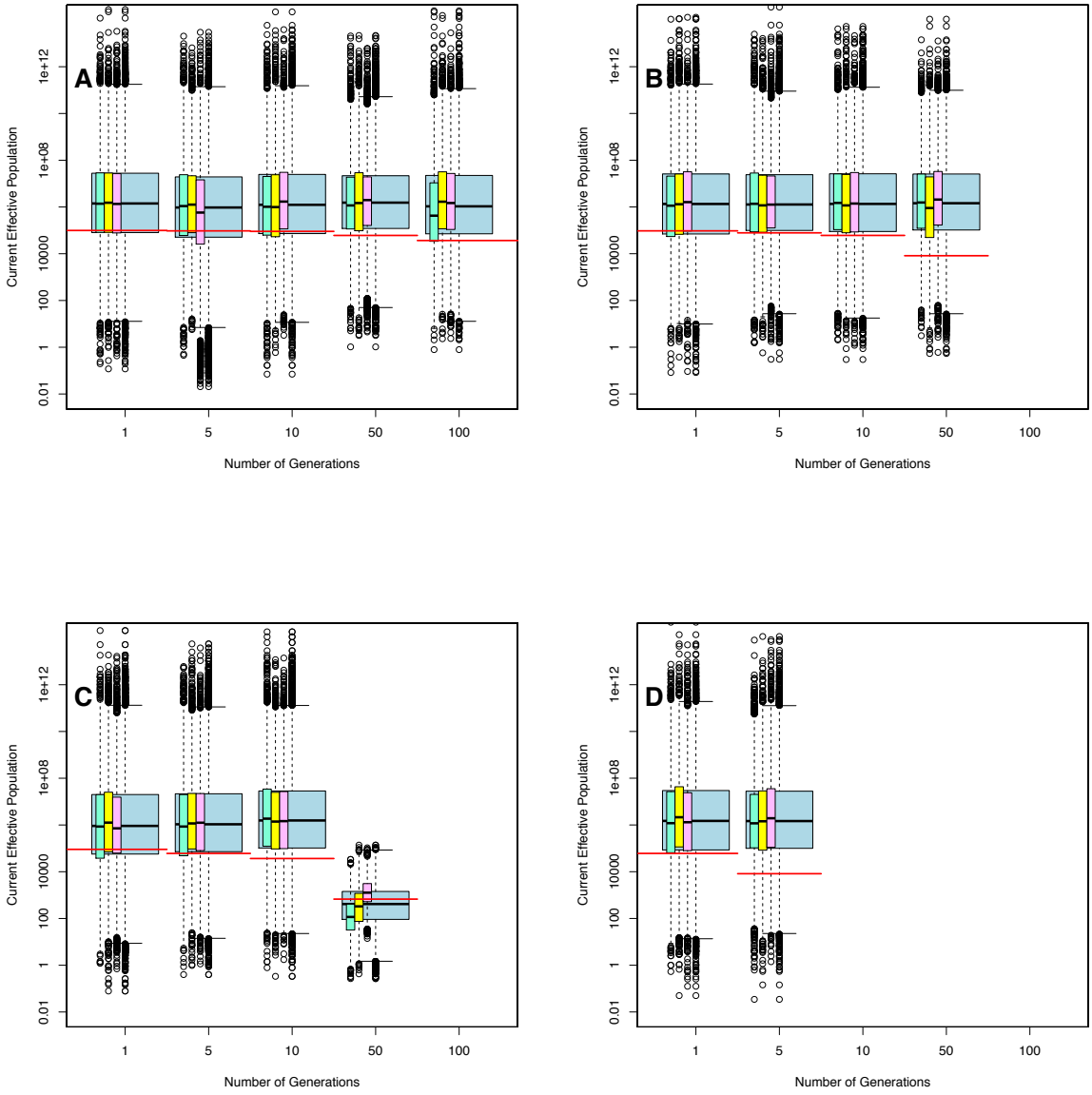

Figure 22. Example posterior probability plot for μ. Results are from a demographic scenario of -1% decline over 100 generations from an ancestral population size of 10,000. The sampling scenario involved 20 individuals genotyped at 50 loci. The red line indicates the known value parameter value; posterior distributions for the three independent runs are shown as blue, green, and purple curves..

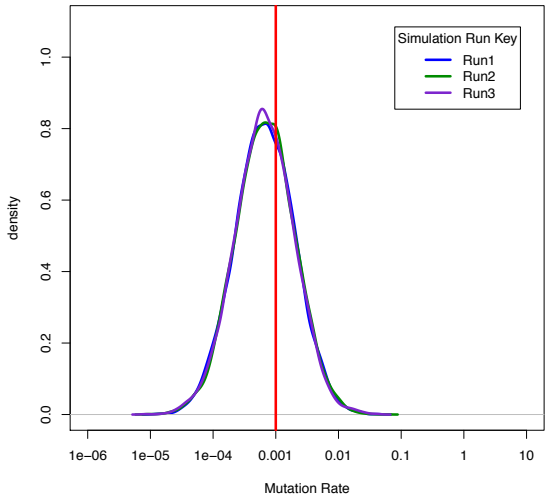

Figure 23. Estimated vs. known μ for scenarios with 20 individuals, 50 microsatellite loci, and N_A =1000. (A) -1% decline, (B) -5% decline, (C) -10% decline, (D) -50% decline. Red lines indicate the known values of μ at each timepoint. Results are shown only for analyses that converged. Individual runs are shown in green (run 1), yellow (run 2), and pink (run 3), with the pooled results of the three runs in blue.

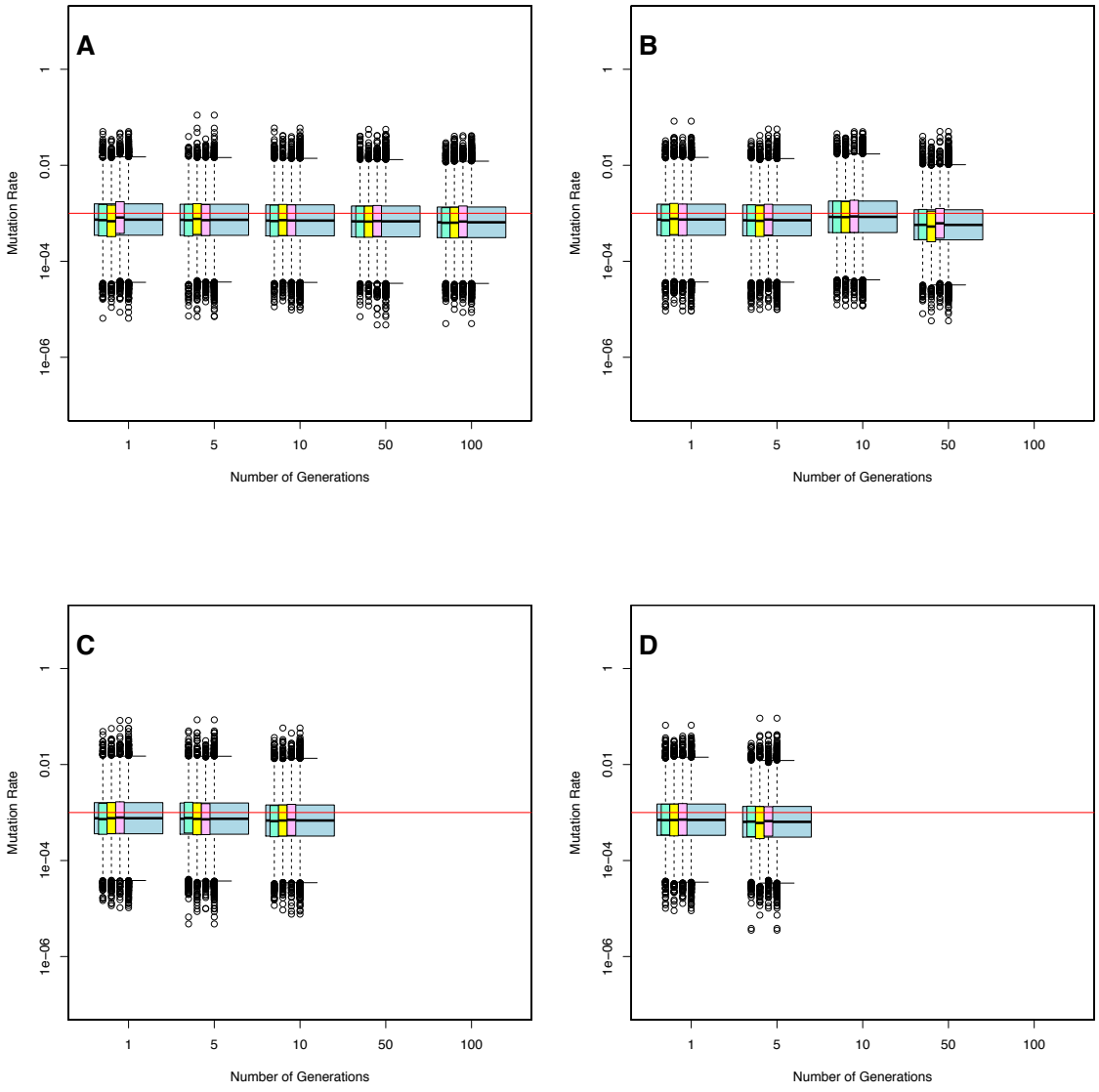

Figure 24 Estimated vs. known μ for scenarios with 20 individuals, 50 microsatellite loci, and N_A =10,000. (A) -1% decline, (B) -5% decline, (C) -10% decline, (D) -50% decline. Red lines indicate the known values of μ at each timepoint. Results are shown only for analyses that converged. Individual runs are shown in green (run 1), yellow (run 2), and pink (run 3), with the pooled results of the three runs in blue.

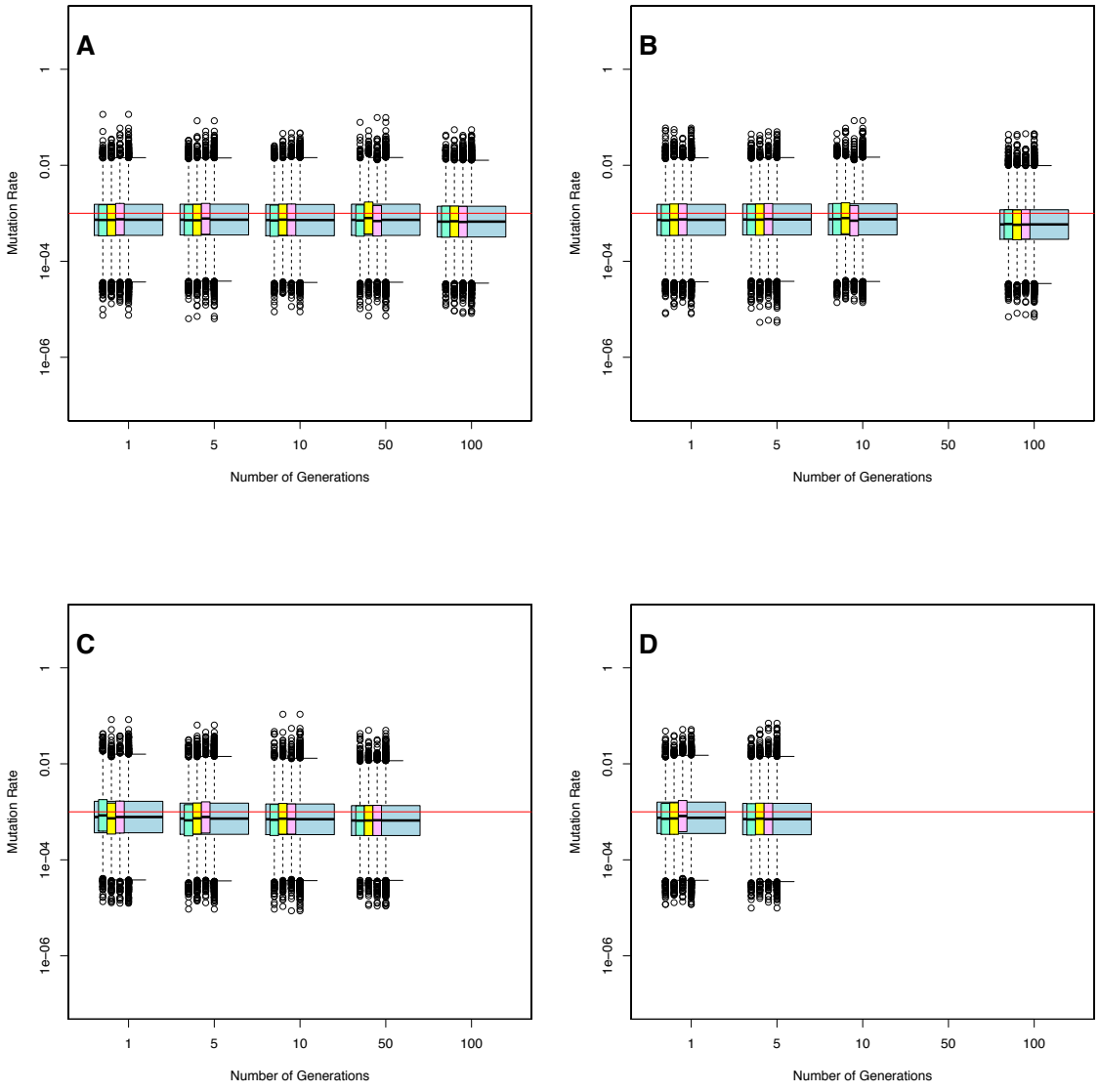

Figure 25. Estimated vs. known μ for scenarios with 20 individuals, 50 microsatellite loci, N_A =100,000, and -1% decline. Red lines indicate the known values of μ at each timepoint. Results are shown only for analyses that converged. Results of individual runs are shown with each box plot in green (run 1), yellow (run 2), and pink (run 3), with the pooled results of the three runs in blue.

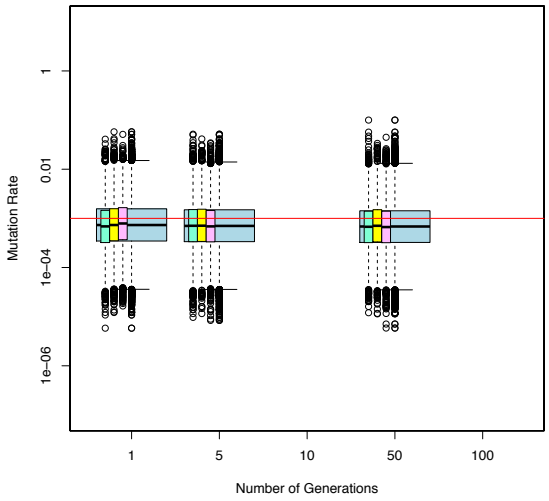

Figure 26. Estimated vs. known μ for scenarios with 50 individuals, 10 microsatellite loci, and N_A =1000. (A) -1% decline, (B) -5% decline, (C) -10% decline, (D) -50% decline. Red lines indicate the known values of μ at each timepoint. Results are shown only for analyses that converged. Individual runs are shown in green (run 1), yellow (run 2), and pink (run 3), with the pooled results of the three runs in blue.

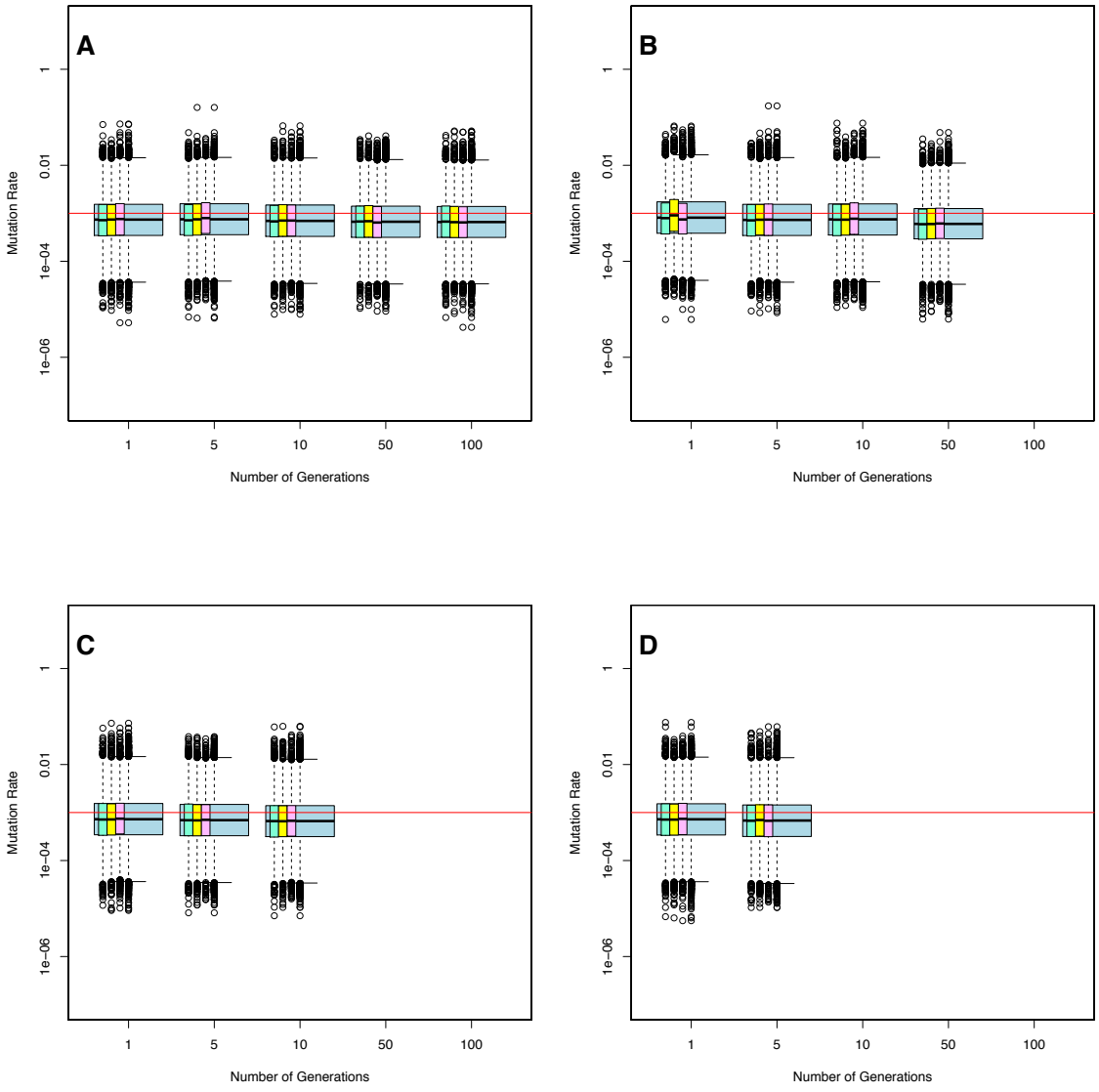

Figure 27. Estimated vs. known μ for scenarios with 50 individuals, 10 microsatellite loci, and N_A =10,000. (A) -1% decline, (B) -5% decline, (C) -10% decline, (D) -50% decline. Red lines indicate the known values of μ at each timepoint. Results are shown only for analyses that converged. Individual runs are shown in green (run 1), yellow (run 2), and pink (run 3), with the pooled results of the three runs in blue.

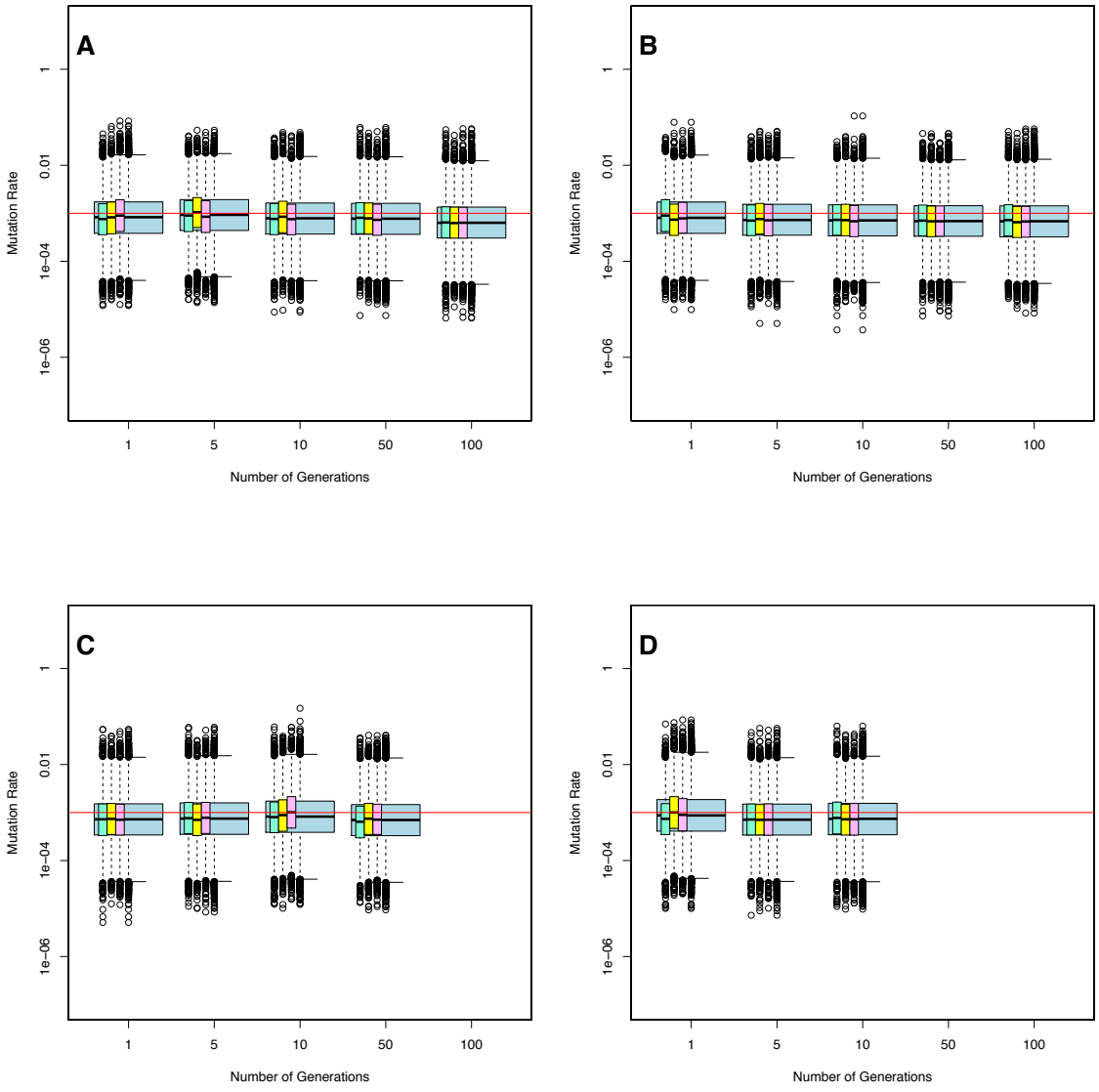

Figure 28. Estimated vs. known μ for scenarios with 50 individuals, 10 microsatellite loci, and N_A =100,000. (A) -1% decline, (B) -5% decline, (C) -10% decline, (D) -50% decline. Red lines indicate the known values of μ at each timepoint. Results are shown only for analyses that converged. Individual runs are shown in green (run 1), yellow (run 2), and pink (run 3), with the pooled results of the three runs in blue.

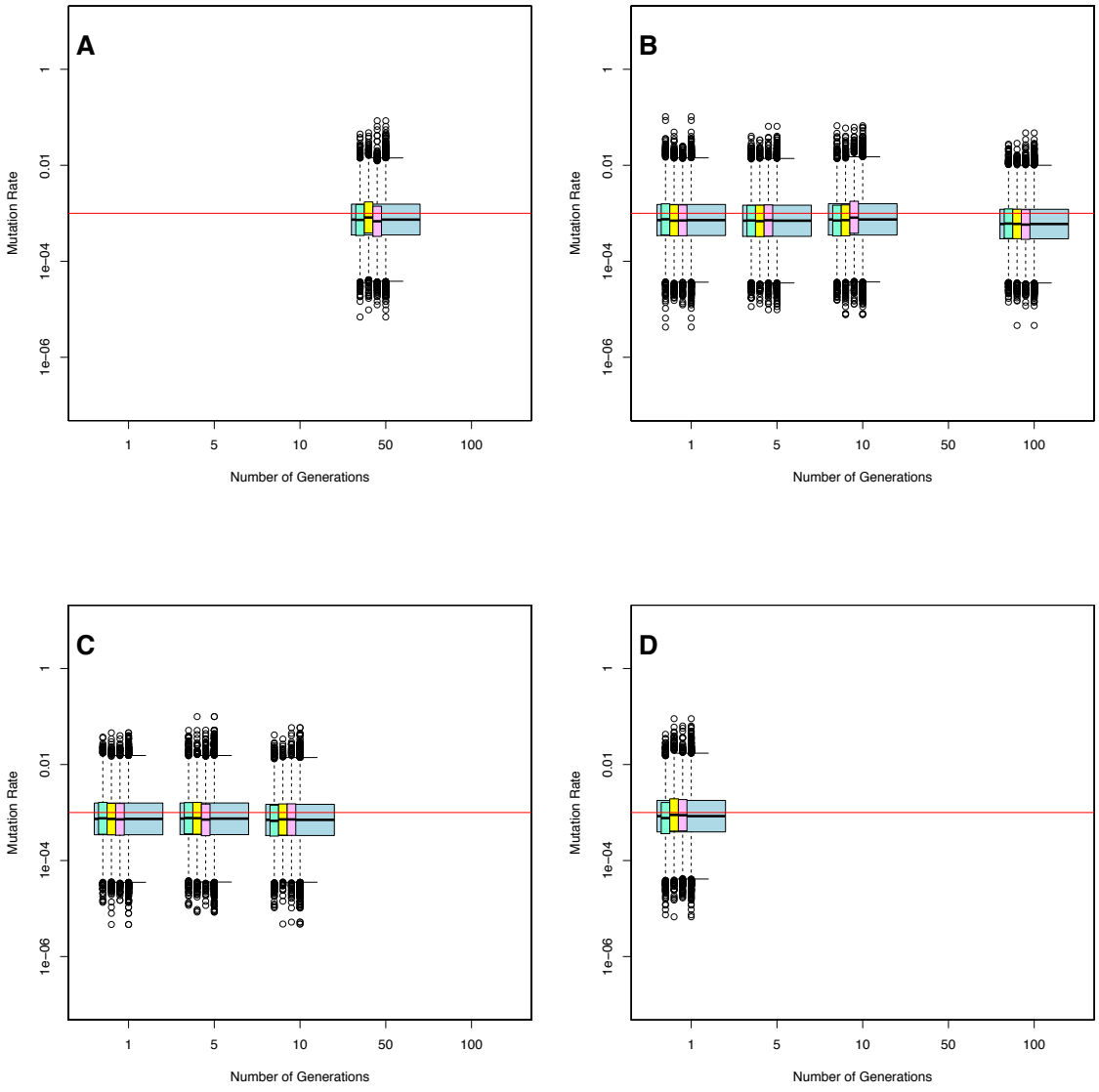

Figure 29. Estimated vs. known μ for scenarios with 20 individuals, 10 microsatellite loci, and N_A =1000. (A) -1% decline, (B) -5% decline, (C) -10% decline, (D) -50% decline. Red lines indicate the known values of μ at each timepoint. Results are shown only for analyses that converged. Individual runs are shown in green (run 1), yellow (run 2), and pink (run 3), with the pooled results of the three runs in blue.

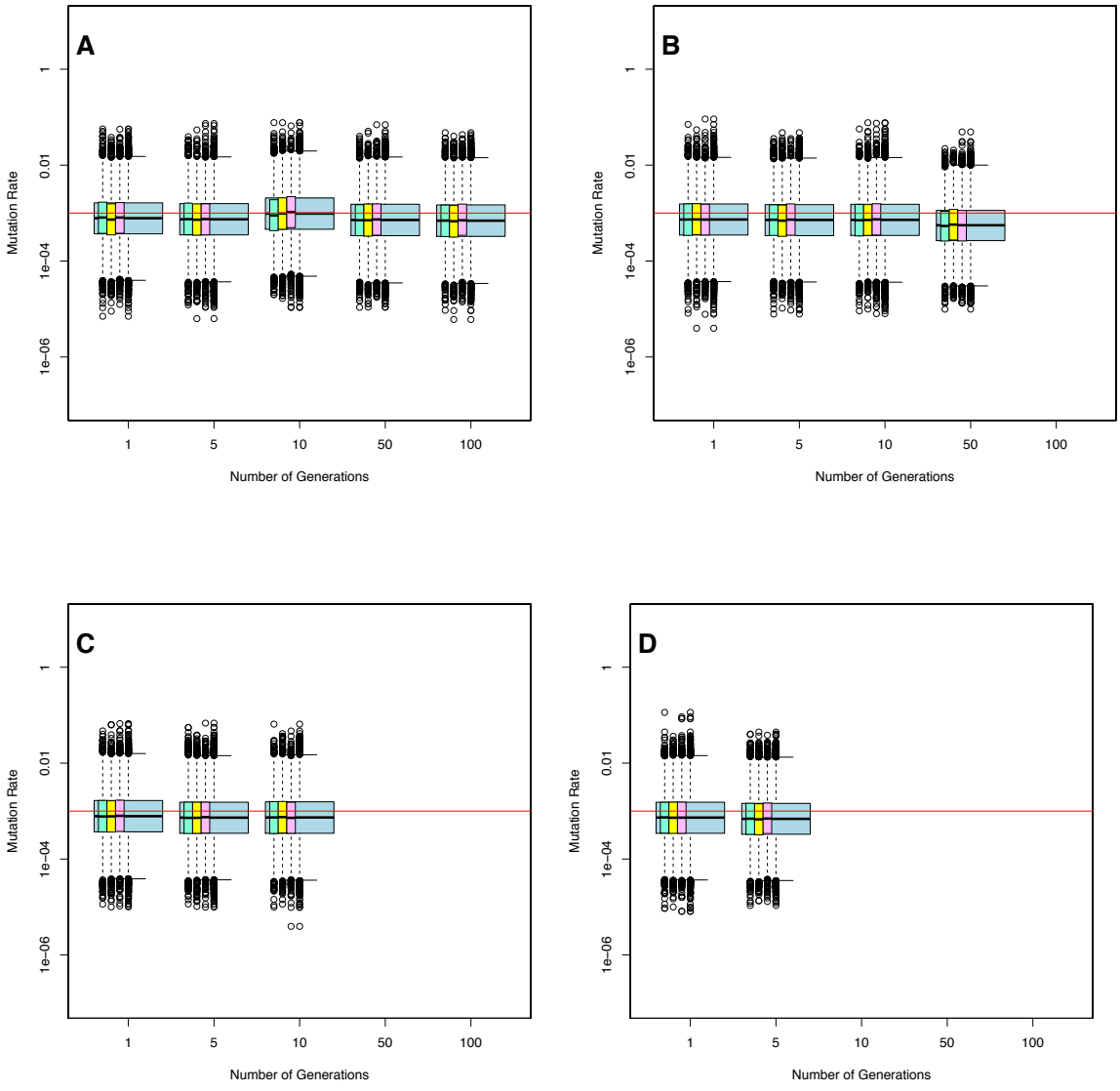

Figure 30. Estimated vs. known μ for scenarios with 20 individuals, 10 microsatellite loci, and N_A =10,000. (A) -1% decline, (B) -5% decline, (C) -10% decline, (D) -50% decline. Red lines indicate the known values of μ at each timepoint. Results are shown only for analyses that converged. Individual runs are shown in green (run 1), yellow (run 2), and pink (run 3), with the pooled results of the three runs in blue.

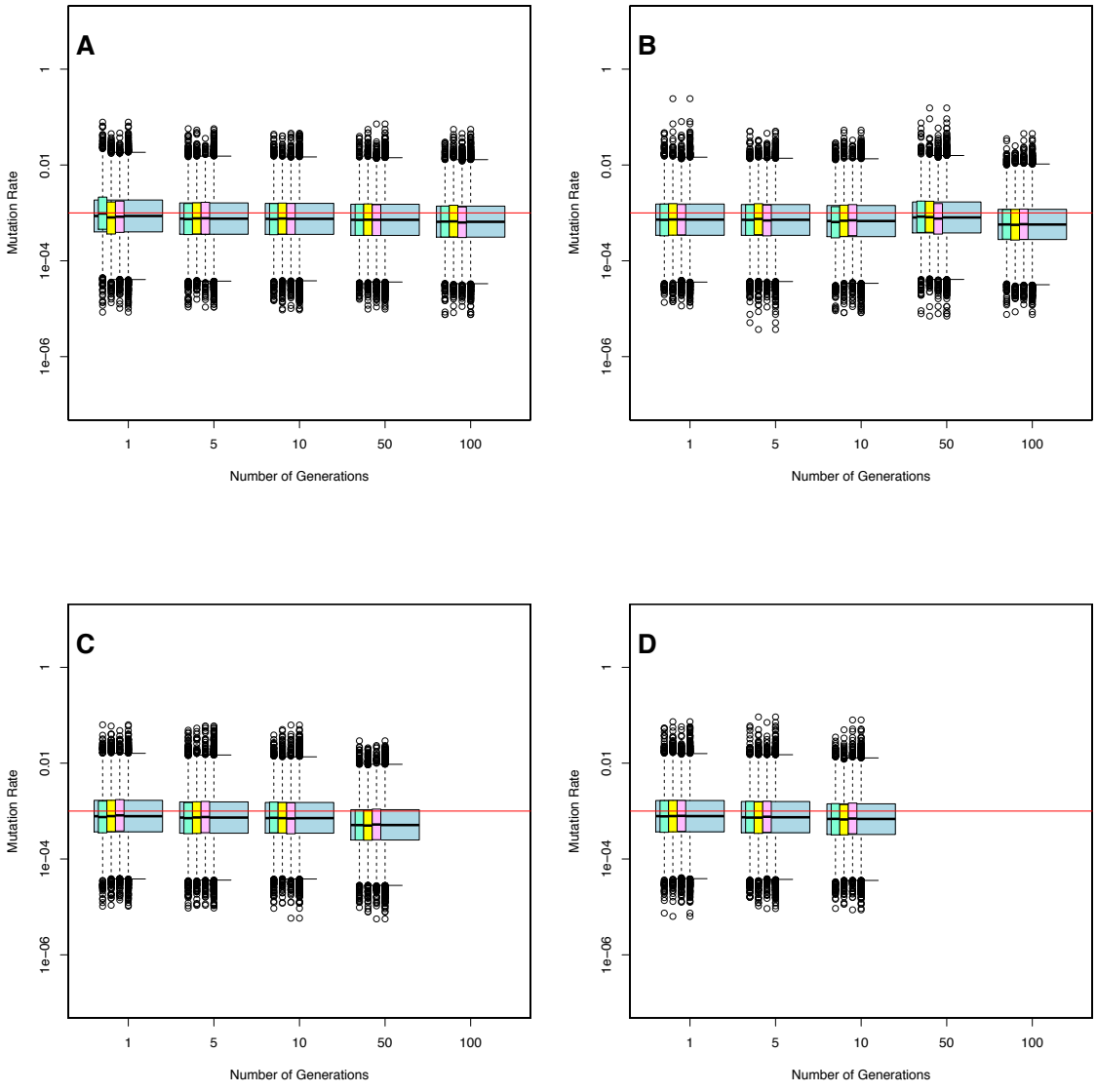

Figure 31. Estimated vs. known μ for scenarios with 20 individuals, 10 microsatellite loci, and N_A =100,000. (A) -1% decline, (B) -5% decline, (C) -10% decline, (D) -50% decline. Red lines indicate the known values of μ at each timepoint. Results are shown only for analyses that converged. Individual runs are shown in green (run 1), yellow (run 2), and pink (run 3), with the pooled results of the three runs in blue.

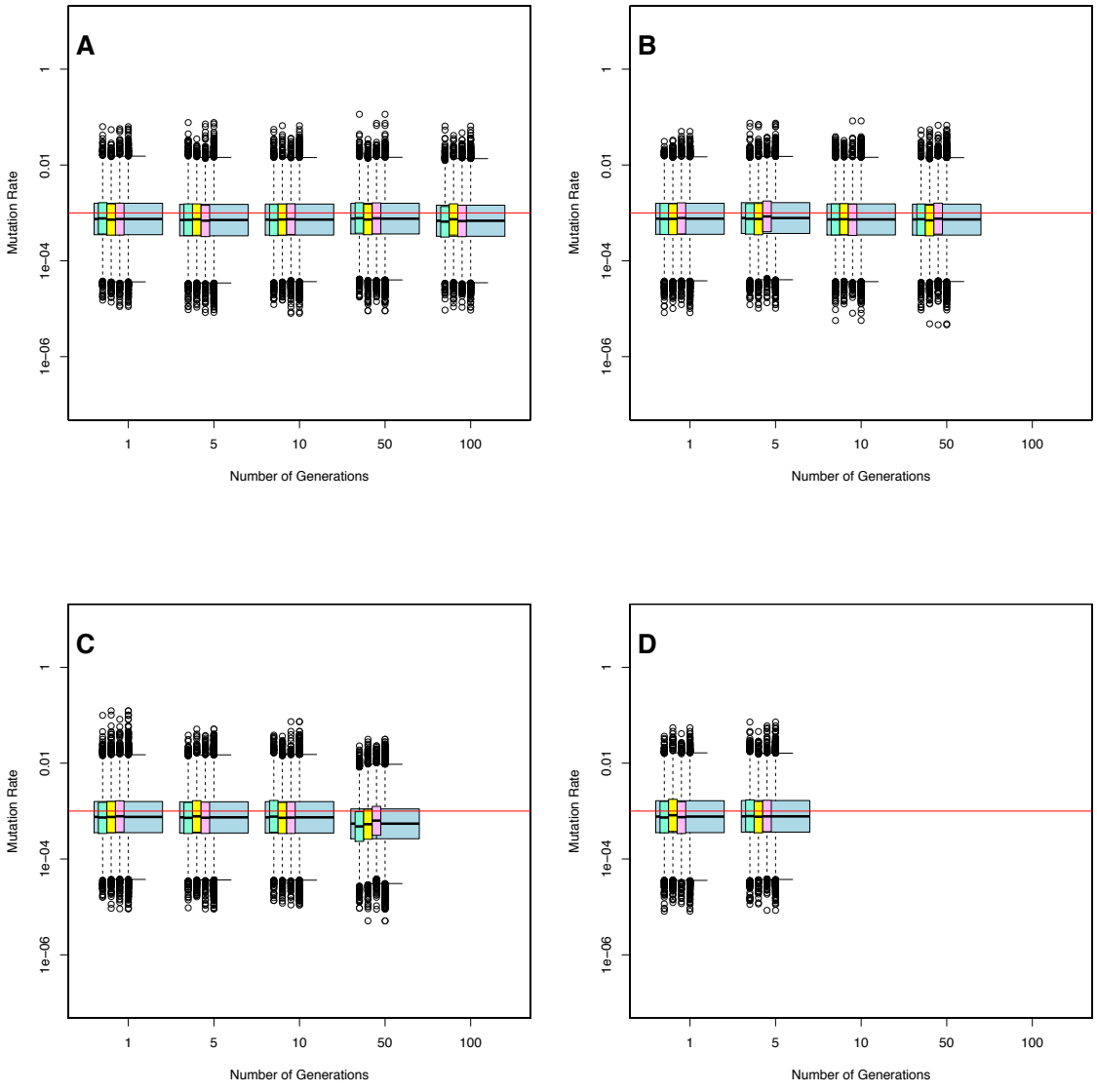

Figure 32. Example posterior probability plots for *t*. Red lines indicate the known parameter value at each timepoint; posterior distributions for the three independent runs are shown as blue, green, and purple curves. A. Results from a demographic scenario of -1% decline over 1 generation from an ancestral population size of 10,000 and a sampling scenario of 20 individuals and 50 loci. B. Results from a demographic scenario of -50% decline over 100 generations from an ancestral population size of 10,000 and a sampling scenario of 50 individuals and 10 loci. C. Results from a demographic scenario of -10% decline over 50 generations from an ancestral population size of 1000 and a sampling scenario of 20 individuals and 50 loci. D. Results from a demographic scenario of -50% decline over 1 generation from an ancestral population size of 10,000 and a sampling scenario of 20 individuals and 50 loci.

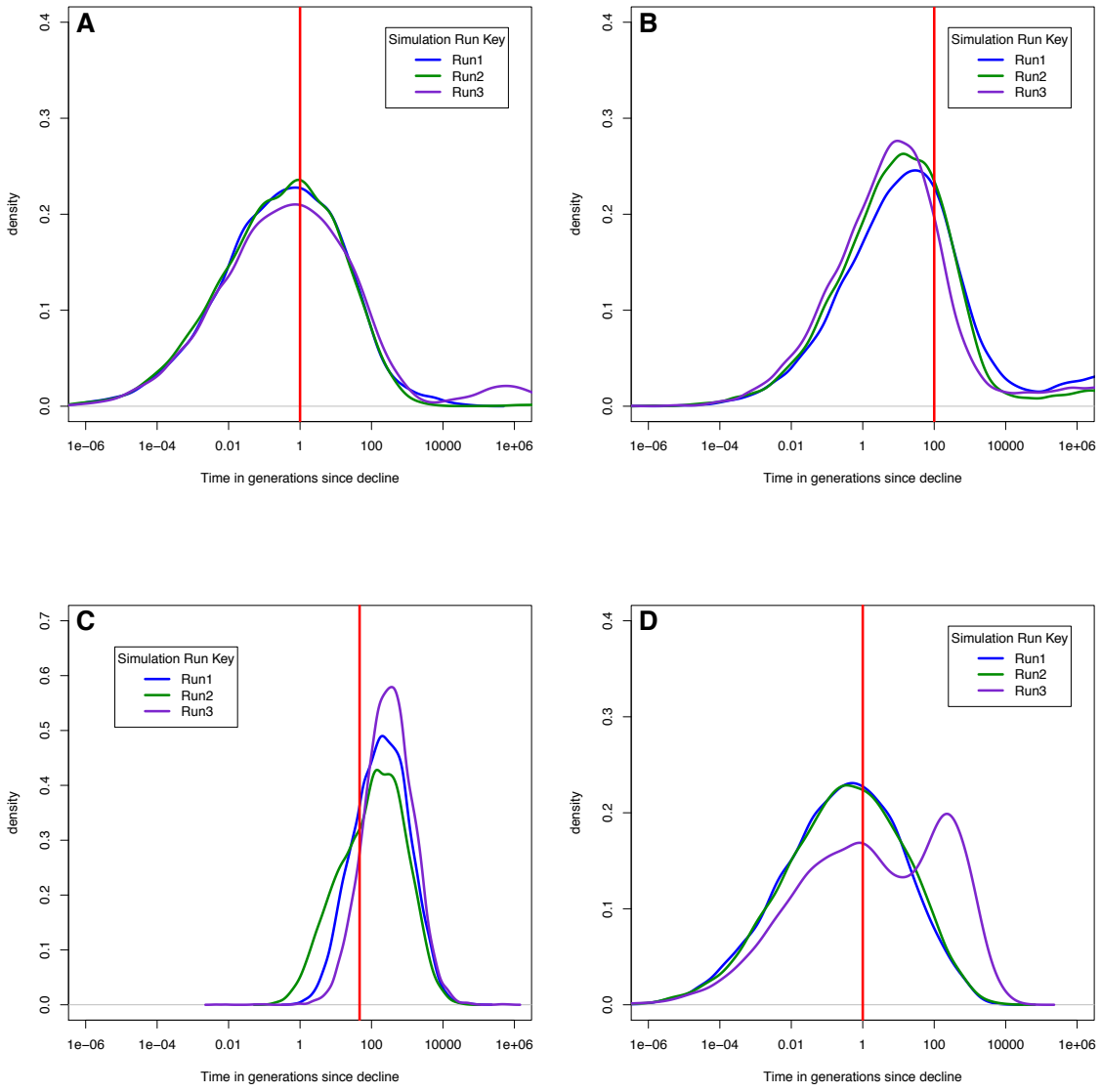

Figure 33. Estimated vs. known generations since decline (t) for scenarios with 20 individuals, 50 microsatellite loci, and N_A =1000. (A) -1% decline, (B) -5% decline, (C) -10% decline, (D) -50% decline. Red lines indicate the known values of t at each timepoint. Results are shown only for analyses that converged. Results of individual runs are shown in green (run 1), yellow (run 2), and pink (run 3), with the pooled results of the three runs in blue.

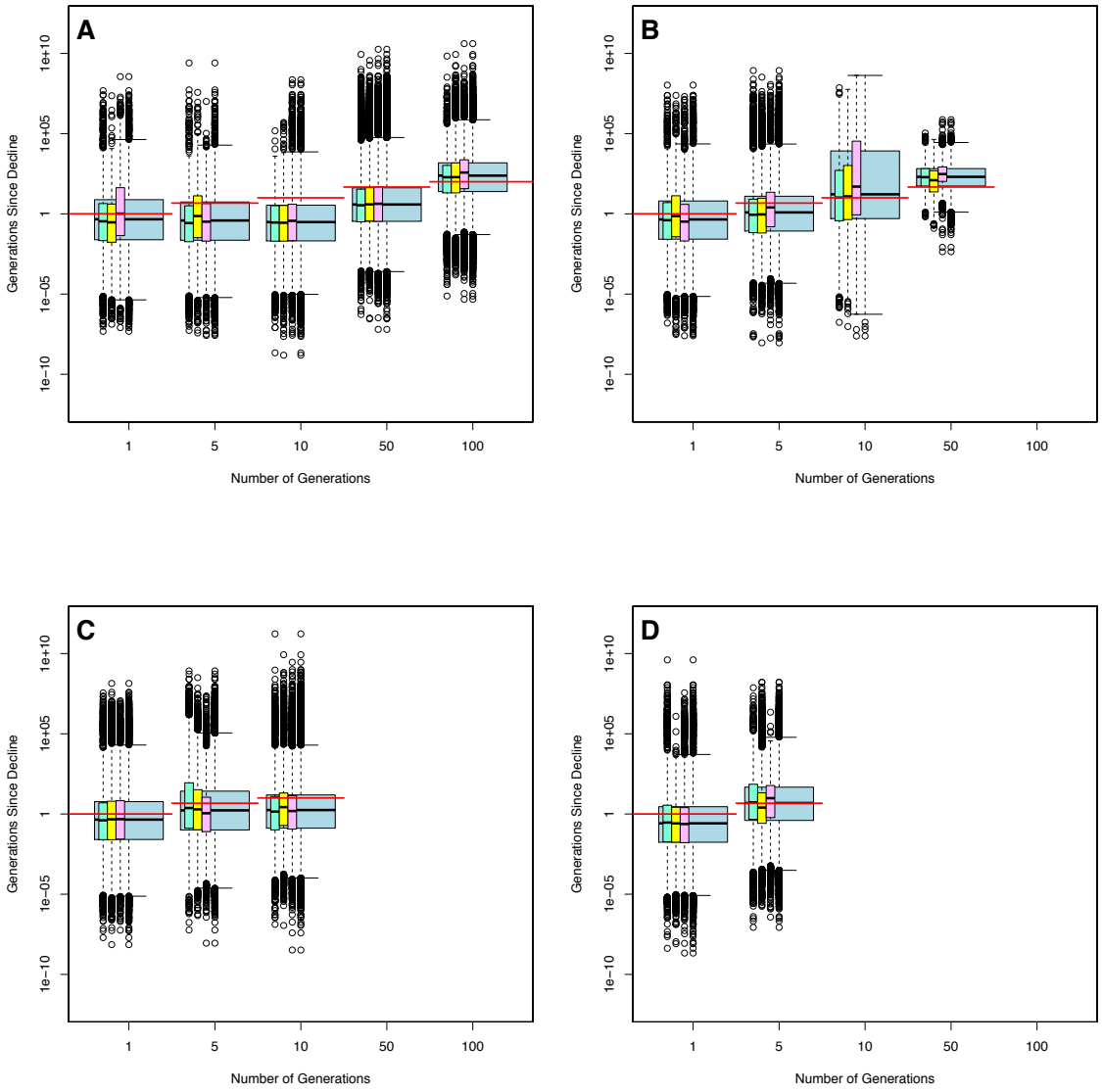

Figure 34. Estimated vs. known generations since decline (t) for scenarios with 20 individuals, 50 microsatellite loci, and N_A =10,000. (A) -1% decline, (B) -5% decline, (C) -10% decline, (D) -50% decline. Red lines indicate the known values of t at each timepoint. Results are shown only for analyses that converged. Results of individual runs are shown in green (run 1), yellow (run 2), and pink (run 3), with the pooled results of the three runs in blue.

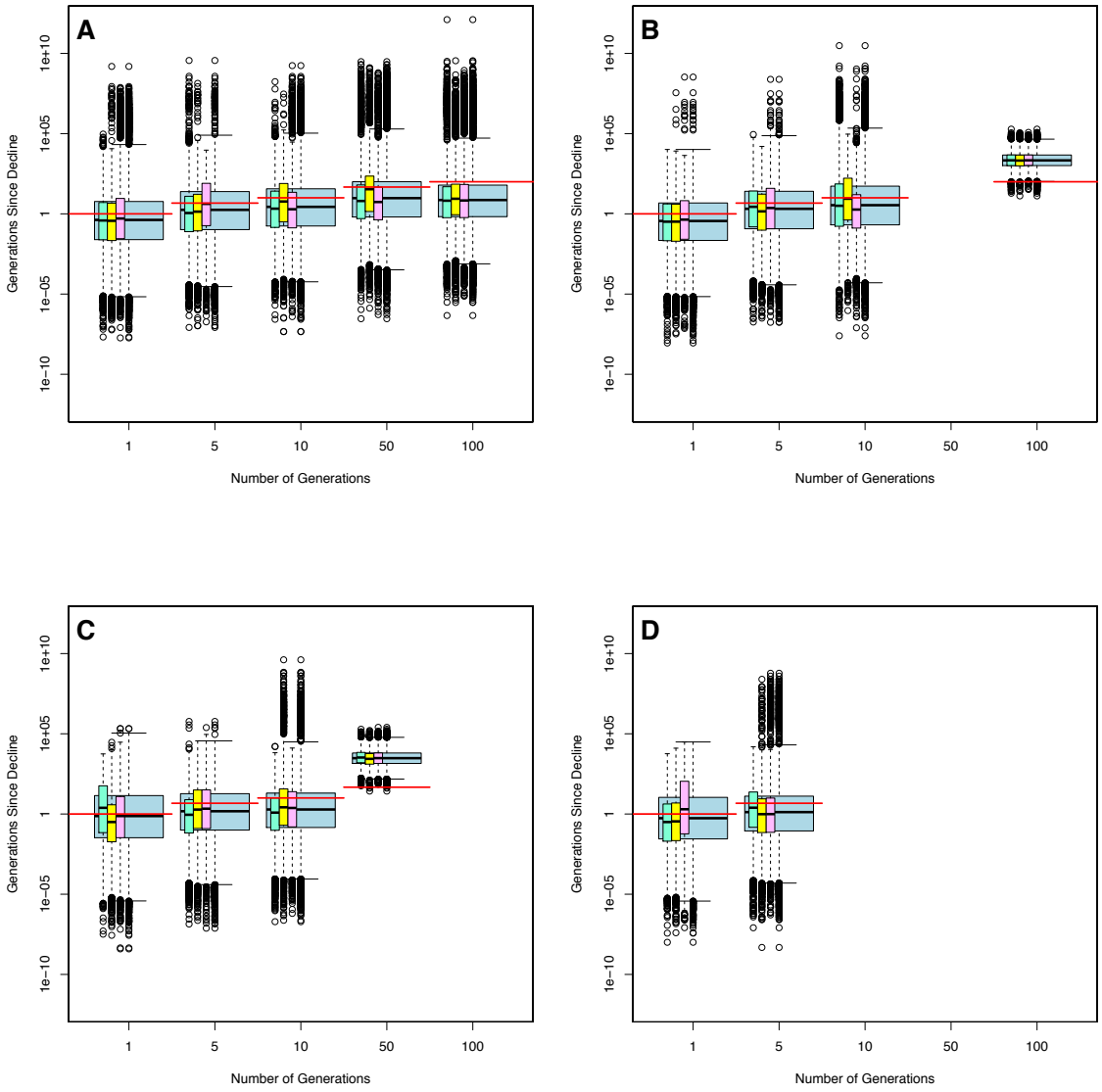

Figure 35. Estimated vs. known generations since decline (t) for scenarios with 20 individuals, 50 microsatellite loci, N_A =100,000, and -1% decline. Red lines indicate the known values of t at each timepoint. Results are shown only for analyses that converged. Results of individual runs are shown in green (run 1), yellow (run 2), and pink (run 3), with the pooled results of the three runs in blue.

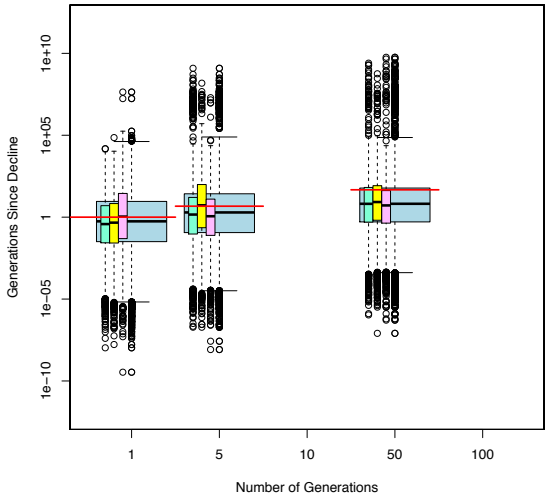

Figure 36. Estimated vs. known generations since decline (t) for scenarios with 50 individuals, 10 microsatellite loci, and N_A =1000. (A) -1% decline, (B) -5% decline, (C) -10% decline, (D) -50% decline. Red lines indicate the known values of t at each timepoint. Results are shown only for analyses that converged. Results of individual runs are shown in green (run 1), yellow (run 2), and pink (run 3), with the pooled results of the three runs in blue.

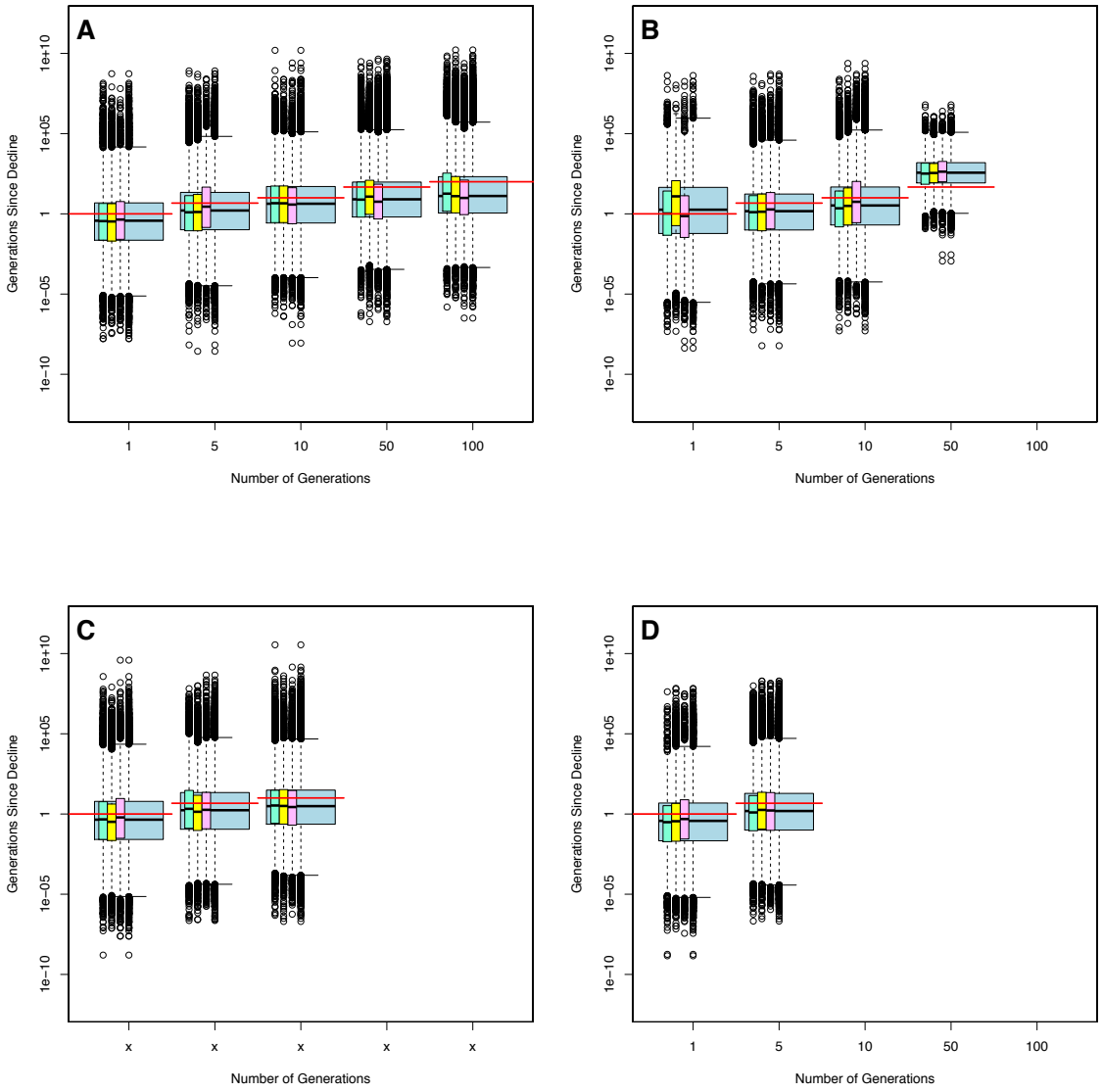

Figure 37. Estimated vs. known generations since decline (t) for scenarios with 50 individuals, 10 microsatellite loci, and N_A =10,000. (A) -1% decline, (B) -5% decline, (C) -10% decline, (D) -50% decline. Red lines indicate the known values of t at each timepoint. Results are shown only for analyses that converged. Results of individual runs are shown in green (run 1), yellow (run 2), and pink (run 3), with the pooled results of the three runs in blue.

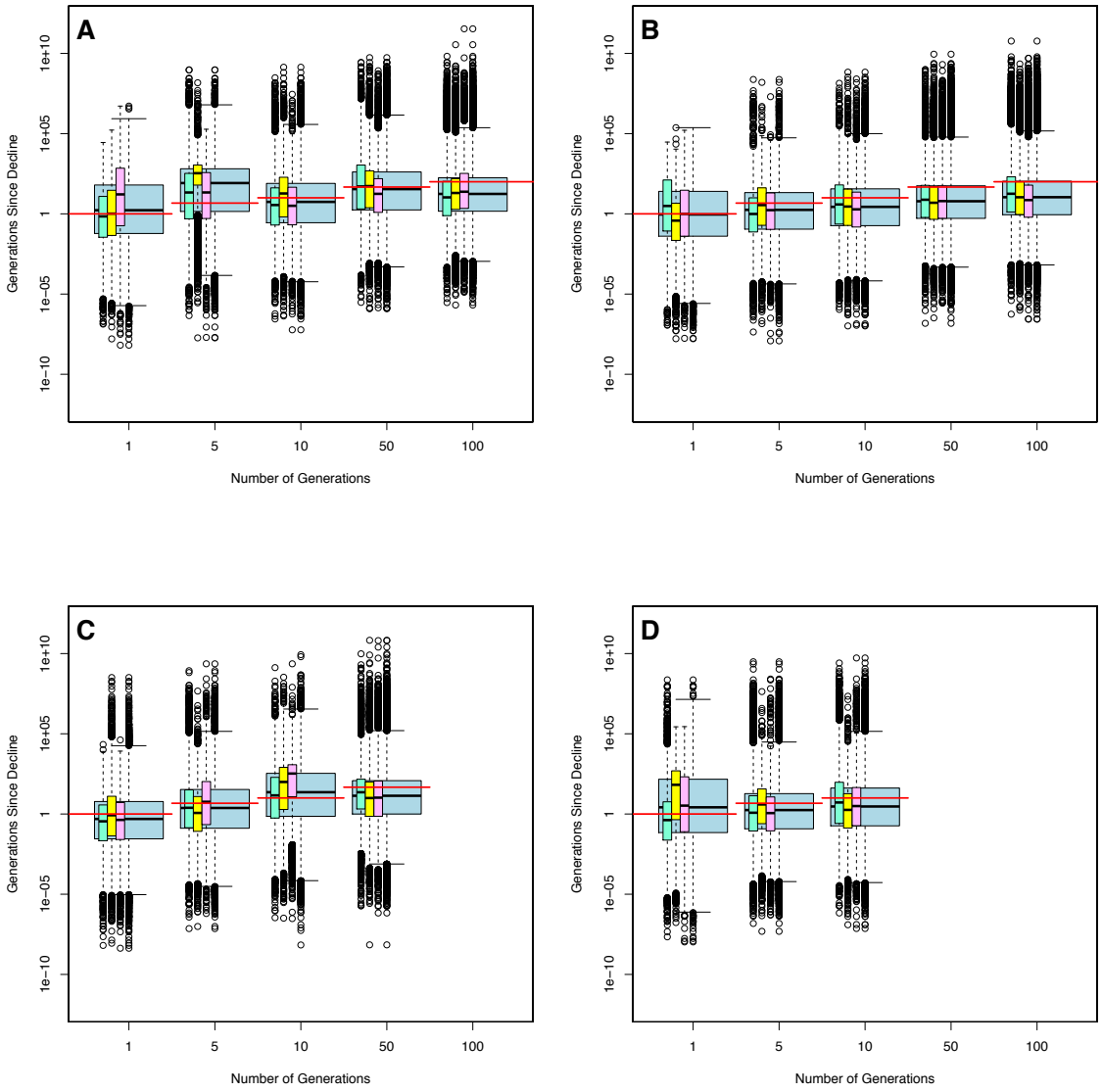

Figure 38. Estimated vs. known generations since decline (t) for scenarios with 50 individuals, 10 microsatellite loci, and N_A =100,000. (A) -1% decline, (B) -5% decline, (C) -10% decline, (D) -50% decline. Red lines indicate the known values of t at each timepoint. Results are shown only for analyses that converged. Results of individual runs are shown in green (run 1), yellow (run 2), and pink (run 3), with the pooled results of the three runs in blue.

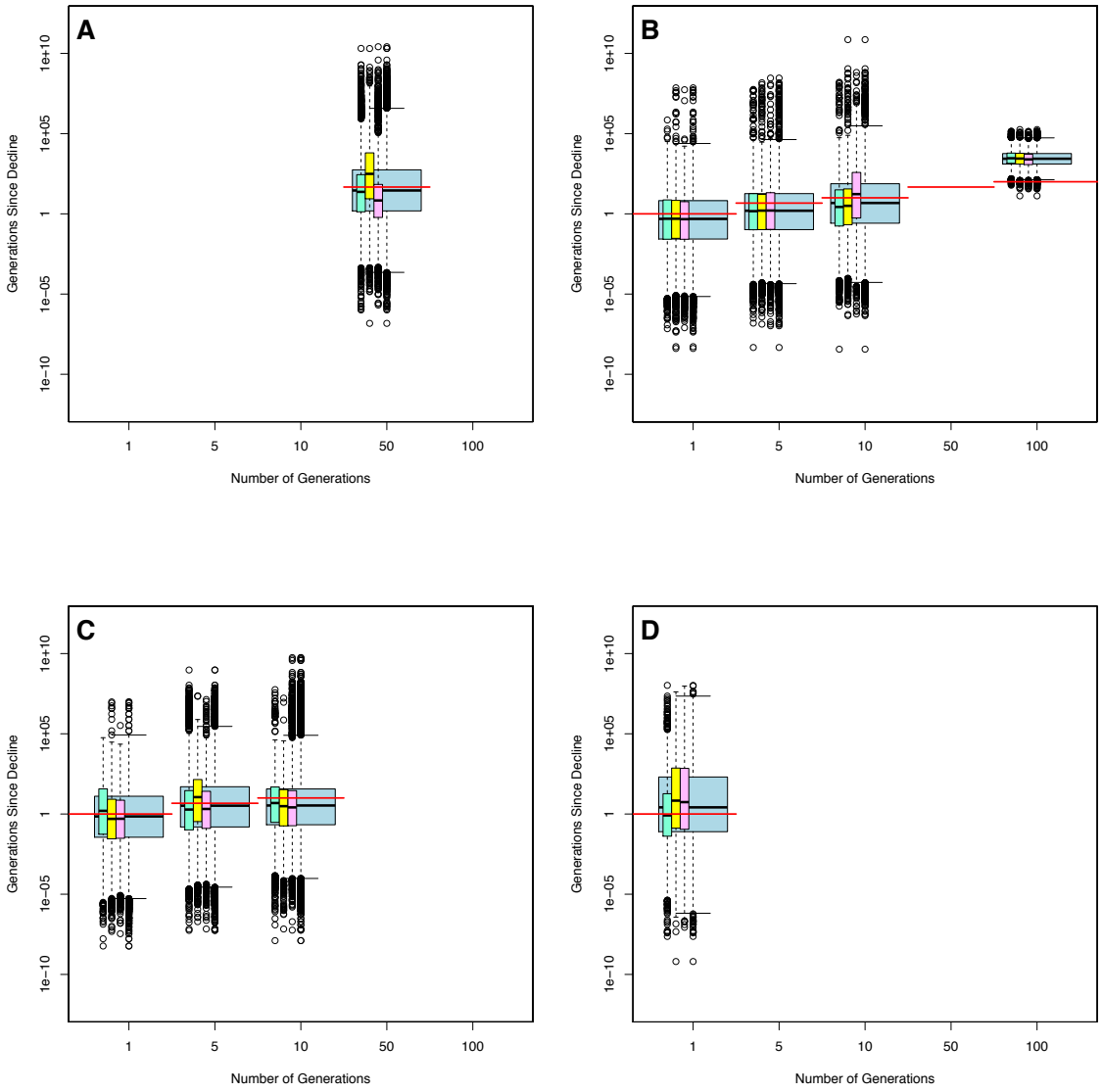

Figure 39. Estimated vs. known generations since decline (t) for scenarios with 20 individuals, 10 microsatellite loci, and N_A =1000. (A) -1% decline, (B) -5% decline, (C) -10% decline, (D) -50% decline. Red lines indicate the known values of t at each timepoint. Results are shown only for analyses that converged. Results of individual runs are shown in green (run 1), yellow (run 2), and pink (run 3), with the pooled results of the three runs in blue.

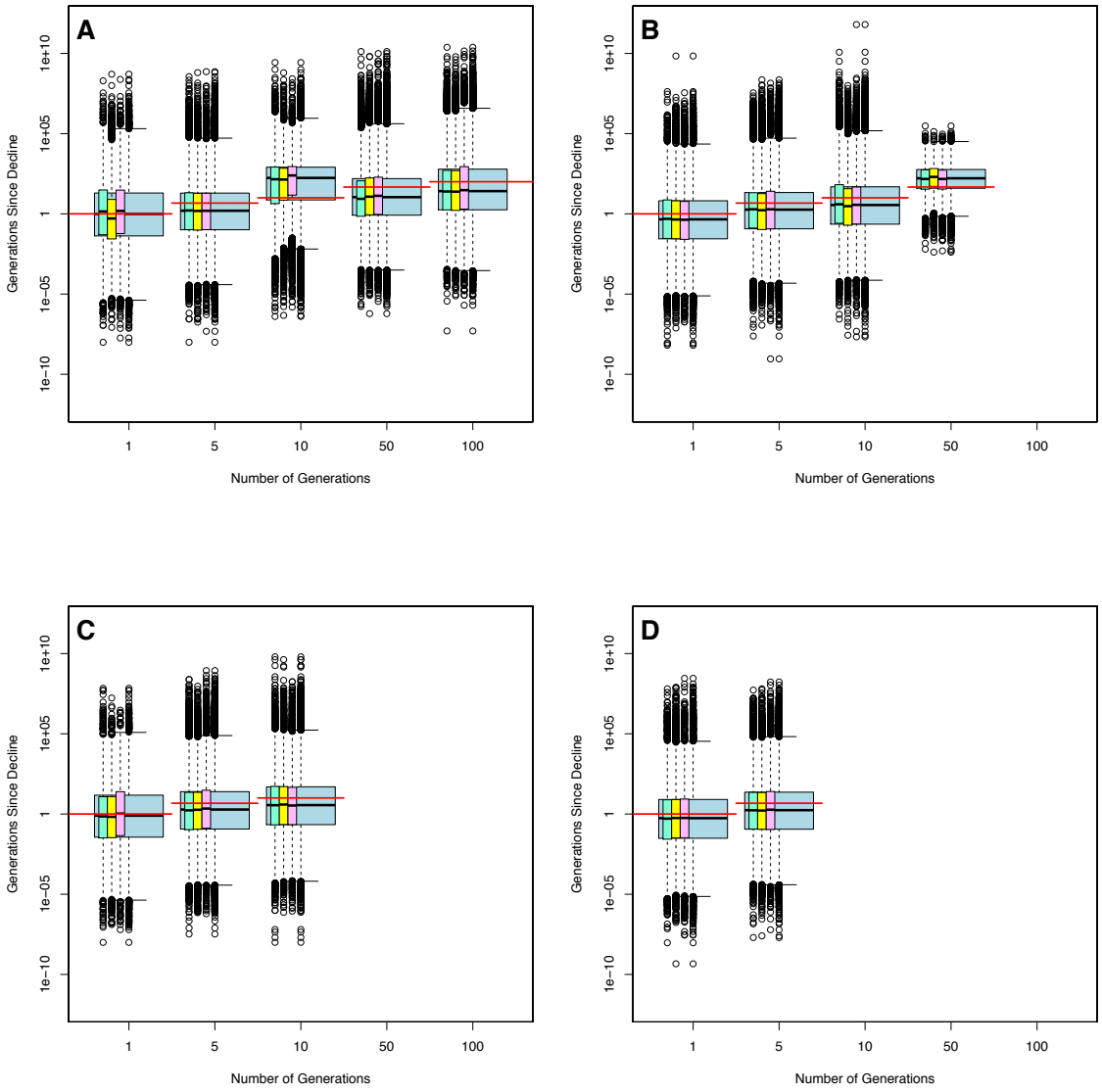

Figure 40. Estimated vs. known generations since decline (t) for scenarios with 20 individuals, 10 microsatellite loci, and N_A =10,000. (A) -1% decline, (B) -5% decline, (C) -10% decline, (D) -50% decline. Red lines indicate the known values of t at each timepoint. Results are shown only for analyses that converged. Results of individual runs are shown in green (run 1), yellow (run 2), and pink (run 3), with the pooled results of the three runs in blue.

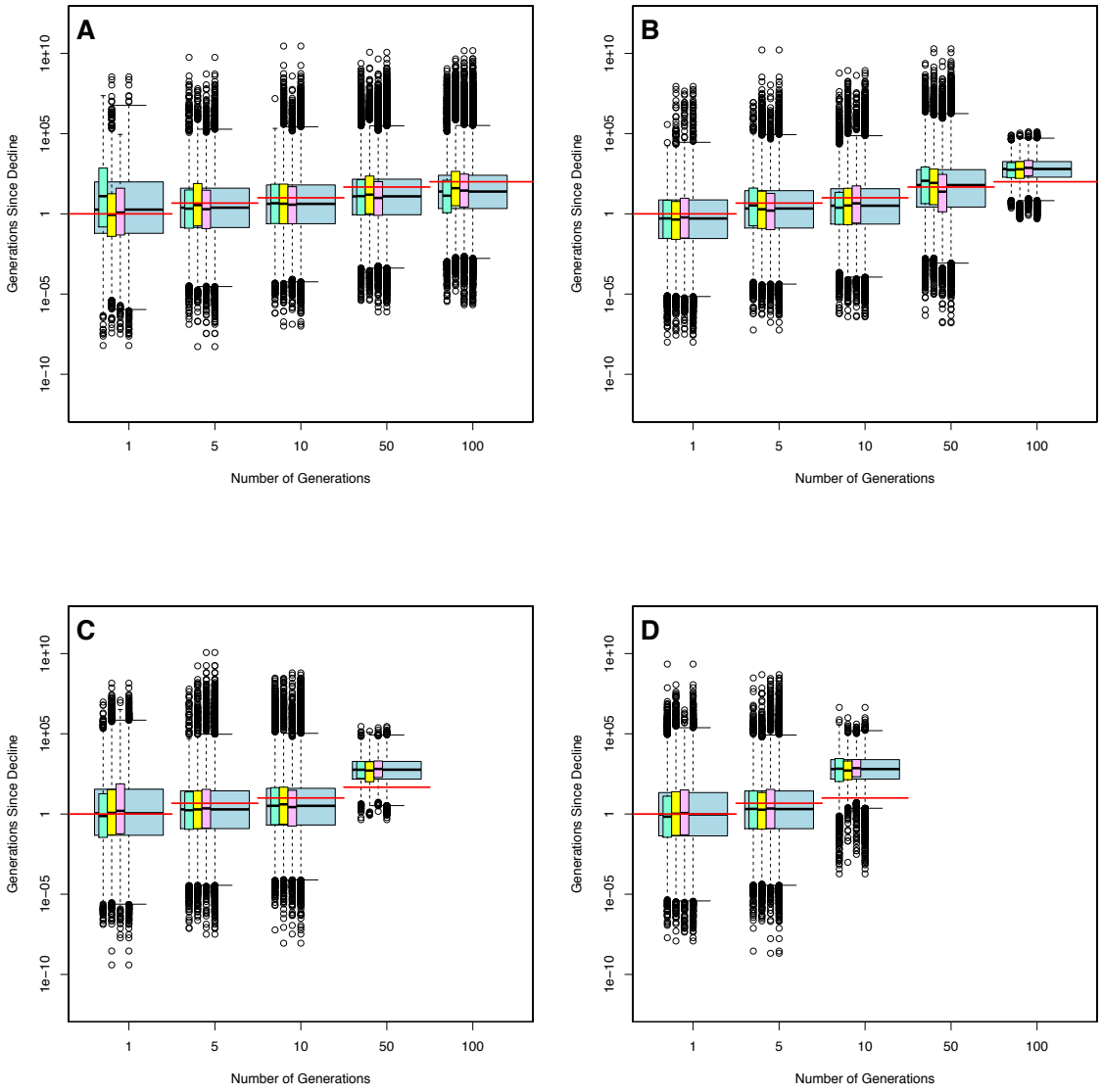

Figure 41. Estimated vs. known generations since decline (t) for scenarios with 20 individuals, 10 microsatellite loci, and N_A =100,000. (A) -1% decline, (B) -5% decline, (C) -10% decline, (D) -50% decline. Red lines indicate the known values of t at each timepoint. Results are shown only for analyses that converged. Results of individual runs are shown in green (run 1), yellow (run 2), and pink (run 3), with the pooled results of the three runs in blue.

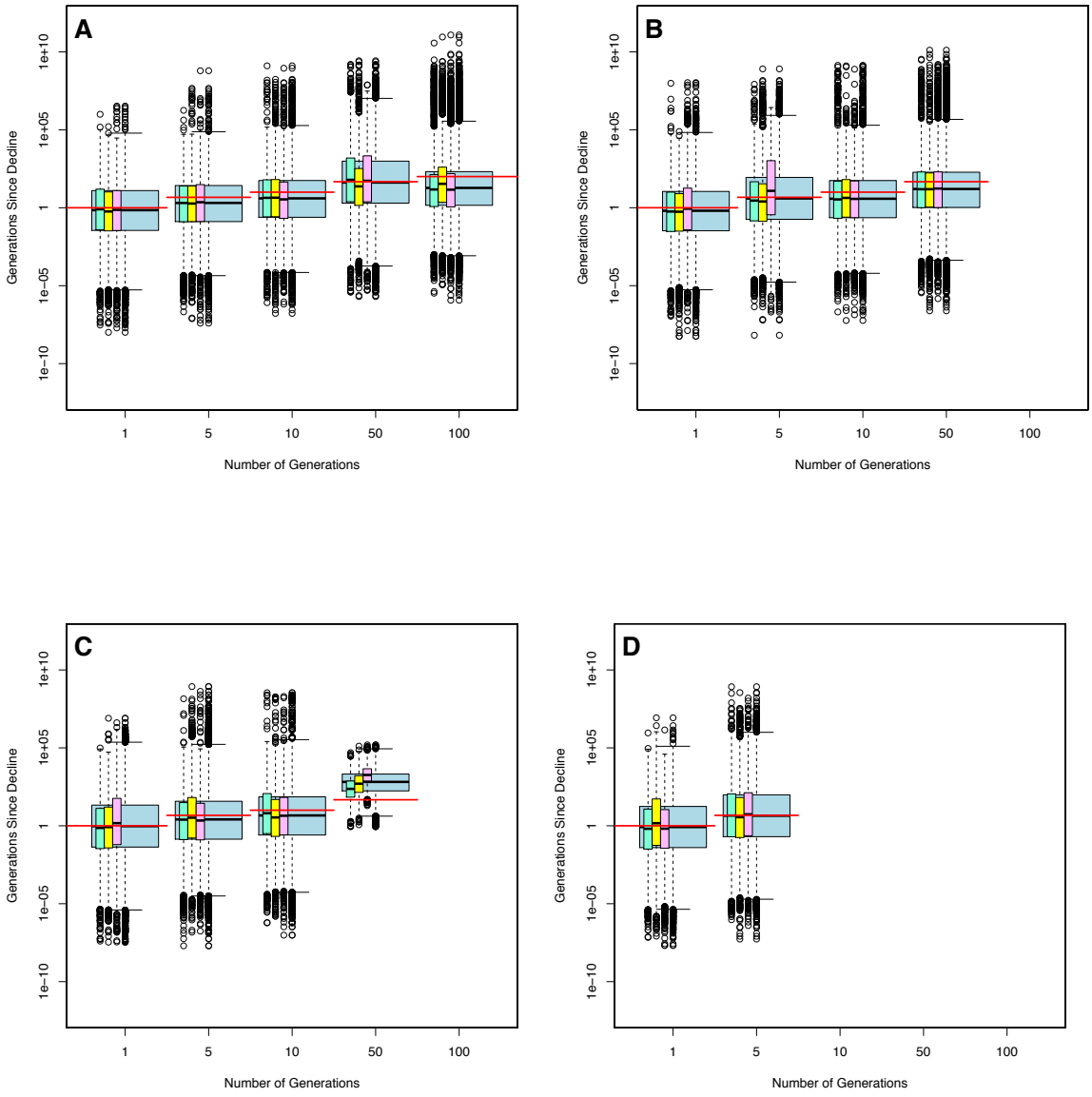

REFERENCES:

Allendorf FW, Luikart G, Aitken SN (2013) *Conservation and the Genetics of Populations, 2nd edn.* Wiley-Blackwell Publishing, West Sussex.

Amos W, Balmford A (2001) When does conservation genetics matter? *Heredity,* **87**, 257-265.

Anmarkrud JA, Kleven O, Augustin J, Bentz KH, Blomqvist D, *et al.* (2011) Factors affecting germline mutations in a hypervariable microsatellite: a comparative analysis of six species of swallows (Aves: Hirundinidae). *Mutation Research*, **708**, 37-43.

Antao T, Perez-Figueroa A, Luikart G (2011) Early detection of population declines: high power of genetic monitoring using effective population size estimators. *Evolutionary Applications,* **4**, 144-154.

Ardren WR, Kapuscinski AR (2003) Demographic and genetic estimates of effective population size (N_e) reveals genetic compensation in steelhead trout. *Molecular Ecology*, **12**, 35-49.

Arnett EB, Baerwald EF (2013) Impacts of wind energy development on bats: implications for conservation. In *Bat Evolution, Ecology, and Conservation* (eds. Adams RA, Pederson SC), pp. 435-456. Springer Science & Business Media, New York.

Arnett EB, Brown K, Erickson WP, Fiedler JK, Hamilton BL, *et al.* (2008) Patterns of bat fatalities at wind energy facilities in North America. *Journal of Wildlife Management*, **72**, 61-78.

Arnett EB, Hein CD, Schirmacher MR, Huso MM, Szewczak JM (2013) Evaluating the effectiveness of an ultrasonic acoustic deterrent for reducing bat fatalities at wind turbines. *PLoS ONE*, **8**, e65794.

Arroyo-Cabrales J, Miller B, Reid F, Cuarón AD, de Grammont PC (2008) *Lasiurus borealis*. The IUCN Red List of Threatened Species. Version 2015.2 www.iucnredlist.org. Downloaded on 30 July 2015.

Barclay R, Baerwald EF, Gruver JC (2007) Variation in bat and bird fatalities at wind energy facilities: assessing the effects of rotor size and tower height. *Canadian Journal of Zoology,* **85**, 381-387.

Bartley D, Bagley M, Gall G, Bentley B (1992) Use of linkage disequilibrium data to estimate effective size of hatchery and natural fish populations. *Conservation Biology*, **6**, 365-375.

Baum JK, Myers RA, Kehler DG, Worm B, Harley SJ, *et al.* (2003) Collapse and conservation of shark populations in the northwest Atlantic. *Science*, **299**, 389.

Beaumont MA (1999) Detecting population expansion and decline using microsatellites. *Genetics*, **153**, 2013-2029.

Beaumont MA, Zhang W, Balding DJ (2002) Approximate Bayesian computation in population genetics. *Genetics*, **162**, 2025-2035.

Blehert DS, Hicks AC, Behr M, Meteyer CU, Berlowski-Zier BM, *et al.* (2009) Bat white-nose syndrome: an emerging fungal pathogen? *Science,* **323**, 227.

Bourke BP, Frantz AC (2010) Genetic signatures of population change in the British golden eagle (*Aquila chrysaetos*). *Conservation Genetics*, **11**, 1837-1846.

Brinkmann B, Klintschar M, Neuhuber F, Hühne J, Rolf B (1998) Mutation rate in human microsatellites: influence of the structure and length of the tandem repeat. *American Journal of Human Genetics*, **62**, 1408-1415.

Coleman JTH, Reichard JD (2014) Bat white-nose syndrome in 2014: a brief assessment seven years after discovery of a virulent fungal pathogen in North America. *Outlooks on Pest Management*, **25**, 374-377.

Cornuet JM, Luikart G (1996) Description and power analysis of two tests for detecting recent population bottlenecks from allele frequency data. *Genetics,* **144**, 2001-2014.

Cornuet JM, Piry S, Luikart G, Estoup A, Solignac M (1999) New methods employing multilocus genotypes to select or exclude populations as origins of individuals. *Genetics*, **153**, 1989-2000.

Cryan PM (2011) Wind turbines as landscape impediments to the migratory connectivity of bats. *Environmental Law*, **41**, 355-370.

Cryan PM, Barclay R (2009) Causes of bat fatalities at wind turbines: hypotheses and predictions. *Journal of Mammalogy,* **90**, 1330-1340.

Cryan PM, Jameson JW, Baerwald EF (2012) Evidence of late-summer mating readiness and early sexual maturation in migratory tree-roosting bats found dead at wind turbines. *PLoS ONE,* **7**, e47586.

David L, Blum S, Feldman MW, Lavi U, Hillel J (2003) Recent duplication of the common carp (*Cyprinus carpio* L.) genome as revealed by analyses of microsatellite loci. *Molecular Biology and Evolution*, **20**, 1425-1434.

Dietrich W, Katz H, Lincoln S, Shin HS, Friedman J, *et al.* (1992) A genetic map of the mouse suitable for typing intraspecific crosses. *Genetics*, **131**, 423-447.

Driscoll DA (1999) Genetic neighbourhood and effective population size for two endangered frogs. *Biological Conservation*, **88**, 221-229.

Edwards AL, Hammond HA, Jin L, Caskey CT, Chakraborty R (1992) Genetic variation at five trimeric and tetrameric tandem repeat loci in four human population groups. *Genomics*, **12**, 241-253.

Ellegren H (1995) Mutation rates at porcine microsatellite loci. *Mammalian Genome*, **6**, 376-377.

Ellison LE, Wunder MB, Jones CA, Mosch C, Navo KW, *et al.* (2003) Colorado bat conservation plan. Colorado Committee of the Western Bat Working Group. Available at http://www.cnhp.colostate.edu/teams/zoology/cbwg/pdfs/ColoradoBatConservationPlanFebruary2004.pdf

Felsenstein J (2006) Accuracy of coalescent likelihood estimates: do we need more sites, more sequences, or more loci? *Molecular Biology and Evolution*, **23**, 691-700.

Frankham R (1995) Conservation genetics. *Annual Review of Genetics*, **29**, 305-327.

Frankham R (2005) Genetics and extinction. *Biological Conservation*, **126**, 131-140.

Fu YX (2006) Exact coalescent for the Wright-Fisher model. *Theoretical Population Biology*, **69**, 385-394.

Garza JC, Williamson EG (2001) Detection of reduction in population size using data from microsatellite loci. *Molecular Ecology,* **10**, 305-318.

Girod C, Vitalis R, Leblois R, Fréville H (2011) Inferring population decline and expansion from microsatellite data: a simulation-based evaluation of the msvar method. *Genetics*, **188**, 165-179.

Goldstein DB, Pollock DD (1997) Launching microsatellites: a review of mutation processes and methods of phylogenetic inference. *Journal of Heredity*, **88**, 335-342.

Groombridge JJ, Jones CG, Bruford MW, Nichols RA (2000) 'Ghost' alleles of the Mauritius kestrel. *Nature*, **403**, 616.

Gutenkunst RN, Hernandez RD, Williamson SH, Bustamante CD (2009) Inferring the joint demographic history of multiple populations from multidimensional SNP frequency data. *PLoS Genetics*, **5**, e1000695.

Haasl RJ, Payseur BA (2010) The number of alleles at a microsatellite defines the allele frequency spectrum and facilitates fast accurate estimation of θ. *Molecular Biology and Evolution*, **27**, 2702-2715.

Halliday TR (1980) The extinction of the passenger pigeon *Ectopistes migratorius* and its relevance to contemporary conservation. *Biological Conservation*, **17**, 157-162.

Hare MP, Nunney L, Schwartz MK, Ruzzante DE, Bruford M (2011) Understanding and estimating effective population size for practical application in marine species management. *Conservation Biology*, **25**, 438-449.

Harrad H, Jackson T (1961) *Mammals of Wisconsin*. University of Wisconsin Press, Madison.

Harvey MJ, Altenback JS, Best TR (2011) *Bats of the United States and Canada.* The Johns Hopkins University Press, Baltimore.

Hauser L, Adcock GJ, Smith PJ, Bernal Ramirez JH, Carvalho GR (2002) Loss of microsatellite diversity and low effective population size in an overexploited population of New Zealand snapper (*Pagrus auratus*). *Proceedings of the National Academy of Sciences, USA*, **99**, 11742-11747.

Hedrick PW, Peterson RO, Vucetich LM, Adams JR, Vucetich JA (2014) Genetic rescue in Isle Royale wolves: genetic analysis and the collapse of the population. *Conservation Genetics*, **15**, 1111-1121.

Hein J, Schierup MH, Wiuf C (2004) *Gene Genealogies, Variation and Evolution: A Primer in Coalescent Theory*. Oxford University Press, Oxford.

Hill WG (1972) Effective size of populations with overlapping generations. *Theoretical Population Biology*, **3**, 278-289.

Hoban S, Arntzen JA, Bruford MW, Godoy JA, Hoelzel AR, *et al*. (2014) Comparative evaluation of potential indicators and temporal sampling protocols for monitoring genetic erosion. *Evolutionary Applications*, **7**, 984-998.

Horn JW, Arnett EB, Jensen M, Kunz TH (2008) Testing the effectiveness of an experimental acoustic bat deterrent at the Maple Ridge wind farm. Report prepared for: The Bats and Wind Energy Cooperative and Bat Conservation International, Austin, TX.

Hudson RR (1991) Gene genealogies and the coalescent process. In *Oxford Surveys in Evolutionary Biology* (eds. Futuyma DJ, Antonovics JD), pp. 1-44. Oxford University Press, New York.

Hudson RR (2002) Generating samples under a Wright-Fisher neutral model of genetic variation. *Bioinformatics*, **18**, 337-338.

Hunter ME, Mignucci-Giannoni AA, Pause Tucker K, King TL, Bonde RK, *et al.* (2012) Puerto Rico and Florida manatees represent genetically distinct groups. *Conservation Genetics*, **13**, 1623-1635.

International SNP Map Working Group (2001) A map of human genome sequence variation containing 1.42 million single nucleotide polymorphisms. *Nature*, **409**, 928-933.

Itsara A, Wu H, Smith JD, Nickerson DA, Romieu I, *et al.* (2010) De novo rates and selection of large copy number variation. *Genome Research*, **20**, 1469-1481.

Jackson JBC, Kirby MX, Berger WH, Bjorndal KA, Botsford LW, *et al.* (2001) Historical overfishing and the recent collapse of coastal ecosystems. *Science*, **293**, 629-638.

Johnson GD, Perlik MK, Erickson WP, Strickland MD (2004) Bat activity, composition, and collision mortality at a large wind plant in Minnesota. *Wildlife Society Bulletin,* **32**, 1278-1288.

Jones G, Jacobs DS, Kunz TH, Willig MR, Racey PA (2009) Carpe noctem: the importance of bats as bioindicators. *Endangered Species Research*, **8**, 93-115.

Jones G, Rebelo H (2013) Responses of bats to climate change: learning from the past and predicting the future. In *Bat Evolution, Ecology, and Conservation* (eds. Adams RA, Pederson SC), pp. 457-478. Springer Science & Business Media, New York.

Jordan MA, Patel D, Sanders KE, Gillespie RB (2013) The relative roles of contemporary and ancient processes in shaping genetic variation of a generalist fist in a catchment dominated by agriculture. *Freshwater Biology*, **58**, 1660-1671.

Kimmel M, Chakraborty R, King JP, Bamshad M, Watkins WS, *et al.* (1998) Signatures of population expansion in microsatellite repeat data. *Genetics*, **148**, 1921-1930.

Kimura M (1968) Genetic variability maintained in a finite population due to mutational production of neutral and nearly neutral isoalleles*. *Genetical Research*, **11**, 247-270.

Kimura M, Crow JF (1963) The measurement of effective population number. *Evolution*, **17**, 279-288.

Kingman JFC (1982) On the genealogy of large populations. *Journal of Applied Probability*, **19**, 27-43.

Kumar S, Subramanian S (2002) Mutation rates in mammalian genomes. *Proceedings of the National Academy of Sciences, USA,* **99**, 803-808.

Kunz TH, Arnett EB, Erickson WP, Hoar AR, Johnson GD, *et al*. (2007) Ecological impacts of wind energy development on bats: questions, research needs, and hypotheses. *Frontiers in Ecology and the Environment*, **5**, 315-324.

Kuo CH, Janzen FJ (2004) Genetic effects of a persistent bottleneck on a natural population of ornate box turtles (*Terrapene ornate*). *Conservation Genetics*, **5**, 425-437.

Lande R (1988) Genetics and demography in biological conservation. *Science*, **241**, 1455-1460.

Lesiński G (2008) Linear landscape elements and bat casualties on roads – an example. *Annales Zoologici Fennici*, **45**, 277-280.

Luikart G, Ryman N, Tallmon DA, Schwartz MK, Allendorf FW (2010) Estimation of census and effective population sizes: the increasing usefulness of DNA-based approaches. *Conservation Genetics,* **11**, 355-373.

Mahtani MM, Willard HF (1993) A polymorphic X-linked tetranucleotide repeat locus displaying a high rate of new mutation: implications for mechanisms of mutations at short tandem repeat loci. *Human Molecular Genetics*, **2**, 431-437.

Malthus T (1798) *An essay on the principle of population, as it affects the future improvement of society with remarks on the speculations of Mr. Godwin, M. Condorcet, and other writers*. St. Paul's Church-yard, London.

Marth GT, Czabarka E, Murvai J, Sherry ST (2004) The allele frequency spectrum in genome-wide human variation data reveals signals of differential demographic history in three large world populations. *Genetics*, **166**, 351-372.

Martin AM (2014) Historical demography and dispersal patterns in the eastern pipistrelle bat (*Perimyotis subflavus*). Unpublished master's thesis, Grand Valley State University, Allendale, MI.

Meyer CFJ, Kalko EKV, Kerth G (2009) Small-scale fragmentation effects on local genetic diversity in two phyllostomid bats with different dispersal abilities in Panama. *Biotropica*, **41**, 95-102.

Möhle M (1998) Robustness results for the coalescent. *Journal of Applied Probability*, **35**, 438-447.

Morin PA, Archer FI, Pease VL, Hancock-Hanser BL, Robertson KM, *et al.* (2012) Empirical comparison of single nucleotide polymorphism and microsatellites for population and demographic analyses of bowhead whales. *Endangered Species Research*, **19**, 129-147.

Morin PA, Luikart G, Wayne RK, SNP workshop group (2004) SNP in ecology, evolution and conservation. *Trends in Ecology and Evolution*, **19**, 208-216.

Moritz C (1994) Applications of mitochondrial DNA analysis in conservation: a critical review. *Molecular Ecology*, **3**, 401-411.

Moussy C, Hosken DJ, Mathews F, Smith GC, Aegerter JN, *et al.* (2013) Migration and dispersal patterns of bats and their influence on genetic structure. *Mammal Review*, **43**, 183-195.

Nei M, Maruyama T, Chakraborty R (1975) The bottleneck effect and genetic variability in populations. *Evolution*, **29**, 1-10.

Nei M, Tajima F (1981) Genetic drift and estimation of effective population size. *Genetics*, **98**, 625-640.

Nielsen R, Slatkin M (2013) *An Introduction to Population Genetics: Theory and Applications.* Sinauer Associates, Inc., Sunderland.

Okello JBA, Wittemyer G, Rasmussen HB, Arctander P, Nyakaana S, *et al.* (2008) Effective population size dynamics reveal impacts of historic climatic events and recent anthropogenic pressure in African elephants. *Molecular Ecology*, **17**, 3788-3799.

Paradis E (2010) Pegas: an R package for population genetics with an integrated-modular approach. *Bioinformatics*, **26**, 419-420.

Peery MZ, Kirby, R, Reid BN, Stoelting R, Doucet-Bëer E, *et al.* (2012) Reliability of genetic bottleneck tests for detecting recent population declines. *Molecular Ecology*, **21**, 3403-3418.

Pidugu SR, Schlötterer C (2006) ms2ms.pl: a PERL script for generating microsatellite data. *Molecular Ecology Notes*, **6**, 580-581.

Pierce BA (2014) *Genetics A Conceptual Approach, 5nd edn.* W. H. Freeman and Company, New York.

Plummer M, Best N, Cowles K, Vines K (2006) CODA: convergence diagnosis and output analysis for MCMC. *R News*, **6**, 7-11.

Pritchard JK, Seielstad MT, Perez-Lezuan A, Feldman MW (1999) Population growth of human Y chromosomes: a study of Y chromosome microsatellites. *Molecular Biology and Evolution*, **16**, 1791-1798.

Qiu F, Kitchen A, Beerli, P, Miyamoto MM (2013) A possible explanation for the population size discrepancy in tuna (genus *Thunnus*) estimated from mitochondrial DNA and microsatellite data. *Molecular Phylogenetics and Evolution*, **66**, 463-468.

R Core Team (2014) R: a language and environment for statistical computing. R Foundation for Statistical Computing, Vienna. http://www.R-project.org/.

Reed DH, Lowe EH, Briscoe DA, Frankham R (2003) Inbreeding and extinction: effects of rate of inbreeding. *Conservation Genetics*, **4**, 405-410.

Rotheray EL, Lepais O, Nater A, Krützen M, Greminger M, *et al*. (2012) Genetic variation and population decline of an endangered hoverfly *Blera fallax* (Diptera: Syrphidae). *Conservation Genetics*, **13**, 1283-1291.

Rubinoff D (2006) Utility of mitochondrial DNA barcodes in species conservation. *Conservation Biology*, **20**, 1026-1033.

Ruiz-Lopez MJ, Gañan N, Godoy JA, Del Olmo A, Garde J, *et al.* (2012) Heterozygosity-fitness correlations and inbreeding depression in two critically endangered mammals. *Conservation Biology,* **26**, 1121-1129.

Russell AL, Butchkoski CM, Saidak L, McCracken GF (2009) Road-killed bats, highway design, and the commuting ecology of bats. *Endangered Species Research,* **8**, 49-60.

Russell AL, Medellín RA, McCracken GF (2005) Genetic variation and migration in the Mexican free-tailed bat (*Tadarida brasiliensis mexicana*). *Molecular Ecology*, **14**, 2207-2222.

Schneider S, Excoffier L (1999) Estimation of past demographic parameters from the distribution of pairwise differences when the mutation rates vary among sites: application to human mitochondrial DNA. *Genetics*, **152**, 1079-1089.

Seber GAF (1973) *The Estimation of Animal Abundance and Related Parameters*. Hafner Press, New York.

Shump KA, Shump AU (1982) *Lasiurus borealis*. *Mammalian Species*, **183**, 1-6.

Siemers BM, Schaub A (2011) Hunting at the highway: traffic noise reduces foraging efficiency in acoustic predators. *Proceedings of the Royal Society B: Biological Sciences*, **278**, 1646-1652.

Simmons JA, Neretti N, Intrator N, Altes RA, Ferragamo MJ, *et al.* (2004) Delay accuracy in bat sonar is related to the reciprocal of normalized echo bandwidth, or *Q*. *Proceedings of the National Academy of Sciences, USA*, **101**, 3638-3643.

Spielman D, Brook BW, Briscoe DA, Frankham R (2004a) Does inbreeding and loss of genetic diversity decrease disease resistance? *Conservation Genetics*, **5**, 439-448.

Spielman D, Brook BW, Frankham R (2004b) Most species are not driven to extinction before genetic factors impact them. *Proceedings of the National Academy of Sciences, USA*, **101**, 15261-15264.

Spong G, Johansson M, Björklund M (2000) High genetic variation in leopards indicates large and long-term stable effective population size. *Molecular Ecology*, **9**, 1773-1782.

Stoner AW, Ray-Culp M (2000) Evidence for Allee effects in an over-harvested marine gastropod: density-dependent mating and egg production. *Marine Ecology Progress Series*, **202**, 297-302.

Storz JF, Beaumont M (2002) Testing for genetic evidence of population expansion and contraction: an empirical analysis of microsatellite DNA variation using a hierarchical Bayesian model. *Evolution*, **56**, 154-166.

Sunnucks P (2000) Efficient genetic markers for population biology. *Trends in Ecology and Evolution*, **15**, 199-203.

Tucker T, Marra M, Friedman JM (2009) Massively parallel sequencing: the next big thing in genetic medicine. *American Journal of Human Genetics,* **85**, 142-154.

Ujvari B, Belov K (2011) Major histocompatibility complex (MHC) markers in conservation biology. *International Journal of Molecular Sciences*, **12,** 5168-5186.

U. S. Energy Information Administration (2015) *Short-term energy outlook.* http://www.eia.gov/forecasts/steo/report/renew_co2.cfm. Downloaded on 22 June 2015.

U. S. Fish and Wildlife Service (2015) Endangered and threatened wildlife and plants; threatened species status for the northern long-eared bat with 4(d) rule. *Federal Register*, **80**, 17974-18033.

Vonhof MJ, Russell AL (2015) Genetic approaches to the conservation of migratory bats: a study of the eastern red bat (*Lasiurus borealis*). *PeerJ*, **3**, e983.

Vors LS, Boyce MS (2009) Global declines of caribou and reindeer. *Global Change Biology*, **15**, 2626-2633.

Wakeley J (2009) *Coalescent Theory: An Introduction.* Roberts & Company Publishers, Greenwood Village.

Wakeley J, Sargsyan O (2009) Extensions of the coalescent effective population size. *Genetics*, **181**, 341-345.

Waples RS (1989) A generalized approach for estimating effective population size from temporal changes in allele frequency. *Genetics*, **121**, 379-391.

Waples RS, Do C (2010) Linkage disequilibrium estimates of contemporary N_e using highly variable genetic markers: a largely untapped resource for applied conservation and evolution. *Evolutionary Applications*, **3**, 244-262.

Weber JL, Wong C (1993) Mutation of human short tandem repeats. *Human Molecular Genetics*, **2**, 1123-1128.

Weissenbach J, Gyapay G, Dib C, Vignal A, Morissette J, *et al.* (1992) A second-generation linkage map of the human genome. *Nature*, **359**, 794-801.

Williamson-Natesan EG (2005) Comparison of methods for detecting bottlenecks from microsatellite loci. *Conservation Genetics*, **6**, 551-562.

Winhold L, Kurta A, Foster R (2008) Long-term change in an assemblage of North American bats: are eastern red bats declining. *Acta Chiropterologica,* **10**, 359-366.